Elbow

8

Stefano Bianchi and Carlo Martinoli

CONTENTS

S. Bianchi, MD
Privat-docent, Université de Genève, Consultant Radiologist,
Fondation et Clinique des Grangettes, 7, ch. des Grangettes,
1224 Genève, Switzerland
C. Martinoli, MD
Associate Professor of Radiology, Cattedra "R" di Radiologia
– DICMI – Università di Genova, Largo Rosanna Benzi 8, 16132
Genova, Italy

8.1
Introduction

Being capable of a wide range of hinged and rotational motion, the elbow is intrinsically predisposed to acute injures and degenerative changes. Although clinical examination and routine radiography are essential to evaluate elbow disorders, US has become increasingly important in the diagnostic investigation of several abnormalities affecting tendons and muscles, joints, ligaments, nerves and other soft-tissue structures around the elbow joint. After US examination, CT and MR imaging may be required to further address the status of the joint cavity, the articular cartilage and the bone.

8.2
Clinical Anatomy

A brief description of the complex anatomy of the elbow with emphasis given to the anatomic features amenable to US examination, including joints and ligament complexes, muscles and tendons, neurovascular structures and bursae, is included here.

8.2.1
Joint and Ligament Complexes

The elbow is composed of three articulations–radio-capitellar, proximal radio-ulnar and trochlea-ulna–sharing in a common joint cavity and stabilized by a number of soft-tissue structures, including the lateral and medial collateral ligaments and the anterior portion of the joint capsule.

8.2.1.1
Elbow Joint

The bone structures about the elbow joint include the proximal ends of the ulna and radius and the distal end of the humerus (Fig. 8.1). The radial head articulates with the humeral capitellum in a pivotal mode and the ulna with the humeral trochlea in a hinge mode. The proximal radio-ulnar articulation is composed of the radial head which revolves within the sigmoid (radial) notch of the ulna allowing pronation-supination movements. These articulations cooperate during complex joint movements allowing a wide degree of flexion, extension and axial rotation. The congruity of the apposing articular surfaces varies in different elbow positions and is maximal with the elbow 90° flexed and the forearm midway between full pronation and full supination. The humeral trochlea, the trochlear notch of the ulna and the radial head, with the exception of its anterolateral portion, are covered by articular cartilage which is approximately 2 mm thick.

The elbow is one of the most stable joints of the body. In normal states, elbow joint motion ranges approximately from 0° to 150° of flexion and from 75° in pronation to 85° in supination. Elbow extension is limited by contact of the olecranon in the posterior humeral fossa, and tightening of the anterior band of the medial collateral ligament, of the joint capsule and of flexor muscles. On the other hand, the bulk of anterior muscles of the arm, the tension of the triceps and the contact of the coronoid process in the anterior humeral fossa limit elbow flexion. Pronation and supination movements are primarily limited by passive muscle constraints rather than ligaments.

The joint capsule invests the entire elbow. Anteriorly, it is attached to the humeral shaft just above the coronoid and radial fossae, to the anterior aspect of the coronoid process and to the annular ligament.
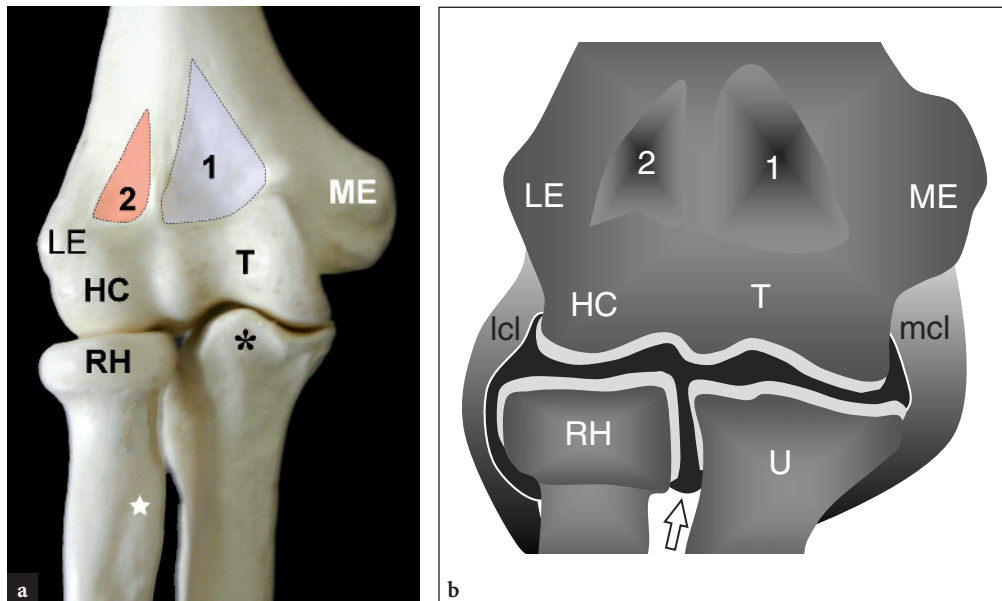
Fig. 8.1a,b. Elbow joint. Articular anatomy. **a** Anterior aspect of the elbow bones illustrates the relationships of the trochlea (T) and capitellum (*HC*) of the distal humerus with the coronoid process of the ulna (*asterisk*) and the radial head (*RH*). The capitellum of the humerus articulates with the superior facet of the radial head forming the radio-capitellar joint, and the trochlea of the humerus articulates with the trochlear notch of the ulna, forming the humero-ulnar joint. Observe the medial (*ME*) and lateral (*LE*) epicondyles and the coronoid *(1)* and radial *(2)* fossae of the humerus. *Star*, radial tuberosity. **b** Schematic drawing of a coronal view through the elbow shows the extension of the joint cavity (*in black*). Note the lateral *(lcl)* and medial *(mcl)* collateral ligaments which delimit the joint cavity on each side and the pouch *(arrow)* of the elbow joint between radius and ulna forming the superior radio-ulnar joint

It is taut in elbow extension and lax in elbow flexion. Posteriorly, the capsule inserts on the posterior aspect of the humerus above the olecranon fossa, and to the upper margins of the olecranon. The anterior bulk of the brachialis muscle, the posterior bulk of the triceps and, on each side, the medial and lateral collateral ligaments reinforce the capsule. The synovial membrane of the elbow joint envelops the inner surface of the capsule and the annular ligament (Fig. 8.1b). It infolds between the radius and the ulna and produces three main synovial recesses. The largest recess is the olecranon (posterior humeral) recess which includes a superior, medial and lateral pouches (Fig. 8.2). On the anterior elbow, the coronoid (anterior humeral) recess extends over the coronoid and radial fossae of the humerus, whereas the annular (periradial) recess surrounds the radial neck. Two small additional recesses are located deep to the medial and lateral collateral ligaments. Some fat pads lie between the fibrous capsule and the synovial membrane in an extrasynovial but intra-articular location. The largest ones fill the coronoid and radial fossae of the humerus underneath the brachialis muscle, and the olecranon fossa deep to the triceps muscle (Fig. 8.2). Any intra-articular expansible process causes displacement and elevation of these fat pads. A crescentic synovial fold, commonly referred to as the "lateral synovial fringe", may be found at the level of radiocapittelar joint. Similar to the knee plicae, this fringe represents a septal remnant (CLARKE 1988) and may cause symptoms, such as elbow locking and popping, secondary to its

entrapment in the radio-capitellar joint. Other synovial plicae may project into the anterior humeral recess from the anterior fat pad and into the olecranon recess from the posterior fat pad, this latter location being more commonly associated with clinical symptoms (locking elbow). They may seldom mimic an intra-articular loose body (AWAYA et al. 2001).

8.2.1.2
Medial Collateral Ligament

The medial collateral ligamentous complex, also known as the ulnar collateral ligament, is composed of three bands in continuity with each other: anterior, posterior and oblique (Fig. 8.3a). The anterior band is the most conspicuous and extends from the medial epicondyle to the medial aspect of the coronoid process, providing the major constraint to valgus stress. The posterior band arises from the posterior aspect of the medial epicondyle and inserts into the medial edge of the olecranon. The oblique band, commonly referred to as the "ligament of Cooper", is the weakest and bridges the insertions of the anterior and posterior bands on the ulna.

8.2.1.3
Lateral Collateral Ligament

The lateral collateral ligamentous complex is more variable than the medial one. It consists of the radial
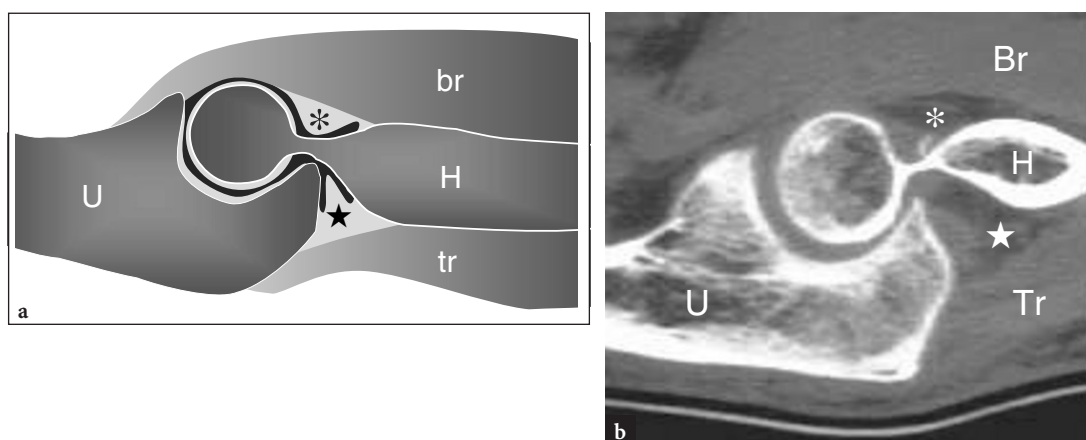
Fig. 8.2a,b. Elbow joint. Articular anatomy. **a** Schematic drawing of a midsagittal view through an extended elbow with **b** CT scan correlation demonstrates the articular relationship between the trochlea of the humerus *(H)* and the trochlear groove of the ulna *(U)*, leading to flexion and extension joint movements. The extrasynovial anterior *(asterisk)* and posterior *(star)* fat pads are closely applied to the distal end of the humerus and lie just superficial to the joint space *(in black)*. Note the insertion of the brachialis *(Br)* and the triceps *(tr)* muscles, which are the main flexor and extensor muscles of the elbow respectively

Fig. 8.3a–c. Collateral ligaments of the elbow. **a** Medial view of the elbow bones showing the position of the medial collateral ligament, including its anterior band *(1)*, posterior band *(2)* and transverse ligament *(3)*. Note that the common flexor tendon origin *(cft)* lies just superficial to the medial ligamentous structures. The medial aspect of the annular ligament *(4)* is also shown. **b** Lateral view of th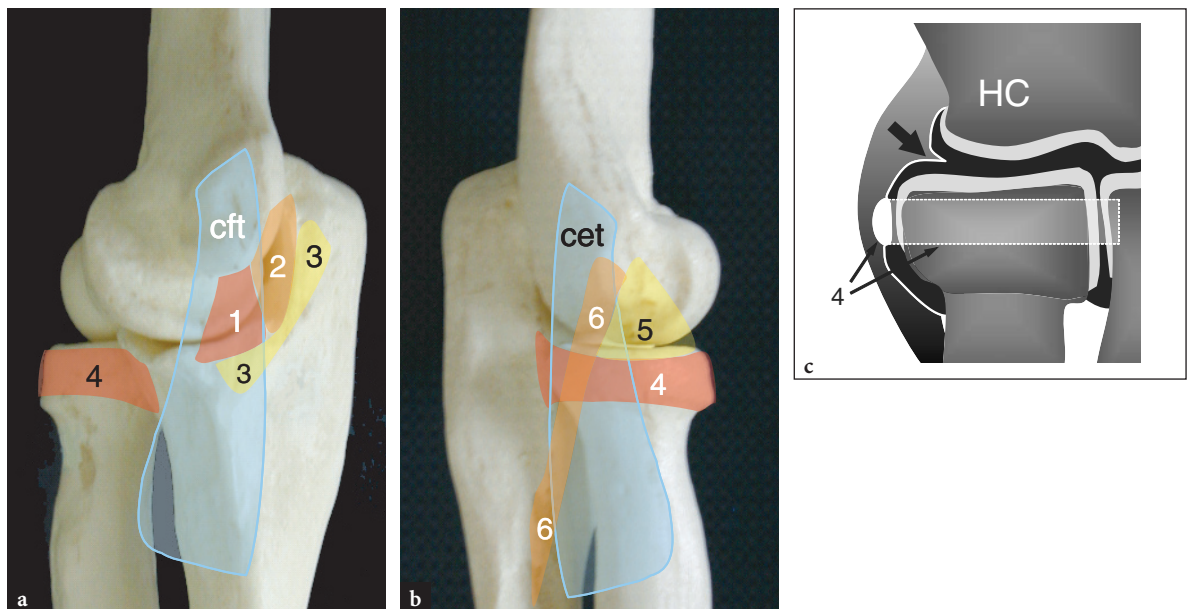e elbow showing the position of the lateral collateral ligamentous complex, including the annular ligament *(4)*, the radial collateral ligament *(5)* and the lateral ulnar collateral ligament *(6)* relative to the common extensor tendon origin *(cet)*. In **a** and **b**, the annular ligament *(4)* is seen encircling the radial head and attaching to the margins of the radial notch of the ulna. **c** Schematic drawing of a coronal view of the lateral elbow illustrates the position of the annular ligament *(4)* relative to the articular structures and the joint cavity *(in black)*. Note the lateral synovial fringe *(arrow)* abutting the joint line. *HC*, capitellum of the distal humerus

collateral ligament, the annular ligament, the lateral ulnar collateral ligament and the accessory lateral collateral ligament (Fig. 8.3b). The radial collateral ligament is a thick band of fibrous tissue which arises from the lateral epicondyle and inserts on the radial notch of the ulna, blending with the fibers of the annular ligament. The annular ligament is a strong ligament which surrounds the radial head and holds it in contact with the ulna by inserting on the anterior and posterior margins of the radial notch of this latter bone (Fig. 8.3). In its short-axis, the annular ligament displays a crescent-shaped profile with a smooth internal appearance and is covered by a synovial membrane (Fig. 8.3c). Proximally, the fibers of the annular ligament blend with the joint capsule and with the adjacent radial collateral ligament. The annular ligament maintains the radial head in close contact with the ulna preventing its withdrawal or inferior displacement from its socket. The lateral ulnar collateral ligament arises from the lateral epicondyle and blends with the fibers of the annular ligament deep to the common extensor tendon origin (Fig. 8.3b). It remains stretched

throughout the full range of elbow flexion-extension movements and plays an essential role as a lateral stabilizer of the trochlea-ulna joint.

8.2.2
Muscles and Tendons

The muscles and tendons around the elbow can be subdivided according to their position into anterior, medial, lateral and posterior.

8.2.2.1
Anterior Elbow

The anterior group of muscles and tendons includes the biceps brachii and the brachialis that lie in the cubital region between the brachioradialis muscle laterally and the pronator teres muscle medially. The biceps brachii muscle is located superficial to the brachialis and has a long distal tendon that is not surrounded by muscle, making it more susceptible
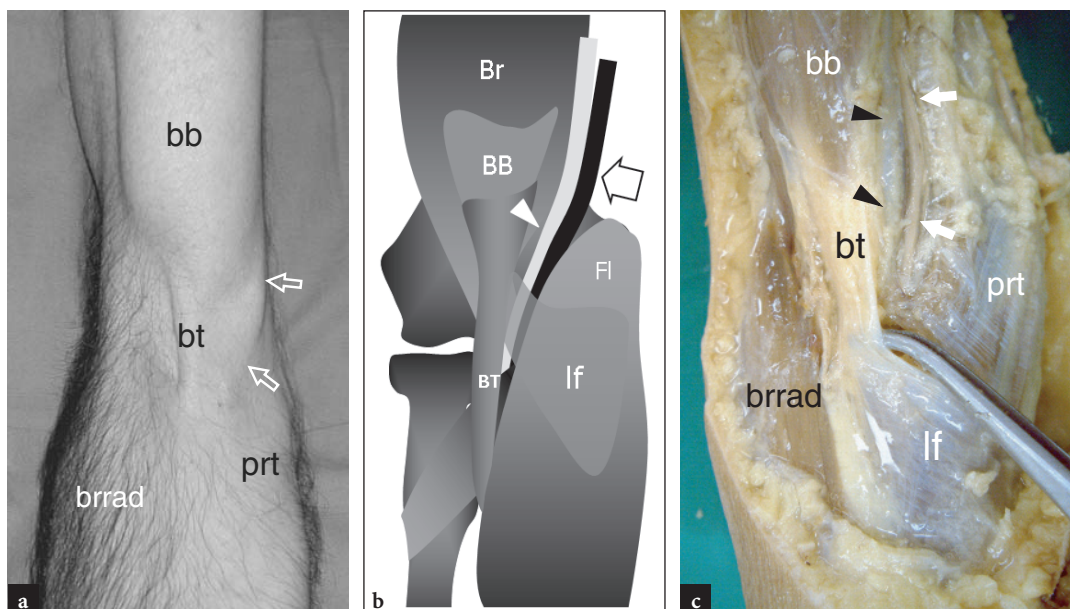
Fig. 8.4a–c. Anatomy of the cubital fossa. **a** Photograph of the anterior aspect of the elbow in a young man showing the main surface features visible during resisted contraction of the biceps muscle keeping the elbow extended and the hand supinated. During this action, the distal tendon *(bt)* of the biceps brachii muscle *(bb)* becomes prominent on the skin and can be palpated as it passes through the mid-antecubital fossa lying between the bulks of the extensor muscles–represented by the brachioradialis *(brrad)*–and the flexor muscles–represented by the pronator teres *(prt)*. Note the prominence of the basilic vein *(arrows)* relative to the distal biceps tendon. **b** Schematic drawing of a coronal view of the elbow illustrates the position of the biceps tendon *(bt)* and the lacertus fibrosus *(lf)* relative to the flexor-pronator group of muscles *(fl)*, the brachial artery *(arrowhead)* and the median nerve *(arrow)*. *br*, brachialis muscle. **c** Gross dissection of the anterior elbow reveals the cubital fossa delimited by the brachioradialis *(brrad)* and the pronator teres *(prt)* muscles. Observe that the brachial artery *(arrowheads)* and the median nerve *(arrows)* course alongside the biceps muscle *(bb)* and tendon *(bt)* and then deep to the lacertus fibrosus *(lf)*

to injury than the brachialis (Fig. 8.4). The distal biceps tendon is a flattened tendon that derives from the union of the two muscle bellies, the long and short heads, of the biceps brachii muscle which join in the lower part of the arm. It is approximately 7 cm long and curves laterally and deep before inserting on the medial aspect of the radial tuberosity. It also has a flattened aponeurotic expansion, commonly referred to as the "lacertus fibrosus", that extends from the myotendinous junction to the medial deep fascia of the forearm. This aponeurosis covers the median nerve and the brachial artery and contributes to keeping the biceps tendon located in the appropriate position (Fig. 8.4b,c). The distal portion of the biceps tendon is covered by an extrasynovial paratenon and is separated from the radial tuberosity by an intervening bursa, the bicipitoradial bursa, which is normally not visible at US unless distended with fluid effusion. The biceps is a powerful flexor of the elbow; when the forearm is supinated, it also acts as a supinator. Deep to the biceps brachii, the brachialis muscle arises from the anterior surface of the

distal half of the humerus and the adjacent medial and lateral intermuscular septa and extends along the anterior joint capsule to insert onto the anterior surface of the coronoid process and the ulnar tuberosity. Its tendon is thinner than the biceps tendon and is surrounded by the muscle bellies down to its insertion. The brachialis essentially acts as a flexor of the elbow regardless of the position of the forearm.

8.2.2.2
Medial Elbow

The medial compartment includes the pronator teres and the superficial flexor muscles of the wrist and hand that arise from the medial epicondyle as the "common flexor tendon". The pronator teres is the most superficial and anterior of the medial muscles. It has two proximal attachments: one (humeral head) immediately proximal to the medial epicondyle and the common flexor tendon, the other (ulnar
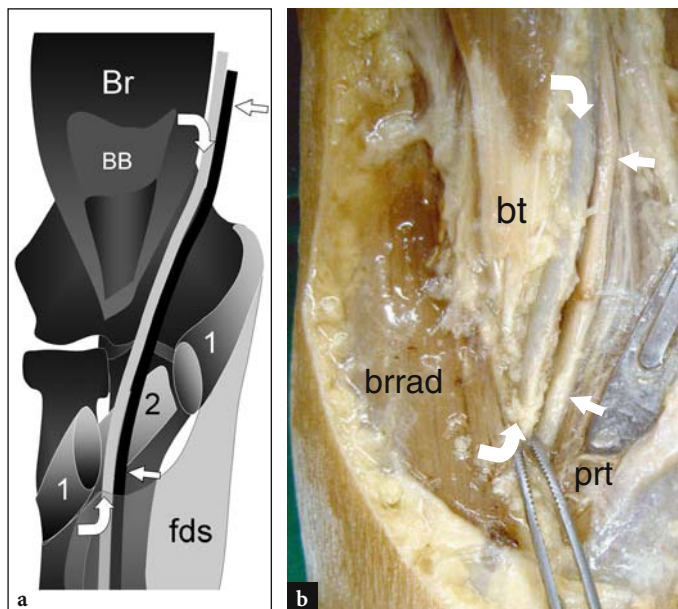
Fig. 8.5a,b. Brachial artery and median nerve. **a** Same schematic drawing as Fig. 8.4b after removal of the distal biceps tendon and the superficial humeral belly of the pronator teres muscle *(1)* reveals the course of the brachial artery *(arrowheads)* and the adjacent median nerve *(straight arrows)* in the pronator area and beneath the "sublimis bridge" *(curved arrow)* of the flexor digitorum superficialis muscle *(fds)*. *Br*, brachialis muscle; *BB*, biceps muscle; *2*, deep (ulnar) belly of the pronator teres muscle. **b** Gross dissection of the cubital fossa demonstrates the brachial artery *(curved arrows)* and the median nerve *(straight arrows)* as they infold in the space between the brachioradialis *(brrad)* and the pronator teres *(prt)* muscles. The distal biceps tendon *(bt)* has previously been removed

head) at the medial aspect of the coronoid process. Distally, the pronator teres inserts along the lateral surface of the radial shaft through a flat tendon (Fig. 8.5a). The median nerve passes in between the two bellies of the pronator teres and is separated from the ulnar artery by the ulnar head of this muscle (Fig. 8.5). During pronation of the forearm, the pronator teres works together with the pronator quadratus. There are four superficial flexor muscles of the hand and wrist that arise from the common flexor tendon, arranged from medial or lateral as the flexor carpi radialis, the palmaris longus, the flexor digitorum superficialis and the flexor carpi ulnaris. The flexor digitorum profundus has a separate more distal origin from the anteromedial aspect of the ulna, the coronoid process and the anterior surface of the interosseous membrane. The superficial and deep flexor muscles are primary flexors of the wrist and fingers. In addition, the common flexor tendon provides dynamic support to the underlying ulnar collateral ligament in resisting valgus stress.

8.2.2.3
Lateral Elbow

The lateral compartment of the elbow includes the extensor muscles of the wrist and hand that arise from the lateral epicondyle as the "common extensor tendon", the brachioradialis, the extensor carpi radialis longus and the supinator muscles.

The common extensor tendon is a flattened tendon which originates from the anterolateral surface of the lateral epicondyle (Fig. 8.3b). It receives contributions of fibers from four superficial extensor muscles: extensor carpi radialis brevis, extensor digitorum communis, extensor digiti minimi and extensor carpi ulnaris. The extensor carpi radialis brevis makes up most of the deep articular fibers, whereas the extensor digitorum contributes to the superficial portion of the common extensor tendon (Connell et al. 2001). The extensor digiti minimi and carpi ulnaris provide only minor components to the common extensor tendon. Overall, these muscles act as extensors of the wrist and/or fingers and also play a role in radial (extensor carpi radialis brevis) and ulnar (extensor carpi ulnaris) deviation of the wrist. The common extensor tendon origin is separated from the joint capsule by the lateral ulnar collateral ligament (Fig. 8.3b). Cranial to and separately from the common extensor tendon, the brachioradialis (anterior) and the extensor carpi radialis longus (posterior) muscles arise from the supracondylar ridge of the humerus and the lateral intermuscular septum. The supinator is the deepest of the lateral muscles. It has two heads between which the posterior interosseous nerve, motor branch of the radial nerve, passes to reach the posterior elbow (Fig. 8.6a) (see also Sect. 8.2.3.2). The superficial head arises from the lateral epicondyle, the lateral collateral and annular ligaments and from behind the supinator crest and fossa of the
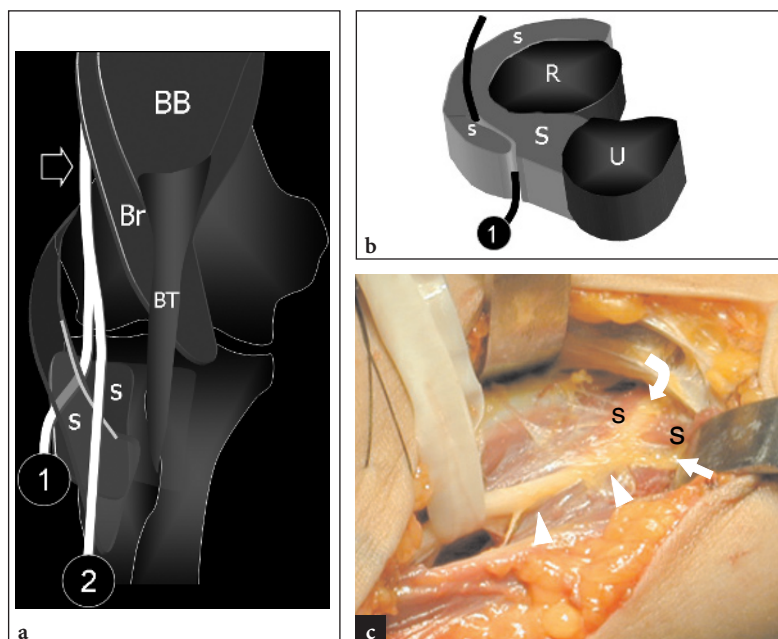
Fig. 8.6a–c. Radial nerve and posterior interosseous nerve. **a** Schematic drawing of a coronal view of the elbow demonstrates the course of the main trunk of the radial nerve *(arrow)* that lies lateral to the brachialis muscle *(br)* and then divides into its terminal branches, the posterior interosseous nerve *(1)* and the superficial sensory branch *(2)*. At the radial neck, the posterior interosseous nerve pierces the supinator muscle *(s)* to reach the posterior compartment of the elbow. *bb*, biceps muscle; *bt*, biceps tendon. **b** Drawing of a cross-section through the proximal forearm shows the bellies of the supinator muscle *(s)* and the posterior interosseous nerve *(1)* that passes in between them. *U*, ulna; *R*, radius. **c** Gross operative appearance of the supinator area. Note the radial nerve *(arrowheads)* that splits into the cutaneous sensory nerve *(curved arrow)* and the posterior interosseous nerve *(straight arrow)* just before this latter enters the supinator muscle *(s)*

ulna; the deep head arises from the supinator fossa of the ulna. This muscle as a whole wraps around the radial neck to insert into the proximal aspect of the radial shaft (Fig. 8.6b). In up to 35% of individuals, the origin of the superficial head unite to form a fibrous arch, which is commonly known as the "arcade of Frohse" (Fig. 8.6c). The supinator muscle acts in synergy with the biceps to supinate the forearm when the elbow is extended.

8.2.2.4
Posterior Elbow

The posterior compartment includes the triceps and the anconeus muscles. The triceps is a large muscle made up of three heads–medial, lateral and long–from which it derives its name. The muscle bellies converge into a single thick tendon which attaches on the posterior aspect of the olecranon process. To increase the strength of extension of the elbow joint, the triceps tendon does not insert on the tip of the olecranon, but approximately 1 cm distal

to it (Fig. 8.2). On the lateral side of the olecranon, opposite the cubital tunnel, the anconeus muscle is a small triangular muscle that arises from the posterior aspect of the lateral epicondyle to insert more distally on the upper posterolateral aspect of the shaft of the ulna. It contributes to the dorsolateral soft-tissue bulk of the elbow, assists the triceps in elbow extension and provides dynamic support to the underlying lateral ulnar collateral ligament in resisting varus stress.

The anconeus epitrochlearis is a small accessory muscle (prevalence ranging from 1% to 34%) that forms the roof of the cubital tunnel, replacing the Osborne retinaculum and joins the posterior aspect of the medial epicondyle with the medial aspect of the olecranon.. This muscle is often bilateral and can cause ulnar neuropathy by occupying space within the cubital tunnel and decreasing its free volume during full elbow flexion. Somewhat equivalent to the anconeus epitrochlearis, an anomalous myotendinous junction of the triceps may also be prominent over the posteromedial side of the cubital tunnel (see Sect. 8.5.4.5).
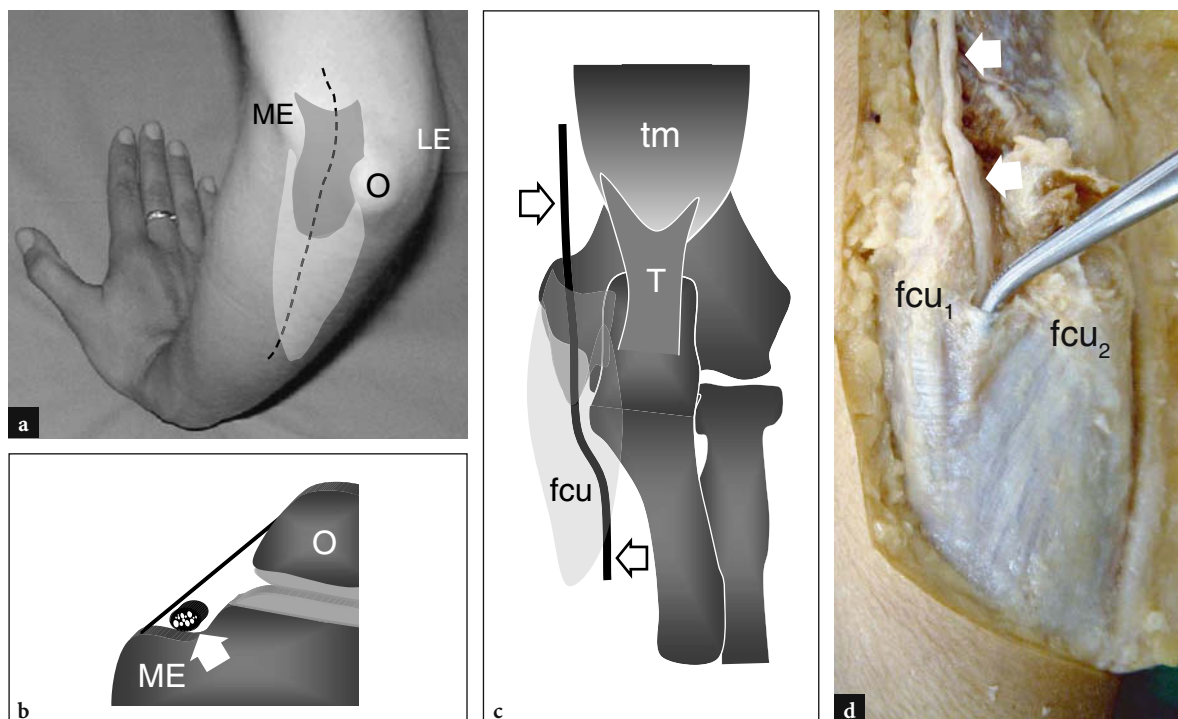
Fig. 8.7a–d. Ulnar nerve and cubital tunnel. **a** Photograph of the posteromedial aspect of the elbow illustrates the course of the ulnar nerve (*dashed black line*) between the bony prominences of the medial epicondyle *(ME)* and the olecranon *(O)* covered by the cubital tunnel retinaculum (*dark gray*) and, more caudally, by the aponeurosis and the belly of the flexor carpi ulnaris muscle (*light gray*). *LE*, lateral epicondyle. **b** Schematic drawing of the cubital tunnel on cross-section view reveals the relationships of the ulnar nerve (*arrow*) with the medial epicondyle *(ME)* and the olecranon *(O)*. Note the Osborne retinaculum that covers the cubital tunnel as a roof. **c** Schematic drawing of the posterior aspect of an extended elbow demonstrates the ulnar nerve (*arrows*) as it passes through the cubital tunnel, beneath the Osborne retinaculum (*dark gray*) and the flexor carpi ulnaris muscle *(fcu, light gray)*. *tm*, triceps muscle; *T*, distal triceps tendon. **d** Gross dissection of the cubital tunnel shows the triangular arcuate ligament that unites the humeral *(fcu$_1$)* and ulnar *(fcu$_2$)* heads of the flexor carpi ulnaris muscle. The forceps elevate the ligament making the course of the nerve (*arrows*) visible

8.2.3
Neurovascular Structures

The elbow is traversed by the ulnar, median and radial nerves that cross through its posteromedial, anterior and lateral aspects respectively. In the elbow area, the median nerve is accompanied by the brachial artery, the radial nerve gives off a main motor branch, the posterior interosseous nerve, and the ulnar nerve travels across an osteofibrous tunnel, the cubital tunnel.

8.2.3.1
Median Nerve and Brachial Artery

In the cubital fossa, the median nerve courses behind the lacertus fibrosus and superficial to the brachialis

muscle. More distally, it progressively deepens to pass between the ulnar and humeral heads of the pronator teres muscle in more than 80% of individuals. At the elbow, the median nerve gives off small muscular branches to the pronator teres, palmaris longus, flexor carpi radialis and flexor carpi ulnaris. Then, it courses deep to the tendinous bridge connecting the humero-ulnar and radial heads of the flexor digitorum superficialis muscle, the so-called sublimis bridge (Fig. 8.5).

At the elbow, the brachial artery is superficial and courses along the medial border of the biceps muscle and tendon overlying the brachialis (Figs. 8.4b,c, 8.5). Then, it passes between the median nerve (medial) and the biceps tendon (lateral) beneath the bicipital aponeurosis to divide, at the proximal forearm, into the radial and ulnar arteries.

8.2.3.2
Radial Nerve and Posterior Interosseous Nerve

At the proximal elbow, the radial nerve is located between the brachialis and the brachioradialis muscles anterior to the lateral epicondyle. It divides into a deep purely motor branch, the posterior interosseous nerve, and a superficial sensory branch. The posterior interosseous nerve pierces the supinator muscle, passing between its superficial and deep parts to gain access to the posterior compartment of the elbow (Fig. 8.6). At the proximal edge of the supinator muscle, a fibrous arch bridging the nerve, which is commonly referred to as the "arcade of Frohse", can cause nerve impingement.

8.2.3.3
Ulnar Nerve

In its passage around the posteromedial aspect of the elbow, the ulnar nerve lies in the condylar groove, an osteofibrous ring formed between the olecranon process and the medial epicondyle bridged by a fascial sheet, the cubital tunnel retinaculum, also referred to as the Osborne retinaculum (Fig. 8.7). The floor of this tunnel is formed by the posterior band of the medial collateral ligament. Approximately 1 cm distal to this tunnel, the ulnar nerve enters the proper cubital tunnel, a hiatus between the ulnar and humeral heads of the flexor carpi ulnaris muscle that are connected by an aponeurotic arch, the "arcuate ligament" (Fig. 8.7). This ligament represents a distal expansion of the Osborne retinaculum. In the cubital groove, the ulnar nerve is very superficial and may be palpable immediately posterior to the tip of the epicondyle. During elbow flexion and extension, the cubital tunnel changes shape (from slightly ovoid to elliptical) and volume, because of the eccentric origin of the retinaculum. It must be considered that, as the ulnar nerve curves over the medial epicondyle, a traction-related flattening and elongation of the nerve normally occurs as the elbow flexes; in addition, up to a 55% decrease in the nerve cross-sectional area and a sixfold increase in interstitial pressure of the cubital tunnel occur as a result of increasing tension of the retinaculum and bulging of the medial collateral ligament (GELBERMAN et al. 1998). It is conceivable that these conditions may predispose the nerve to any extrinsic compression at this level. Within the cubital tunnel, the small posterior ulnar recurrent artery and veins course in between the ulnar nerve and the olecranon. In general, these vessels are much smaller than the nerve.

8.2.4
Bursae

Several synovial bursae around the elbow joint lessen friction between bones and the overlying skin and soft-tissue structures. The most important are the olecranon bursa and the bicipitoradial bursa. The olecranon bursa is a large subcutaneous bursa which intervenes between the skin and the olecranon process over the posterior aspect of the elbow. The bicipitoradial bursa (cubital bursa) lies deep in the anterior compartment of the elbow, between the distal biceps tendon and the radial tuberosity, to reduce friction between, especially during pronation of the forearm (SKAF et al. 1999). In fact, the radial tuberosity rotates posteriorly during pronation and wraps the tendon around the radial cortex. During this movement, the bursa is tracked between the tendon and the bone (Fig. 8.8). When distended by fluid, the bicipitoradial bursa may surround the biceps tendon completely and may cause a mass effect on the adjacent branches of the radial nerve.
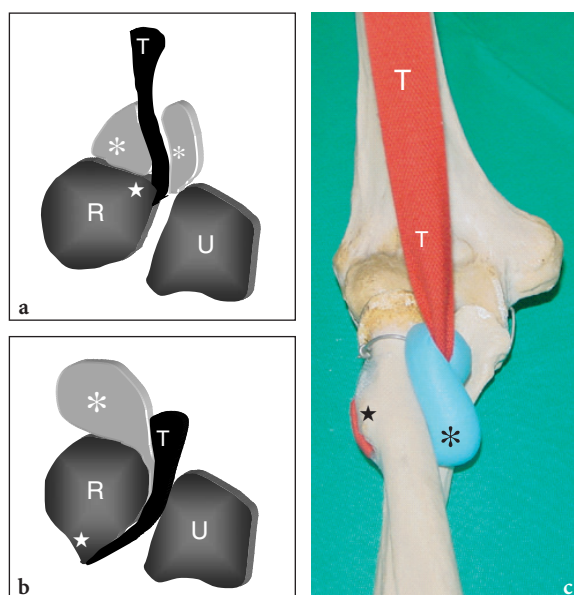

Fig. 8.8a–c. Bicipitoradial bursa. **a,b** Schematic drawings illustrate the position of the bicipitoradial bursa (*asterisks*) relative to the distal biceps tendon *(T)* during **a** supination and **b** pronation. In pronation, the long axis of the radius *(R)* and the radial tuberosity (*star*) rotate compressing the bursa between the distal biceps tendon *(T)* and the bone. *U*, ulna. (Drawings modified by SKAF et al. 1999.) **c** Skeletal model showing the relationship of the bicipitoradial bursa (*asterisk*) with the distal biceps tendon *(T)* in full pronation. Note the posterior and lateral position of the radial tuberosity (*star*) onto which the biceps tendon inserts

8.3
Essentials of Clinical History and Physical Examination

In the history of the patient complaining of elbow pain or dysfunction the examiner has to consider possible systemic articular diseases (rheumatoid arthritis and similar conditions), occupational disorders (drill diseases which can cause joint osteoarthritis) and traumas (missed radial head fractures may be a cause of long-lasting discomfort), even if sustained in the past. Sport activities are also a critical part of the history: tennis and golf practice can cause microtrauma and overuse injuries to the common extensor and flexor tendon origins with the onset of clearly defined clinical syndromes. With chronic symptoms, it is important to analyze as accurately as possible how the pain radiates and where it is localized, as well as its eliciting factors, because these characteristics can help to focus the US examination and suggest the correct diagnosis.

At physical examination, the range of elbow motion and the end-point of motion must be investigated at the level of both the radio-capitellar and trochlea-ulnar joints (flexion/extension) as well as at the proximal radio-ulnar joint (pronation/supination). Then, previous standard radiographs, if any, must be reviewed before starting the US examination in order to exclude bone abnormalities that may be overlooked or misinterpreted at US, such as joint erosions, osteoarthritic changes and heterotopic calcifications. In a post-traumatic setting, a careful review of the radiographs should be obtained prior to the US examination to rule out subtle fractures, especially involving the radial head, that may be overlooked at first observation.

8.3.1.1
Tendon Abnormalities

When a tendon lesion is suspected, specific resisted movements must be checked. Due to its superficial position, the distal biceps tendon can easily be palpated during resisted flexion while keeping the elbow 90° flexed and supinated. The rupture of this tendon is typically associated with retraction of the muscle into the arm, where it can be appreciated as a lump (see Sect. 8.5.1.1). Nevertheless, the retracted muscle belly can be difficult to detect in obese patients or when local swelling and pain limit proper physical examination. The distal triceps tendon can also be palpated without difficulty on the posterior elbow with the joint 90° flexed. Its integrity can be assessed by asking the patient to extend the elbow against resistance: a complete tear of the distal triceps tendon causes complete loss of extension power (see Sect. 8.5.4.1). In the case of a patient with suspected lateral epicondylitis, the examiner should immobilize the patient's elbow with one hand while compressing the common extensor tendon origin with the fingers over the lateral epicondyle. In lateral epicondylitis, this maneuver elicits pain radiating from the epicondylar area down through the forearm. Pain is typically exacerbated by extending the wrist against resistance (see Sect. 8.5.3.1). In medial epicondylitis, pain can be elicited by firm pressure over the medial common tendon or by resisted wrist flexion (see Sect. 8.5.2.1).

8.3.1.2
Ligament Instability

Specific clinical tests may be helpful in the setting of ligament instability. To evaluate the integrity of the lateral and medial collateral ligaments, the examiner may grasp the posterior aspect of the patient's elbow with one hand and the patient's wrist with the other. While locking the elbow, a valgus or varus stress is applied to assess the integrity of the medial and lateral collateral ligaments respectively. These clinical maneuvers are more reliably performed by placing the probe over the ligament in order to demonstrate even minor widening of the joint space during stressing (Fig. 8.9) (see Sects. 8.5.2.2, 8.5.3.2).

8.3.1.3
Cubital Tunnel Syndrome

A useful clinical maneuver to assess the state of the ulnar nerve is the "Froment's test". The patient is asked to pinch a sheet of paper between thumb and index finger. In case of overt ulnar neuropathy, the patient grasps the paper by flexing the thumb (activation of the median-innervated flexor pollicis longus as a compensation for the weakness of dorsal interosseous muscles) (see Sect. 8.5.4.3). In patients with cubital tunnel syndrome, palpation of the ulnar nerve at the cubital tunnel may be painful and may reproduce symptoms.
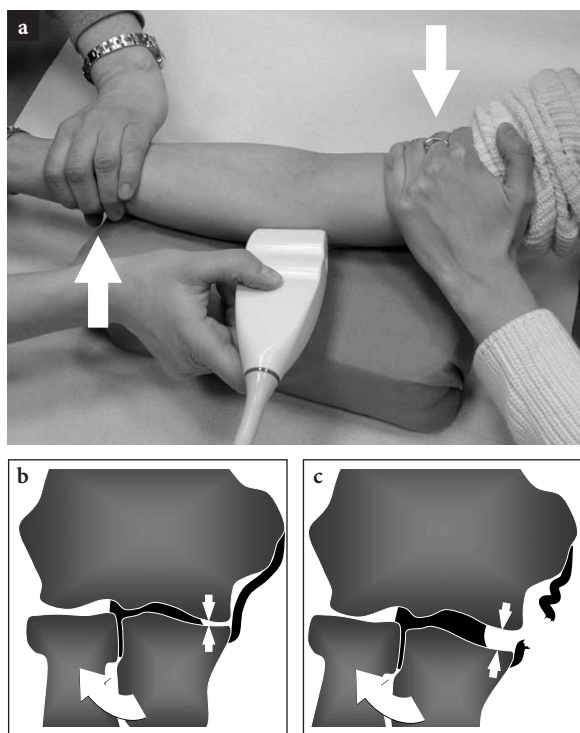
Fig. 8.9a–c. a Photograph illustrating the scanning technique to image the medial collateral ligament with dynamic stress (*arrows*). The elbow lies extended on a pillow while the distal arm is pushed toward the midline by the patient and the examiner pulls laterally on the distal forearm. If the patient is cooperating, this technique does not require further personnel assistance. **b,c** Schematic drawings of a coronal view of the elbow illustrate the appearance of the trochlea-ulna joint *(straight arrows)* under valgus stress (*curved arrow*) **b** when the medial collateral ligament (*in black*) is intact and **c** in the case of complete ligament rupture. When the ligament is torn, valgus stress causes widening of the trochlea-ulna joint

8.4
Ultrasound Anatomy and Scanning Technique

Generally speaking, the elbow is believed to be one of the easier joints to be examined with US, even for beginners (VANDERSCHUEREN et al. 1998). The main technical requirement is availability of a modern linear-array transducer with a frequency band ranging from 5 to 15 MHz. Adequate transducers should not be excessively wide to allow scanning around the elbow in various degrees of flexion without limiting the accessibility around prominent bones. More than in other sites of the limbs, the anatomic structures of the elbow are intrinsically predisposed to anisotropic effects as the probe sweeps over bony fossae, curvilinear surfaces and bone prominences. This requires careful scanning technique, especially when examining tendons, ligaments and nerves. As default settings, the field-of-view of the US image and the focal zone should be adjusted for the examination of small superficial parts, somewhat equal to those currently used for the examination of the wrist. Except for the insertion of the distal biceps tendon and the bicipitoradial bursa, most soft-tissue structures of the elbow are very superficial and require a high magnification scale. In the examination of the cubital tunnel, a stand-off pad or a generous amount of gel can help to improve the contact of the transducer with the skin.

In general, the US examination of the elbow should be tailored directly to the appropriate structure as indicated by the clinical findings. Focusing the US examination on a definite region of the elbow instead of a full elbow examination reduces the scanning time and improves the effectiveness of the study. Accordingly, in this chapter we have arbitrarily subdivided the elbow into a four-quadrant approach, consisting of its anterior, lateral, medial and posterior aspects. In most cases, the examination of the opposite side is neither requested nor required except for comparing the size of a pathologic structure with the healthy one. Nevertheless, this may be helpful for beginners (and especially in cases of mild lateral epicondylitis) to establish whether or not subtle changes in tendon or ligament thickness and echogenicity are real.

Dynamic examination is particularly helpful for the examination of the collateral ligaments because it can show widening of the joint during valgus and varus stress maneuvers, thus confirming the findings obtained on static scanning. Examining the cubital fossa during pronation and supination can demonstrate changes occurring in the bicipitoradial bursa. Anterior instability of the ulnar nerve can be easily evaluated on transverse US scans obtained during progressive flexion of the elbow. In nerve instability, the ulnar nerve can be seen either subluxating over the apex of the medial epicondyle or dislocating outside the tunnel. When associated with a synovial effusion, intra-articular loose bodies can be better evaluated during joint movements and application of pressure over different aspects of the joint in an effort to displace the intra-articular fluid. This can cause changes in position of the loose fragments and allows a more confident diagnosis.

8.4.1
Anterior Elbow

US examination of the anterior elbow may be performed with the patient facing the examiner with the elbow extended resting on a table (BARR and BABCOCK 1991). A slight bending of the patient's body towards the examined side makes full supination and assessment of some structures of the anterior compartment, such as the distal biceps tendon, easier. A full elbow extension can be obtained by placing a pillow under the joint. Raising the table can also be helpful and allows for a more comfortable examination for both the patient and the examiner. If the patient is unable to obtain a complete elbow extension, longitudinal scans can be difficult to perform, particularly when using large-sized probes. As an alternative in the elderly or for severely traumatized patients, the anterior aspect of the elbow can also be examined with the patient supine holding his or her arm along the body.

The main anterior structures amenable to US examination are: the brachialis muscle, the distal biceps muscle and tendon, the brachial artery, the median and radial nerve, the anterior synovial recess with the anterior fat pad and the radio-capitellar and trochlea-ulna joints. Transverse US images are first obtained by sweeping the probe from approximately 5 cm above to 5 cm below the trochlea-ulna joint, perpendicular to the humeral shaft. Cranial US images of the supracondylar region reveal the two main muscles of the anterior aspect of the distal arm: the superficial biceps muscle and the deep brachialis muscle (Fig. 8.10a). The biceps lies just deep to the subcutaneous tissue surrounded by the brachial fascia. It has a bipennate appearance with a central hyperechoic layer reflecting the aponeurosis. The brachialis muscle is located between the biceps and the humeral bony cortex and is much larger than the biceps. The brachial artery and the median nerve course alongside these muscles: the artery typically lies lateral to the nerve (Fig. 8.10b). Shifting the transducer more distally, the distal biceps tendon appears as a hyperechoic structure that overlies the brachialis muscle (Fig. 8.10b,c). A careful scanning technique is required to image this tendon. The distal biceps tendon is best examined on longitudinal planes with the patient's forearm in maximal supination to bring the tendon insertion on the radial tuberosity into view (Fig. 8.11) (MILLER
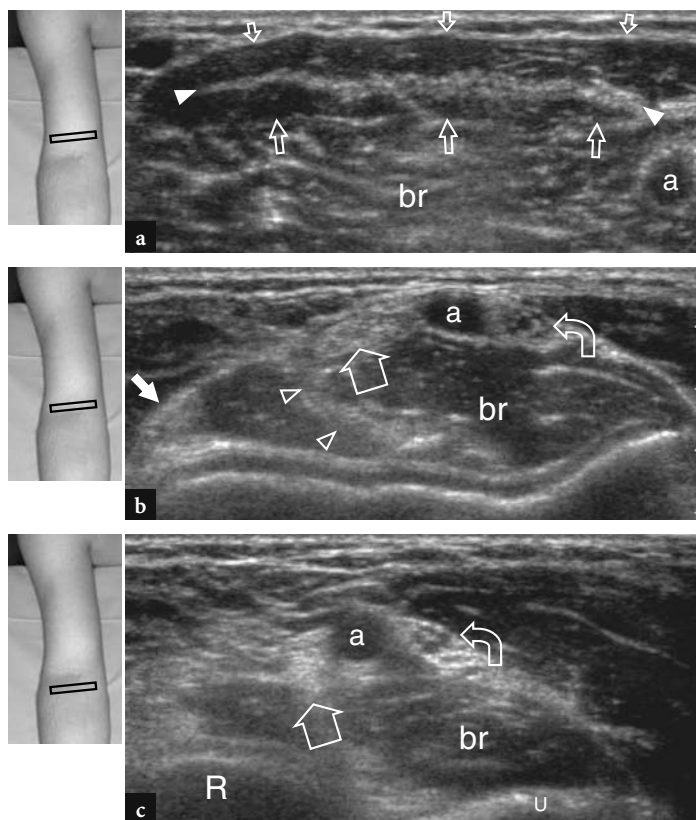

Fig. 8.10a–c. Normal distal biceps tendon. Transverse 12−5 MHz US images obtained over the anterior elbow in a healthy subject demonstrate the distal biceps tendon: **a** at the myotendinous junction, **b** at the level of the humeral trochlea and **c** below the joint line, just before its insertion. In **a**, the distal biceps tendon takes its origin from a wide echogenic aponeurosis (*arrowheads*) that is located centrally within the muscle (*arrows*). Note the brachialis muscle (*br*) that lies deep to the biceps. **a**, brachial artery. In **b** and **c**, the distal biceps tendon (*large arrow*) appears as an oval hyperechoic structure that lies superficial to the brachialis (*br*). Close to its medial side, the brachial artery (*a*) and the median nerve (*curved arrow*) are seen, whereas the radial nerve (*small arrow*) lies more laterally between the brachialis and brachioradialis muscles. Note the aponeurosis (*arrowheads*) of the brachialis *R*, radius; *u*, ulna. The inserts at the upper left side of the figures indicate probe positioning
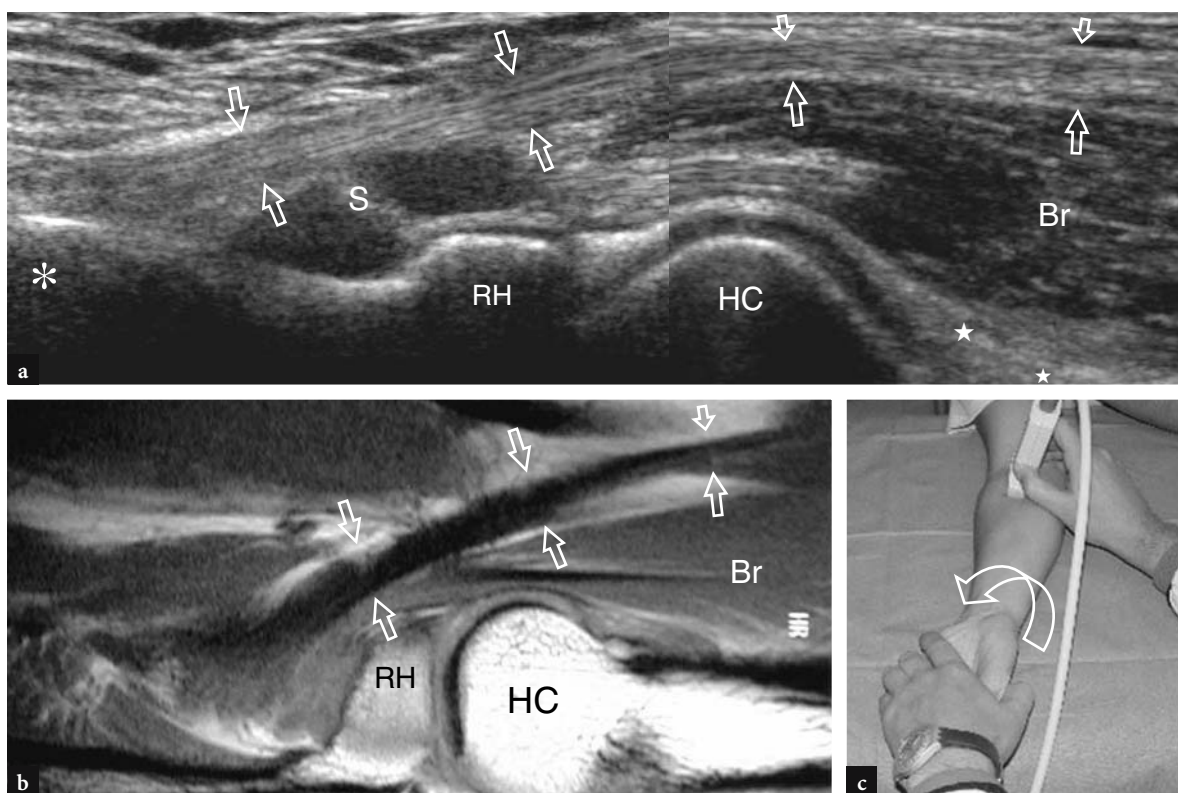
Fig. 8.11a–c. Normal distal biceps tendon. **a** Long-axis 12–5 MHz US image of the anterior elbow with **b** sagittal T1-weighted (T1w) SE MR imaging correlation shows the curved appearance of the distal biceps tendon (*arrows*) that inserts on the bicipital tuberosity (*asterisk*) of the radius. The tendon has a fibrillar appearance and courses superficial to the brachialis (*Br*) and the supinator (*S*) muscles. Observe the squared appearance of the radial head (*RH*), the rounded humeral capitellum (*HC*) covered by a band of hypoechoic cartilage and the anterior fat pad (*stars*). **c** Photograph illustrating the scanning technique to image the distal portion of the biceps tendon. The patient's forearm is kept in maximal supination (*curved arrow*) and the inferior edge of the transducer is pushed against the patient's skin.

and ADLER 2000). Because of an oblique course from surface to depth, portions of this tendon may appear artifactually hypoechoic if the probe is not maintained parallel to it (Fig. 8.12a,c). Accordingly, the distal half of the probe must be gently pushed against the patient's skin to ensure parallelism between the US beam and the distal biceps tendon, thus allowing a complete visualization of its echogenic fibrillar pattern (Fig. 8.12b,d). In thick large elbows, however, the distal portion of this tendon may be difficult to examine owing to its deep location. In general, transverse planes are less useful for examining the distal part of the biceps tendon because slight changes in transducer orientation may produce dramatic variation in tendon echogenicity and this create confusion between the tendon and the surrounding strucutres. In conditions of maximal anisotropy, the tendon and the artery may exhibit the same size and echogenic pattern on transverse scans (Fig. 8.12e,f).

As stated earlier, the median nerve courses on the internal side of the brachial artery, whereas the radial nerve can be appreciated between the brachioradialis and the brachialis muscle (Figs. 8.10b,c; 8.13). The coronoid fossa appears as a concavity of the anterior surface of the humerus filled with hyperechoic tissue related to the anterior fat pad (Fig. 8.14). The fat pad has a triangular shape with its base located anteriorly, deep to the brachialis muscle. At this level, the anterior capsule is imaged inconsistently with US (MILES and LAMONT 1989). In normal states, a small amount of fluid can be recognized between the fat pad and the humerus (Fig. 8.14). On transverse US images, the anterior aspect of the distal humeral epiphysis appears as a wavy hyperechoic line covered by a thin layer (2 mm thick) of hypoechoic articular cartilage (Fig. 8.15). Its lateral third corresponds to the humeral capitellum that shows a typical convex shape and articulates with the radial head. The medial two thirds of
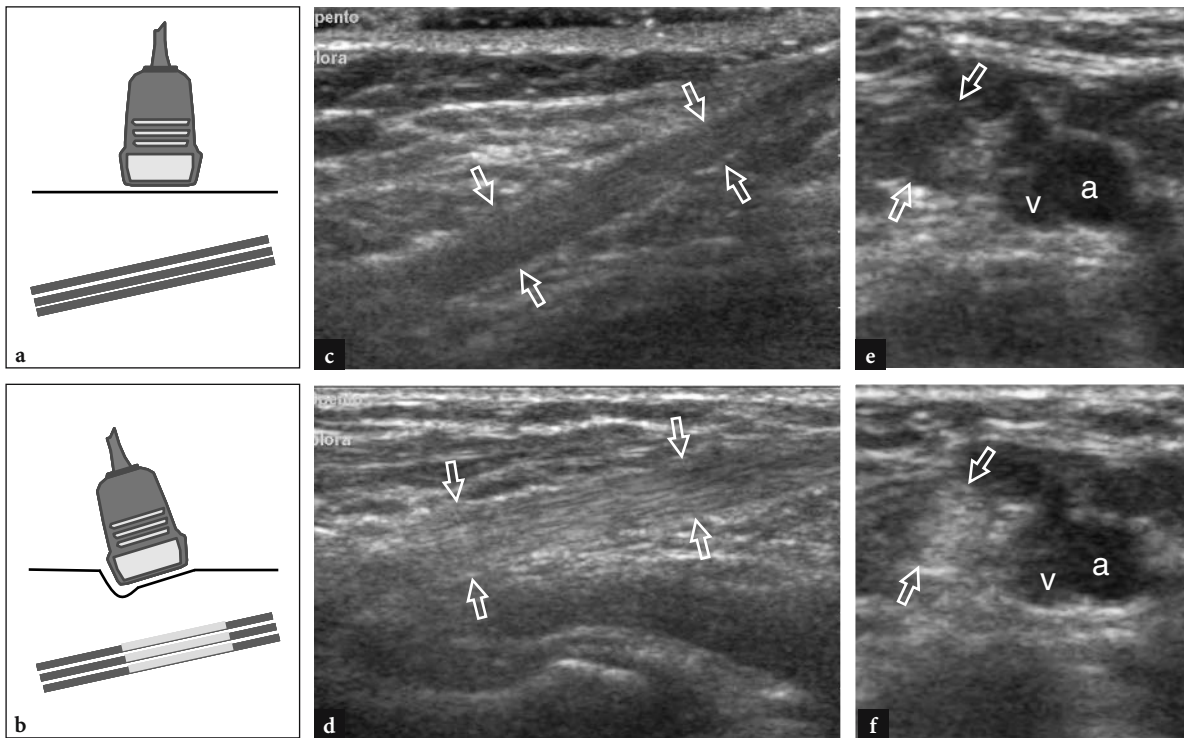
Fig. 8.12a–f. Normal distal biceps tendon and anisotropy. **a,b** Schematic drawings and **c,d** corresponding long-axis 12-5MHz US images of the biceps tendon obtained with oblique (**a,c**) or perpendicular (**b,d**) incidence of the US beam. **e,f** Respective short-axis scans. In **c** and **e**, an inadequate orientation of the US beam leads to a hypoechoic appearance of the tendon (*arrows*) relative to the surrounding fat due to anisotropy. When incorrectly imaged, the tendon can be distinguished from the adjacent brachial artery *(a)* and cubital vein *(v)* with difficulty because all look hypoechoic
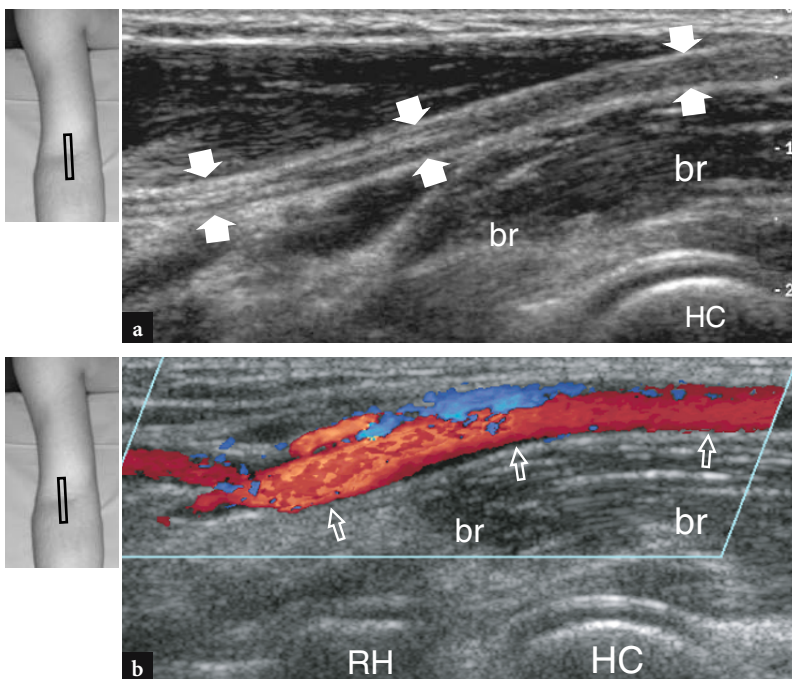

Fig. 8.13a,b. Median nerve and brachial artery. Longitudinal gray-scale (**a**) and color Doppler (**b**) 12−5 MHz US images over the antecubital fossa demonstrate the normal appearance of the median nerve (*white arrows* in **a**) and the brachial artery (*open arrows* in **b**). Both lie superficial to the brachialis muscle *(br)*. Note the humeral capitellum *(HC)* and the radial head *(RH)*. The inserts at the upper left side of the figures indicate probe positioning

Fig. 8.14a,b. Anterior joint recess. **a** Longitudinal 12−5 MHz US image at the anterior aspect of the elbow with **b** diagram correlation identifies the anterior joint recess (*arrowheads*) cranial to the hyperechoic bony surfaces of the coronoid process *(CP)* and the trochlea *(T)* and deep to the brachialis muscle *(br)*. Note the anterior fat pad *(asterisk)* as a hyperechoic tissue delimiting this recess anteriorly. The insert at the upper left side of the figure indicates probe positioning
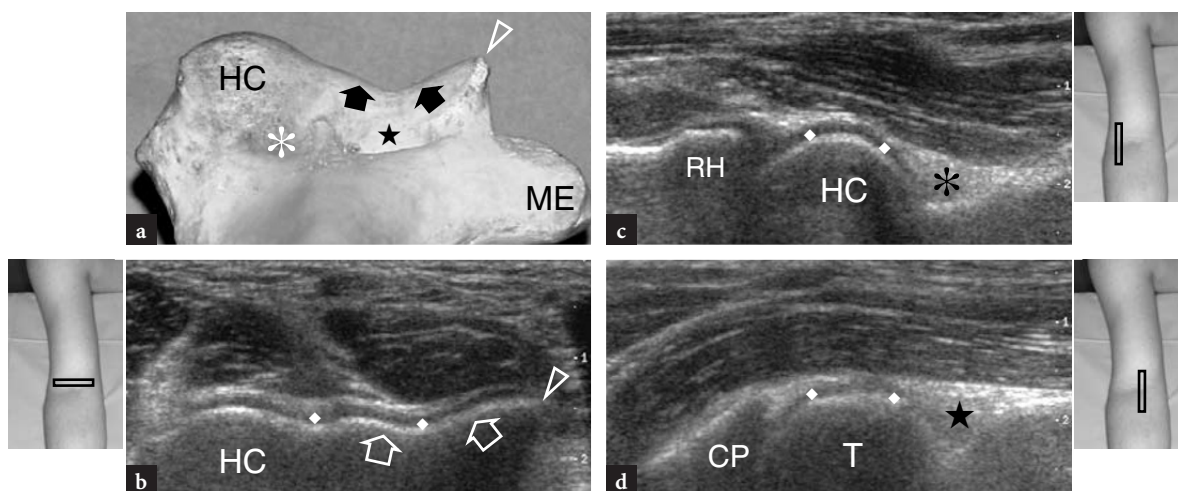

Fig. 8.15a–d. Ultrasound anatomy of bones. **a** Axial view of the anterior aspect of the distal humerus gives a projection of the capitellum *(HC)* and the trochlea *(arrows)* as being visualized with ultrasound. Observe the abrupt medial end *(arrowhead)* of the trochlea and the radial *(asterisk)* and coronoid *(star)* fossae, which lie just proximal to the articular surfaces of the humerus. *ME*, medial epicondyle. **b** Corresponding transverse 12−5 MHz US image of the anterior elbow reveals the anterior distal humerus as a wavy continuous hyperechoic line covered by a hypoechoic layer of cartilage *(rhombi)* in which the capitellum *(HC)* and the trochlea *(arrows)* can easily be distinguished. **c,d** Sagittal 12−5 MHz US images over the radial (**c**) and the coronoid (**d**) fossae show the hyperechoic anterior fat pad *(asterisk and star)* filling these depressions. Note the squared appearance of the radial head *(RH)* in **c** and the pointed shape of the coronoid process *(CP)* in **d**. *T*, trochlea. The inserts placed alongside the figures indicate probe positioning

the humeral epiphysis relate to the humeral trochlea that articulates with the ulna. The trochlea looks like a groove delimited by medial and lateral facets (Fig. 8.15a,b). In longitudinal images obtained more laterally, the radial head exhibits a squared appearance. Its articular facet is covered by a thin rim of cartilage. In mid-sagittal anterior scans, the coronoid process of the ulna appears as a prominent triangular hyperechoic structure onto which the cranial part of the brachialis tendon inserts (Fig. 8.16).

8.4.2
Medial Elbow

The medial aspect of the elbow is examined with the elbow extended, resting on a table. Then, the patient is asked to lean toward the side with the forearm in forceful external rotation (Barr and Babcock 1991). On the medial side of the elbow, there are two main structures amenable to US evaluation: the common flexor tendon and the medial collateral ligament.
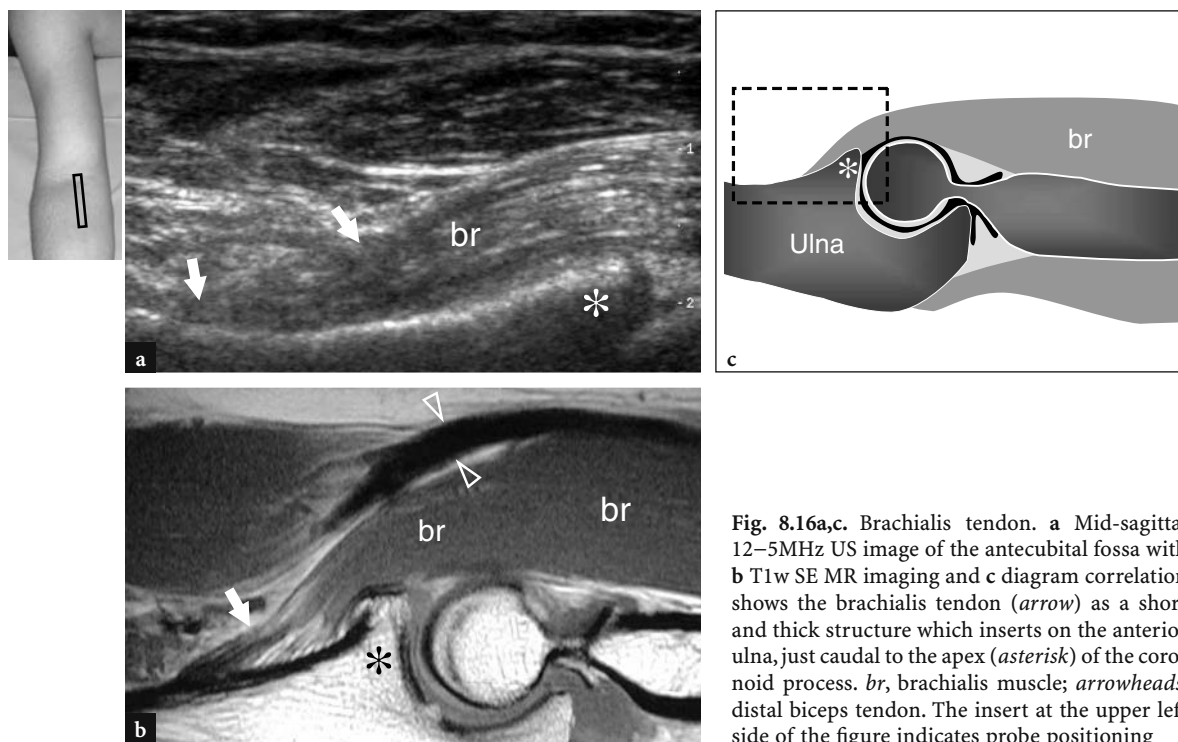
Fig. 8.16a,c. Brachialis tendon. **a** Mid-sagittal 12−5MHz US image of the antecubital fossa with **b** T1w SE MR imaging and **c** diagram correlation shows the brachialis tendon (*arrow*) as a short and thick structure which inserts on the anterior ulna, just caudal to the apex (*asterisk*) of the coronoid process. *br*, brachialis muscle; *arrowheads*, distal biceps tendon. The insert at the upper left side of the figure indicates probe positioning

The common flexor tendon is best examined in longitudinal planes. It appears shorter than the common extensor tendon origin and inserts onto the medial aspect of the epitrochlea (Fig. 8.17a). Deep to this tendon, the anterior bundle of the medial collateral ligament appears as a cord-like structure that joins the epitrochlea with the more cranial aspect of the ulna, the so-called sublimis tubercle (Fig. 8.17a,b). The proper positioning for examination of the anterior bundle of the medial collateral ligament is obtained with the patient supine keeping the shoulder abducted and externally rotated and the elbow in 90° of flexion (Ward et al. 2003). At US examination, the anterior component of the medial collateral ligament has a fibrillar pattern and a fanlike shape (Ward et al. 2003). It looks hyperechoic: however, the ligament echogenicity may vary depending on patient and probe positioning (Fig. 8.17a,b). With the patient's elbow in the extension position lying on the examination table, it usually appear hypoechoic in comparison with the overlying flexor tendon. In a recent US study with cadaveric correlation, the ligament thickness was reported to range from approximately 2.6 to 4 mm, without significant differences in sidedness, stress application or hand dominance (Ward et al. 2003). The other components of this ligament, namely the posterior and transverse bundles, are not depicted as accurately as the anterior one on US examination, even using high-resolution transducers. However, these latter portions are a less frequent source of morbidity and play a minor role in stabilizing the elbow against valgus stress.

8.4.3
Lateral Elbow

The lateral aspect of the elbow is best examined with both elbows in extension, thumbs up, palms of the hands together (Barr and Babcock 1991). When examining the radial collateral ligament and the capsule, the elbow should be extended, keeping the hand pronated. Along the lateral elbow, high-resolution US can demonstrate the common extensor tendon, the lateral ulnar collateral ligament, the radial nerve with its superficial and deep (posterior interosseous nerve) branches, and the radio-capitellar joint.

The common extensor tendon origin is best visualized in longitudinal planes as a beak-shaped hyperechoic structure located between the subcutaneous tissue and the lateral ulnar collateral ligament (Fig. 8.18). Deep to this tendon, the lateral epicondyle appears as a smooth down-sloping hyperechoic structure. The individual contributions from the extensor muscles to the common extensor tendon cannot be discriminated with US because they are
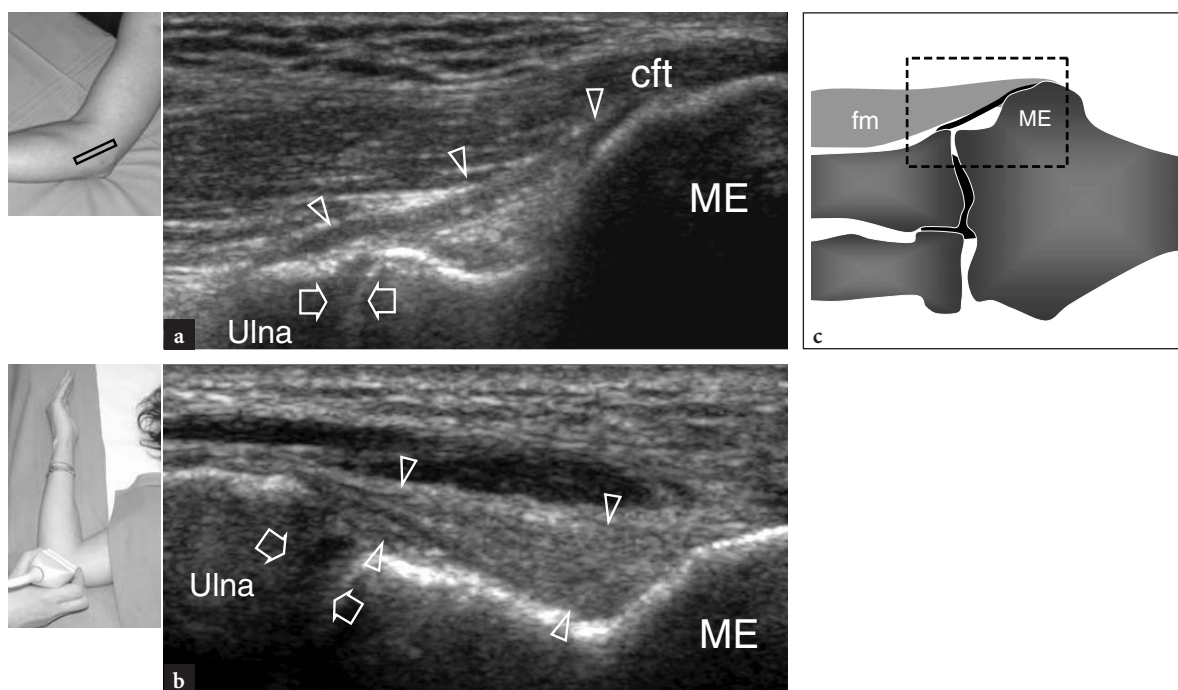
Fig. 8.17a–c. Anterior band of the medial collateral ligament. **a,b** Long-axis 12−5 MHz US images obtained with extended elbow (**a**) and at 90° of flexion (**b**) according to the positioning reported in the inserts at the upper left side of the figures, with **c** diagram correlation. The anterior band of the medial collateral ligament *(arrowheads)* is depicted as an elongated structure crossing the trochlea-ulna joint *(arrows)*. With the elbow flexed, the ligament is taut and its fibrillar pattern is better appreciated. In normal states, the ligament has a uniform thickness and echotexture. *ME,* medial epicondyle; *cft,* common flexor tendon; *fm,* flexor muscles
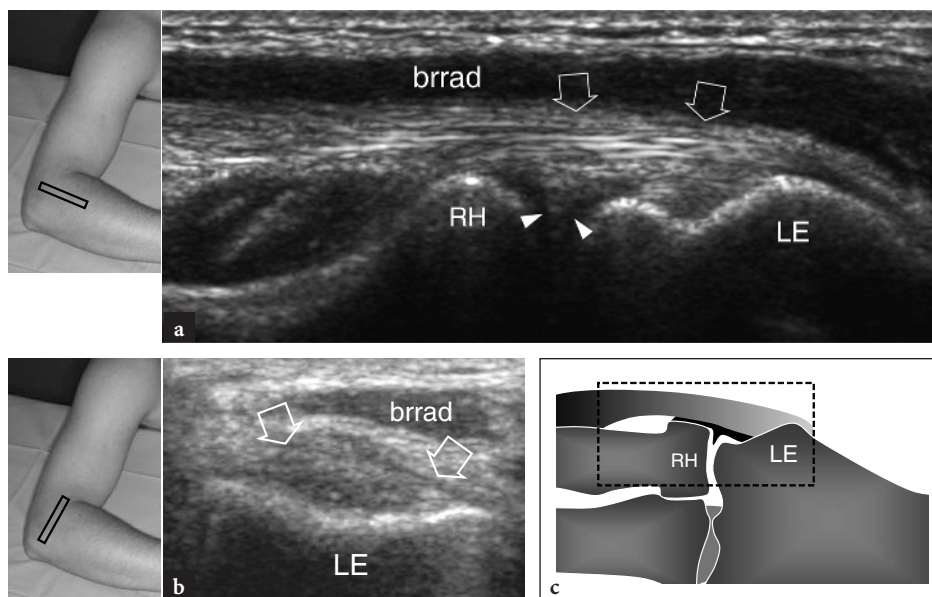

Fig. 8.18a–c. Normal common extensor tendon. **a** Long-axis 12−5 MHz US image obtained over the lateral elbow reveals a normal common extensor tendon origin *(arrows)* characterized by a uniform fibrillar pattern. The tendon is located deep to the brachioradialis muscle *(brrad)* and superficial to the radio-capitellar joint and inserts on the lateral epicondyle *(LE)*. The lateral synovial fringe *(arrowhead)* is depicted as a triangular hyperechoic structure intervening between the capitellum and the radial head *(RH)*. Note the smooth down-sloping appearance of the cortex of the lateral epicondyle and the radial head. **b** Short-axis 12−5 MHz US image over the lateral epicondyle *(LE)* demonstrates the oval cross-sectional shape of the normal common extensor origin *(arrows)*. *Brrad,* brachioradialis muscle. **c** Diagram correlation. The inserts at the upper left side of the figures indicate probe positioning

interwoven with each other. The deep tendon fibers relative to the extensor carpi radialis brevis overlie the lateral ulnar collateral ligament and cannot easily be separated from it. In fact, these structures are intimately related and, although they run in a slightly different direction, they have the same fibrillar appearance (CONNELL et al. 2001). On transverse US images, the common extensor tendon origin has an oval cross-sectional shape and is located just superficial to the lateral epicondyle. Immediately distal to the myotendinous junction, the muscular bellies of the extensor carpi radialis brevis, extensor digitorum, extensor digiti minimi and extensor carpi ulnaris usually appear as a single bulk.

Anterior to the lateral epicondyle, the main trunk of the radial nerve courses between the brachialis and the brachioradialis muscles. It is reliably examined by means of transverse US images obtained between these muscles as a small rounded structure composed of a few scattered hypoechoic dots reflecting the fascicles (Fig. 8.19a) (BODNER et al. 2002). The recurrent radial artery can be seen adjacent to the nerve and should not be confused with one of its fascicles. Color Doppler imaging may be helpful to precisely identify it. High-resolution US is able to visualize the radial nerve as it divides into the superficial cutaneous sensory branch and the posterior interosseous nerve (Fig. 8.19b,c). The fascicles in these latter nerves are very small and a meticulous scanning technique based on tracking the nerve bundle according to its short axis is needed for their visualization. At the lateral elbow, US can visualize the posterior interosseous nerve as it pierces the supinator muscle and enters the arcade
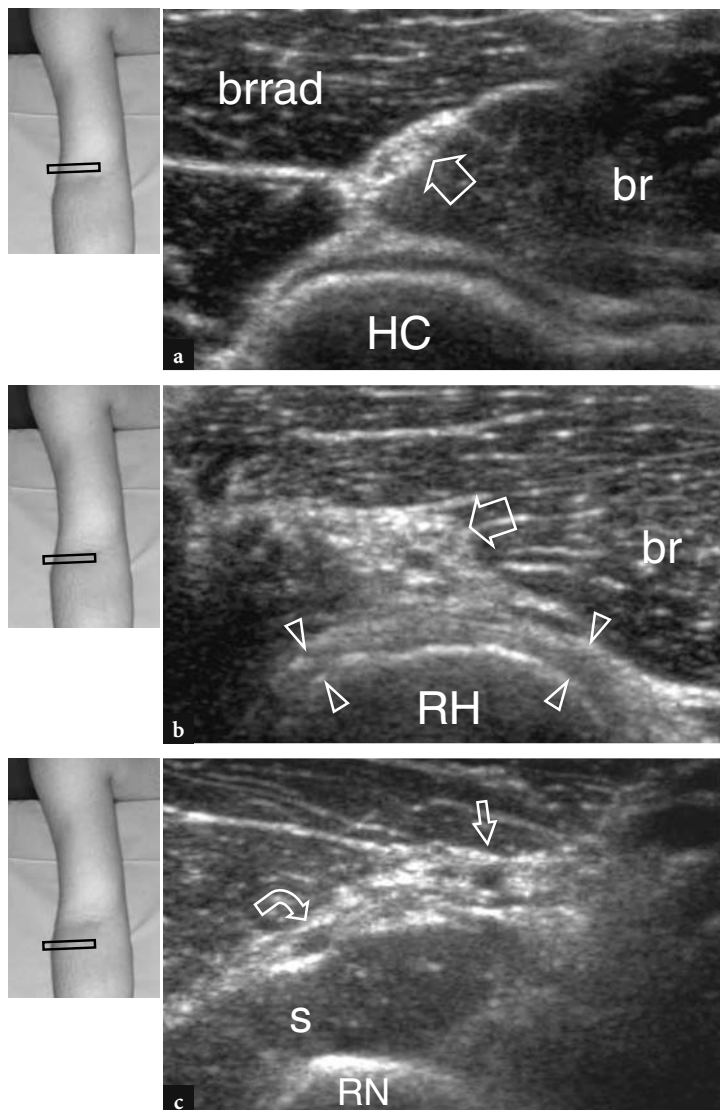

Fig. 8.19a–c. Radial nerve. Transverse 12−5 MHz US images obtained over the anterolateral elbow demonstrate the normal radial nerve and its divisional branches at the level of humeral capitellum (**a**), radial head (**b**) and radial neck (**c**). In **a**, the main trunk of the nerve (*arrow*) lies in the hyperechoic space between the brachialis *(br)* and brachioradialis *(brrad)* muscles, superficial to the humeral capitellum *(HC)*. In **b**, the radial nerve (*arrow*) passes over the radial head (RH) in close relation to the annular ligament (*arrowheads*). Typically, this ligament appears as a curved hyperechoic band that covers the radial head like a belt. In **c**, the cutaneous sensory branch (*straight arrow*) and the posterior interosseous nerve (*curved arrow*) can be appreciated over the supinator muscle *(s)* as a result of bifurcation of the main trunk of the nerve. *RN*, radial neck. The inserts at the upper left side of the figures indicate probe positioning

of Frohse, passing between the superficial and deep parts of this muscle (Fig. 8.20). Across the supinator, the nerve moves toward the posterior compartment. Accordingly, an appropriate scanning technique should include repositioning of the patient with the elbow in semiflexion, placing the forearm forward and more transversely oriented over the examination table. During pronation, the nerve may assume an angulated course at the proximal edge of the arcade of Frohse. One should not mistake this appearance for a pathologic finding. Within or just after leaving the supinator muscle, the posterior interosseous nerve can be seen further subdividing into a few subtle branches directed to the muscles of the posterior forearm. These latter branches are difficult to examine because their size approximates the spatial resolution capability of current US equipment. Once given off anterior to the lateral epicondyle, the superficial cutaneous sensory branch of the radial nerve continues into the anterior forearm. At the proximal forearm, it joins the radial artery and can be demonstrated coursing between the extensor carpi radialis longus and the brachioradialis.

The lateral aspect of the radio-capitellar joint can clearly be delineated with US (Fig. 8.18a). A triangular hyperechoic structure is usually seen filling the peripheral portion of the articular rim between the two bony surfaces. This structure corresponds to a synovial projection, somewhat similar to a meniscus (lateral synovial fringe) (Fig. 8.18a). The appearance of the radial head varies with different degrees of rotation of the forearm: in pronation, the radial head has a more squared appearance, whereas in supination it tends to assume a smoother contour. Dynamic US scanning may be helpful to assess the status of the radial head and to exclude possible occult nondisplaced fractures. Superficial to it, the annular ligament is visible as a belt-like homogeneous hyperechoic structure (Fig. 8.19b). It is best visualized by means of high-resolution transducers. With the probe placed over the radial head, passive supination and pronation movements of the forearm allow a better differentiation of the fixed annular ligament from the rotating radial head. At the radial metaphysis, the annular recess is visualized with US only if distended by fluid.

8.4.4
Posterior Elbow

The posterior aspect of the elbow may be examined by keeping the joint flexed 90° with the palm resting on the table (Barr and Babcock 1991). This posi-
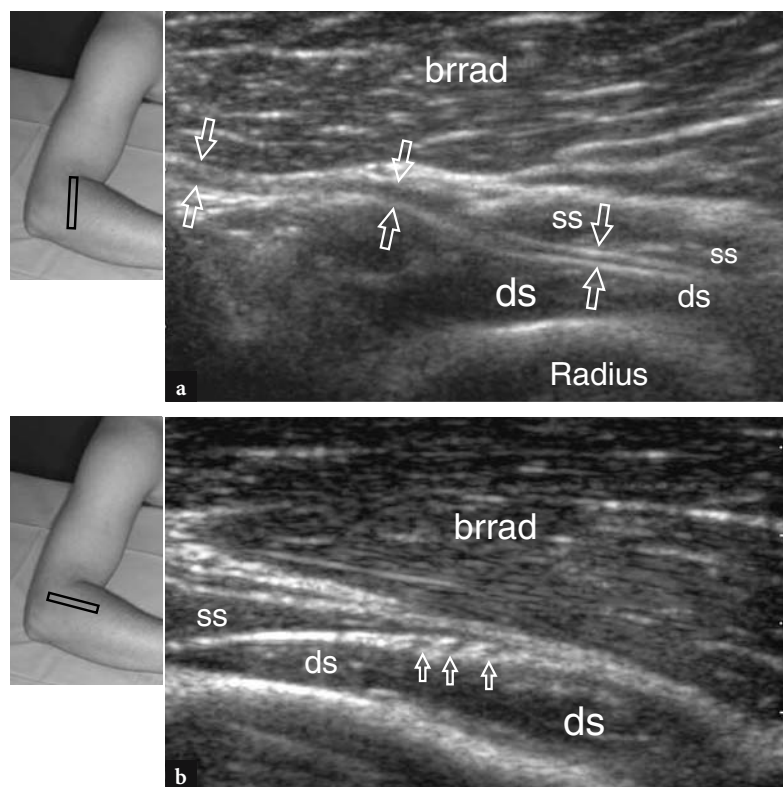

Fig.8.20a,b. Posterior interosseous nerve. **a** Long-axis and **b** short axis 12−5 MHz US images obtained at the proximal forearm over the brachioradialis muscle *(brrad)* demonstrate the normal posterior interosseous nerve as it crosses the supinator muscle. Within the bellies of the supinator *(ss,* superficial part of the supinator muscle; *ds,* deep part of the supinator muscle), the nerve appears as a thin hypoechoic structure composed of a few fascicles *(arrows)* embedded in a hyperechoic fatty plane. The inserts at the upper left side of the figures indicate probe positioning

tion allow easy demonstration of the main structures of the posterior elbow: the cubital tunnel and the ulnar nerve, the triceps muscle and tendon, the posterior fossa with the posterior fat pad and the olecranon bursa.

Cranial to the olecranon, US reveals the hypoechoic bellies of the triceps muscle and its tendon that is located eccentrically and slightly medial with respect to the midline (Fig. 8.21). The distal triceps tendon appears hyperechoic and typically exhibits striations as it fans out toward its insertion on the olecranon, a pattern somewhat similar to the quadriceps. These striations, with alternating hypo- and hyperechoic bands, are more likely due to interposition of fat between the tendon fibers and should not be misinterpreted as tendinosis or tear (Fig. 8.22). If examined in full elbow extension, the distal triceps tendon may also appear wavy, possibly mimicking a rupture. Tendon laxity is particularly evident in the elderly and represents a normal finding (ROSENBERG

et al. 1997). In addition, the preinsertional fibers of this tendon may appear hypoechoic owing to their oblique course (Fig. 8.22). Changes in orientation of the probe allow adequate correction of anisotropic effects in this area. The most distal portion of the triceps tendon should always be evaluated carefully to rule out enthesis calcifications.

The olecranon fossa appears as a wide and deep concavity of the posterior aspect of the humeral shaft filled with the hyperechoic posterior fat pad (Fig. 8.21a) (MILES and LAMONT 1989). At both sides of this fossa, the posterior aspect of the medial and lateral epicondyles can be seen on transverse images. While examining the joint at 45° flexion, intra-articular fluid tends to move from the anterior synovial space to the olecranon recess, thus making the identification of small intra-articular effusions easier. Gentle rocking motion of the patient's elbow during scanning may be helpful to shift elbow joint fluid into the olecranon recess. More distally, the
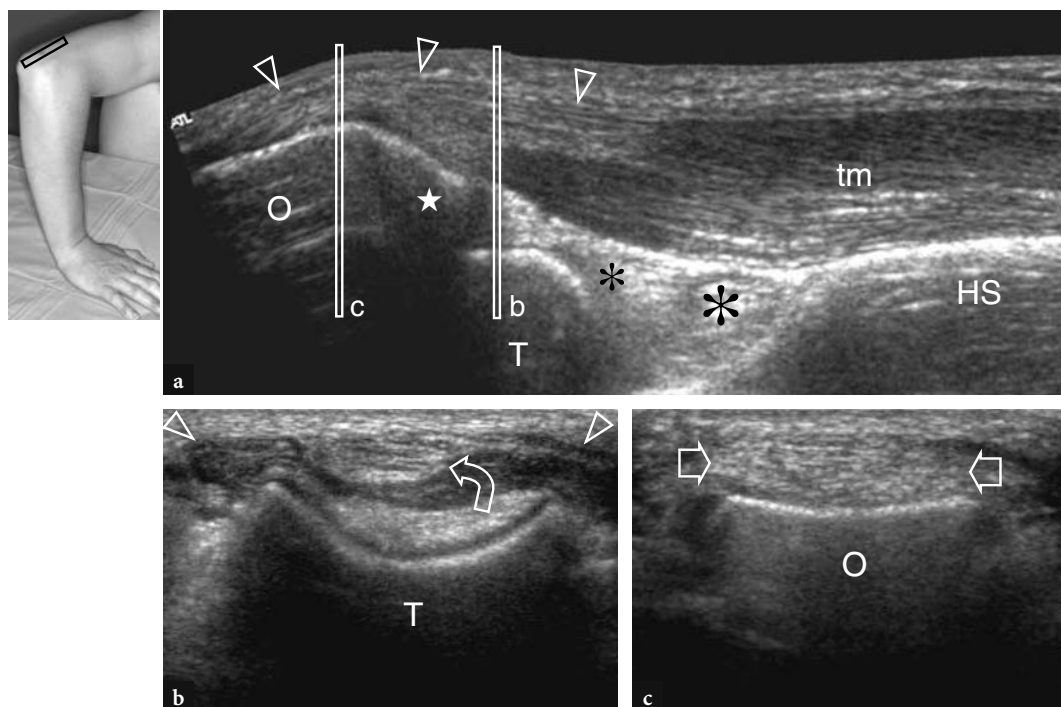

Fig. 8.21a–c. Normal distal triceps tendon and olecranon fossa. **a** Extended-field-of-view mid-sagittal 12−5 MHz US image obtained with the elbow flexed over the olecranon process *(O)* and the posterior aspect of the distal humerus. The distal triceps tendon *(arrowheads)* appears as a beak-shaped hyperechoic structure in continuity with the hypoechoic bellies of the triceps muscle *(tm)* that inserts approximately 1 cm distal to the apex *(star)* of the olecranon. Deep to the triceps, the olecranon fossa is delimited by the hyperechoic spoon-shaped contour of the humerus and the echogenic posterior fat pad *(asterisks)*. Note the posterior rounded appearance of the trochlea *(T)* and the straight profile of the humeral shaft *(HS)* just above the posterior fossa. **b,c** Transverse 12−5 MHz US images obtained at the levels *(vertical white bars)* indicated in **a**. In **b**, the cross-sectional appearance of the distal myotendinous junction of the triceps is seen over the posterior trochlea *(T)*. Observe that the tendon *(curved arrow)* arises slightly eccentrically relative to midline and the distal muscle *(arrowheads)*. In **c**, the oval cross-sectional shape of the distal triceps tendon *(arrows)* is seen lying over the olecranon *(O)*. The insert at the upper left side of the figure indicates probe positioning
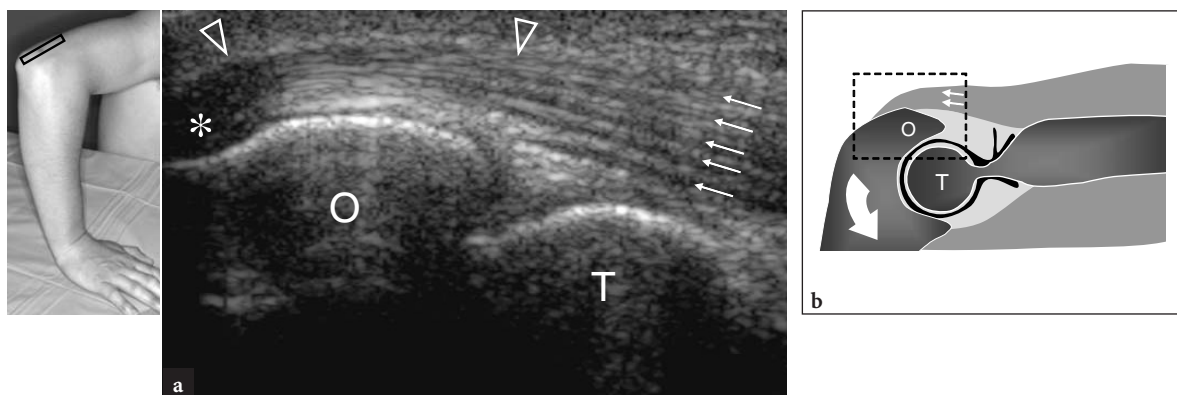
Fig. 8.22a,b. Distal triceps tendon: normal appearance mimicking disease. **a** Long-axis 12−5 MHz US image of the distal triceps tendon (*arrowheads*) with **b** diagram correlation reveals a striated intratendinous pattern composed of alternate hypo- and hyperechoic bands (*arrows*) which are related to fatty tissue strands intervening between the tendon fibers. Also, note the artifactual hypoechoic appearance (*asterisk*) of the tendon as it deflects to insert onto the olecranon process (*O*). This is due to anisotropy. *T*, trochlea. The insert at the upper left side of the figure indicates probe positioning

olecranon process is imaged as a hyperechoic curvilinear structure that is separated from the overlying skin by a thin layer of loose connective tissue containing the synovial olecranon bursa. Because of its thin walls and absence of fluid content, the normal olecranon bursa is not visible at US. Care should be taken not to apply excessive pressure with the probe when evaluating this bursa because small bursal effusions may be squeezed away.

For evaluation of the posteromedial aspect of the joint, including the cubital tunnel and the ulnar nerve, the patient's elbow should be placed in forceful external rotation to enable visualization and palpation of the medial epicondyle and olecranon (Fig. 8.7a). This can be obtained either with the patient seated and the elbow extended and hyperpronated with its dorsal aspect facing the examineror, at least for the right side, with the patient supine and the arm abducted in maximal external rotation, hanging off the table (Martinoli et al. 2000; Jacobson et al. 2001).

To examine the cubital tunnel, the probe should be placed in the transverse plane with one end over the olecranon and the other over the medial epicondyle (Jacobson et al. 2001). Similar to the situation in other sites, bony landmarks work well in routine practice to select the correct probe positioning. Because the nerve passes through a narrow space delimited by prominent bones, small transducers are superior in evaluating this region. Long-axis scans are less useful than short-axis planes for following the ulnar nerve (Fig. 8.23). Systematic scanning in short-axis planes starts at the inner side of the upper arm, where the ulnar nerve courses in a superficial position relative to the triceps. At the humeral groove, the ulnar nerve is located close to
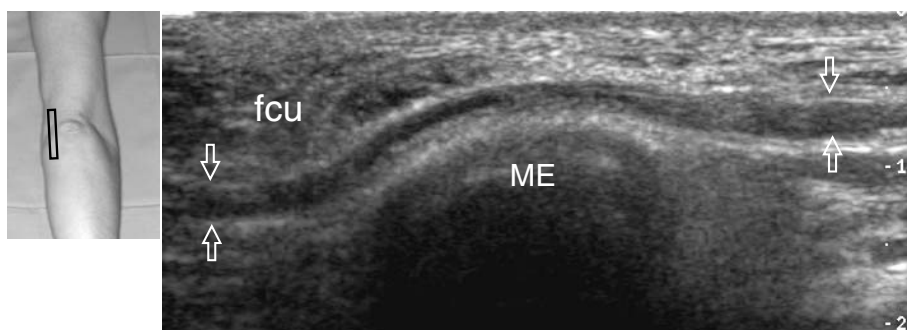

Fig. 8.23. Normal ulnar nerve. Long-axis 12−5 MHz US image of the normal ulnar nerve obtained over the cubital tunnel with extended elbow. The relationships of the nerve (*arrows*) with the medial epicondyle (ME) and the flexor carpi ulnaris muscle (*fcu*) are shown. The ulnar nerve exhibits a hypoechoic appearance and a fairly uniform thickness throughout the tunnel. The insert at the upper left side of the figure indicates probe positioning

the inside slope of the medial epicondyle. It typically appears as an ovoid structure close to the hyperechoic bony cortex of the epicondyle (Fig. 8.24a,b). In the distal portion of the tunnel, the ulnar nerve is visible between the humeral and ulnar heads of the flexor ulnaris carpi muscle (Fig. 8.24c,d). In normal states, the cross-sectional area of the ulnar nerve is slightly greater at the level of the epicondyle (6.8 mm^2) than at the distal arm (5.7 mm^2) and the proximal forearm (6.2 mm^2) (Chiou et al. 1998). One should be careful not to confuse this normal increase in nerve size inside the cubital tunnel for a sign of ulnar neuropathy. Some discrepancies exists in literature on as what the size of the ulnar nerve should be considered normal. A cross-sectional area of $\geq 7.5 \text{mm}^2$ was initially indicated as the threshold value for the cubital tunnel syndrome (Chiou et al. 1998). More recently, 7.9mm^2 has been found as the mean value for the normal ulnar nerve at the cubital tunnel level (Jacob et al. 2004). These discrepancies seem, at least in part, related to differences among races and in study design. In the cubital tunnel, the ulnar recurrent artery and veins can readily be distinguished from the adjacent nerve on color Doppler imaging. In cases of engorgement, these veins become dilated and could mimic swollen individual nerve fascicles. Doppler imaging can help to avoid this pitfall. The cubital tunnel retinaculum and the arcuate ligament consist of thin fascia and, at least in normal states, they are not visualized with US, even using very high frequency US transducers. Dynamic imaging of the cubital tunnel is performed throughout full elbow flexion to assess the position of the ulnar nerve and the medial head of the triceps muscle relative to the medial epicondyle (see Sects. 8.5.4.4, 8.5.4.5) (Fig. 8.25). For this purpose, the probe is placed in the transverse plane over the epicondyle while the patient is asked to slowly flex the elbow (Jacobson et al. 2001). During this maneuver, it should be emphasized that the application of firm pressure on the skin with the transducer must be avoided because it may prevent the dislocation of the nerve from the tunnel.

8.5
Elbow Pathology

A variety of disorders can involve the soft tissues of the elbow. Multiple conditions related to specific anatomic sites may exhibit overlapping symptoms and are easily confused clinically.
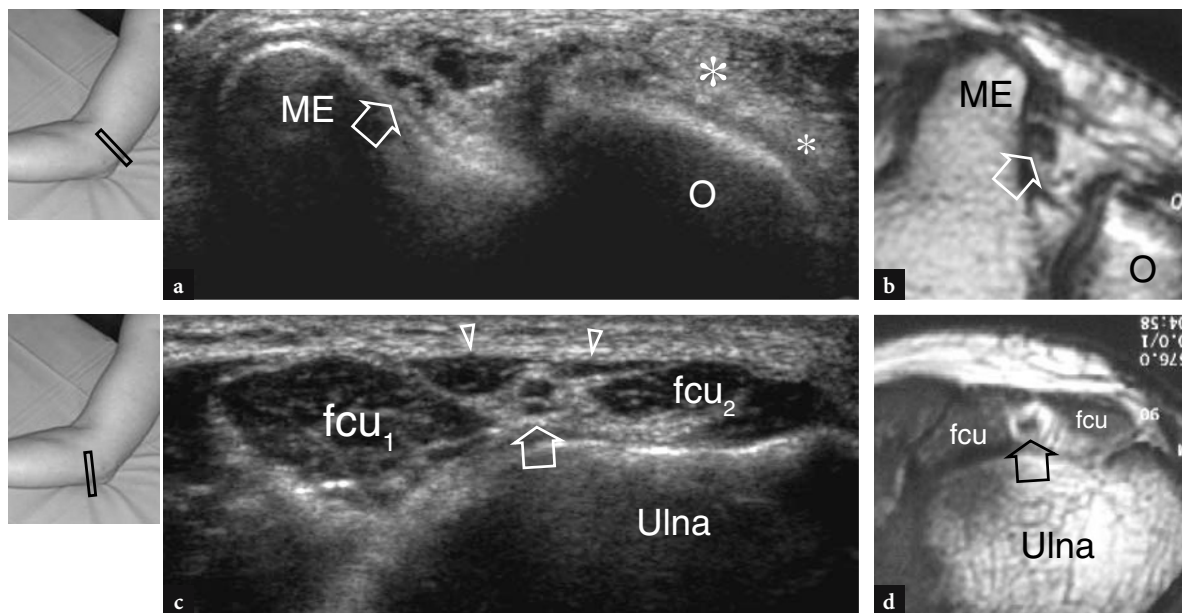

Fig. 8.24a–d. Normal cubital tunnel. **a** Transverse 12−5 MHz US image at the proximal cubital tunnel level (condylar groove) with **b** T1w SE MR imaging correlation show the normal relationship of the ulnar nerve (*arrow*) with the medial epicondyle *(ME)*. Observe the distal triceps tendon (*asterisks*) over the olecranon *(O)*. **c** Transverse 12−5 MHz US image at the distal cubital tunnel level (proper cubital tunnel) with **d** T1w SE MR imaging correlation demonstrates the nerve (*arrow*) beneath the arcuate ligament (*arrowheads*) that joins the humeral *(fcu₁)* and ulnar *(fcu₂)* heads of the flexor carpi ulnaris muscle. The inserts at the upper left side of the figures indicate probe positioning
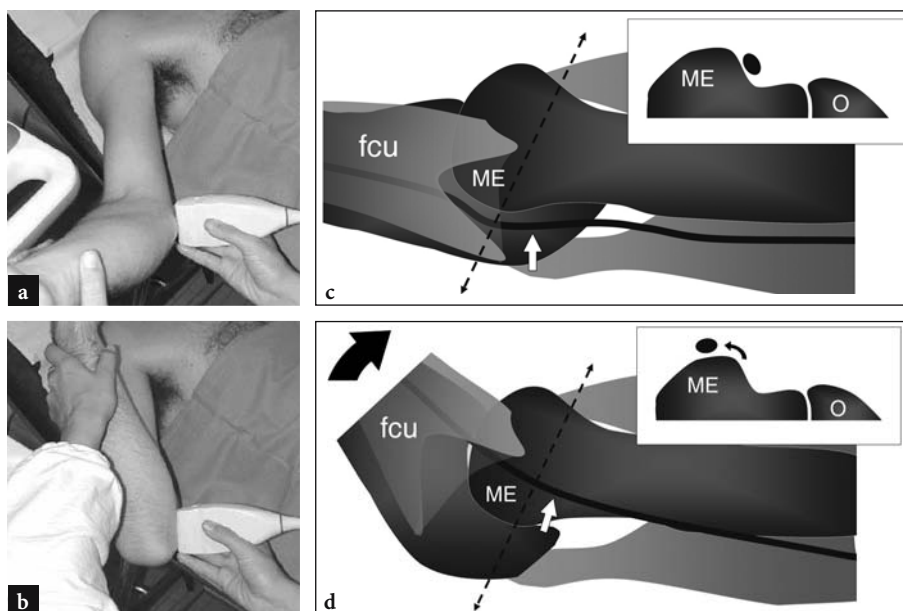
Fig. 8.25a–d. a,b Photographs illustrating the scanning technique to assess the position of the right ulnar nerve relative to the medial epicondyle with elbow extension (**a**) and during progressive degrees of elbow flexion (**b**). Note that the probe remains stabilized on transverse plane between the medial epicondyle and the olecranon during full elbow motion. **c,d** Schematic drawings of the medial elbow examined in **c** extension and **d** flexion illustrate the mechanism of ulnar nerve instability at the cubital tunnel. Note the absence of the Osborne retinaculum (see for comparison Fig. 8.7c). When the elbow is extended, the ulnar nerve (*white arrow*) is contained within the tunnel. Elbow flexion (*black arrow*) dislocates the ulnar nerve anteriorly to the medial epicondyle (*ME*). *fcu*, flexor carpi ulnaris muscle. Dashed line, appropriate probe positioning during scanning

8.5.1
Anterior Elbow Pathology

8.5.1.1
Distal Biceps Tendon Tear

One of the most common causes of acute anterior elbow pain is rupture of the distal biceps tendon. These tears account for less than 5% of all biceps tendon lesions, proximal injuries being far more common (AGINS et al. 1988). They typically occur after 40 years of age (mean 55 years) in manual laborers who attempt to lift a heavy object (or in weightlifters and body builders) or during vigorous eccentric contraction of the biceps against resistance. Distal biceps tendon tears may occur with either avulsion of the tendon by the radial tuberosity (more commonly) or midsubstance tear or injury at its myotendinous junction. Similar to other tendons, there is a relatively hypovascular zone within the distal biceps tendon, approximately 10 mm from its insertion on the radial tuberosity (SEILER et al. 1995). Repetitive impingement of this zone between the radius and the ulna during pronation movements seems to be a predisposing factor to start the degenerative process in the tendon sub-

stance (SEILER et al. 1995). In most cases, the rupture of the distal biceps tendon is associated with tearing of the lacertus fibrosus, but this latter structure may also remain intact. Clinically, a complete tendon tear presents with pain and a palpable defect with a proximal lump in the anterior aspect of the arm related to the retracted muscle (Fig. 8.26). Although weakened, elbow flexion is preserved due to the strong action of the brachialis muscle; on the contrary, supination of the forearm is more severely compromised because of the limited strength of the small supinator muscle. In most cases, the clinical diagnosis is straightforward and does not require an additional imaging study. Nevertheless, occult ruptures are more common than once thought and, in daily practice, they are becoming increasingly diagnosed with US even some time after the trauma. A delayed clinical diagnosis occurs mainly in the absence of significant muscle retraction because of an intact lacertus fibrosus, or when the retracted muscle is hidden from palpation with surrounding edema and hemorrhage.

An early diagnosis of distal biceps tendon rupture is important because surgical outcome is improved in patients treated in the first weeks after trauma before the occurrence of tendon adhesions, degenera-

Fig. 8.26a,b. Distal biceps tendon tear: physical findings. Photographs of two different patients who underwent **a** subacute and **b** chronic complete rupture of the distal biceps tendon. In **a**, the patient injured his left tendon while attempting to lift a heavy object. He presented with hemorrhagic skin over the medial elbow and proximal forearm and with a proximal lump (*arrowheads*) in the anterior aspect of the arm related to the retracted muscle. In **b**, the patient was a competitive body-builder who refused surgical repair of the ruptured tendon. Note the defect (*arrowhead*) in the anterior left arm due to the retracted muscle in comparison with the right side

tive changes and fatty muscle infiltration. The main US features of a complete tear of the distal biceps tendon include nonvisualization of the distal tendon, which appears proximally retracted (up to more than 10 cm from the radial tuberosity), and detection of hypoechoic fluid in the tendinous bed related to hematoma (Fig. 8.27) (Lozano and Alonso 1995; Miller and Adler 2000). The effusion is best recognized around the tendon stump (Fig. 8.28). With high-resolution transducers, US is not sensitive enough to can depict the normal lacertus fibrosus as a very thin fibrillar band over the pronator teres. The status of the lacertus fibrosus is, however, not a critical issue as it is not routinely involved in surgical repair of a torn distal biceps tendon. In addition, there is no evidence that the degree of tendon retraction is in itself predictive of the status of the lacertus fibrosus (Fig. 8.29) (Miller and Adler 2000). In case of its rupture, however, US can recognize perifascial fluid around the anterior and lateral aspects of the flexor-pronator group of muscles and a more striking tendon retraction (Fig. 8.29b).

The less common tendinitis and partial tears of the distal biceps tendon present with localized pain and tenderness over the antecubital fossa. These conditions usually follow repetitive microtrauma or forceful biceps activation. Pain can be exacerbated during resisted elbow flexion or supination of the hand and is worsened by direct palpation of the tendon. At US, partial tears appear as hypoechoic thickening or thinning of the tendon and as contour irregularities or waviness without tendon discontinuity (Fig. 8.30) (Miller and Adler 2000). The assessment of these tears may be difficult with US due to anisotropy related to the oblique course of the tendon and to its deep position. The US appearance of biceps tendinitis is very similar to that of partial tears and the diagnostic accuracy of US for differentiating these conditions relies on availability of a high-quality transducer as well as on the overall experience of the examiner. In doubtful cases, MR imaging is an accurate means to confirm the diagnosis of partial tears (Falchook et al. 1994).

Surgical treatment in complete tendon tears includes repair and reattachment of the retracted tendon to the radial tuberosity or, alternatively, to the brachialis muscle or the ulnar tuberosity. The first technique gives better results in restoring supination but has a significantly higher risk of radial nerve injury. After surgery, the tendon appears thickened and hypoechoic with internal linear hyperechoic images related to sutures (Fig. 8.31).

8.5.1.2
Bicipitoradial (Cubital) Bursitis

The distal biceps tendon is not invested by a synovial sheath but it is covered by a paratenon. Just proximal to the tendon insertion, it is in contact with the bicipitoradial (cubital) bursa. This bursa is located between the
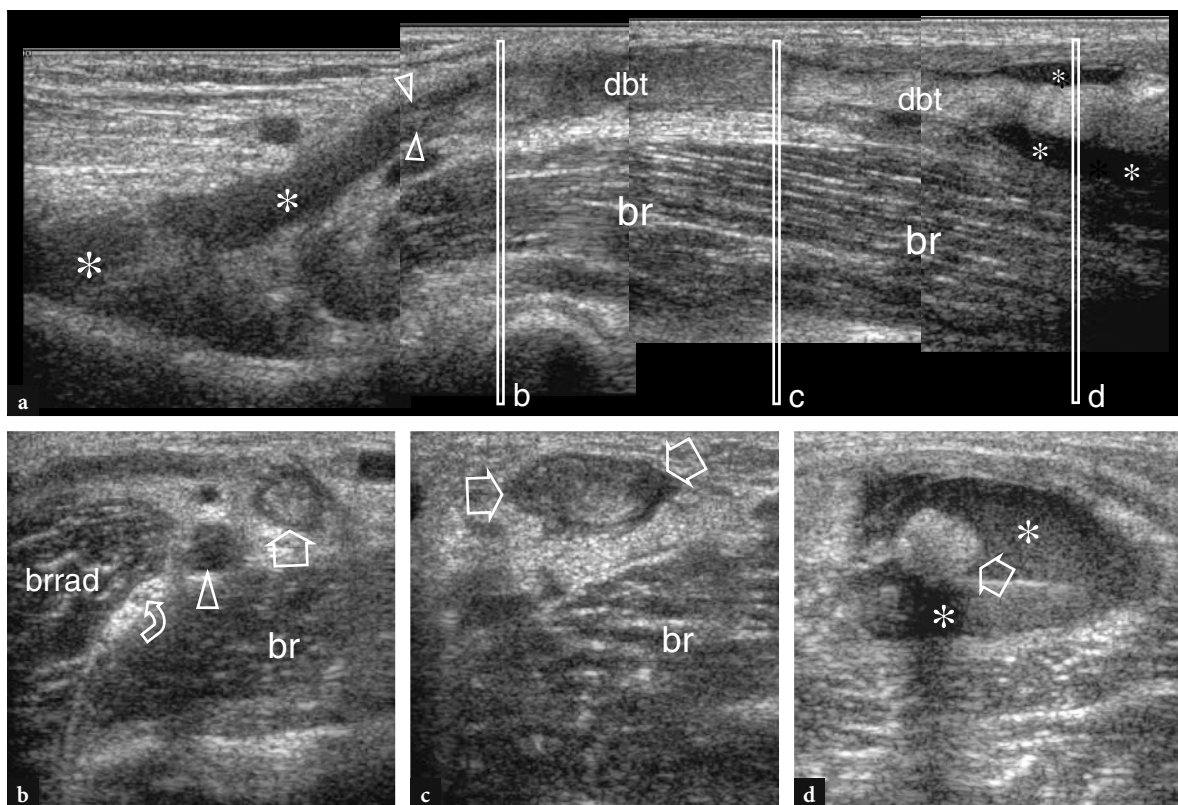
Fig. 8.27a–d. Complete rupture of the distal biceps tendon. **a** Long-axis 12−5 MHz US image over the brachialis muscle *(br)* shows hypoechoic fluid *(asterisks)* filling the distal bed of the retracted distal biceps tendon *(dbt)* and surrounding its myotendinous junction. In this particular case, the tendon edge *(arrowheads)* lies distal to the joint line. **b–d** Short-axis 12−5 MHz US images obtained at the levels *(vertical white bars)* indicated in a demonstrate the torn and retracted tendon end *(straight arrows)* surrounded by hypoechoic hematoma *(asterisks)*. The relationships of the torn tendon with the brachial artery *(arrowhead)*, radial nerve *(curved arrow)*, brachialis *(br)* and brachioradialis *(brrad)* muscles are shown
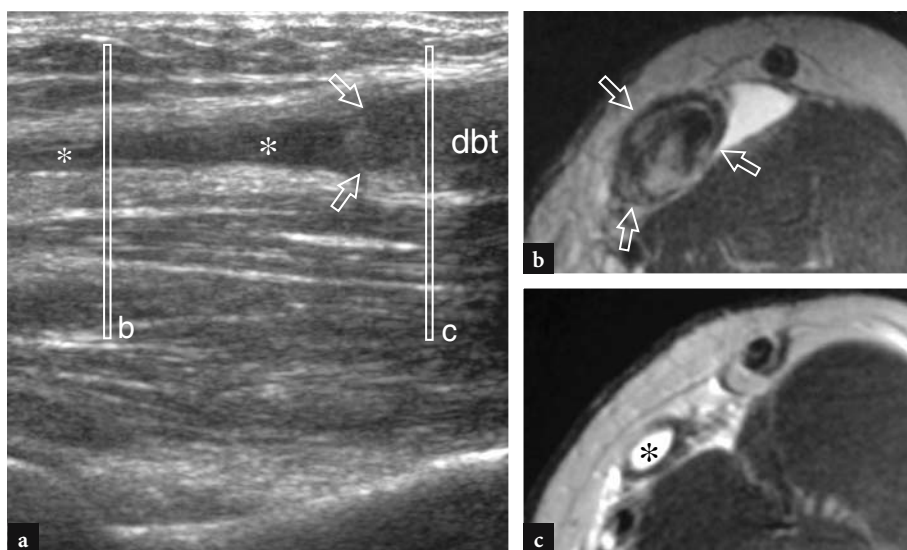
Fig. 8.28a–c. Complete rupture of the distal biceps tendon. **a** Long-axis 12−5 MHz US image obtained proximal to the elbow joint with **b,c** correlative transverse T2w SE MR images acquired at the levels *(vertical white bars)* indicated in a show the retracted edge *(arrows)* of the distal biceps tendon *(dbt)* with hypoechoic fluid *(asterisks)* filling the gap
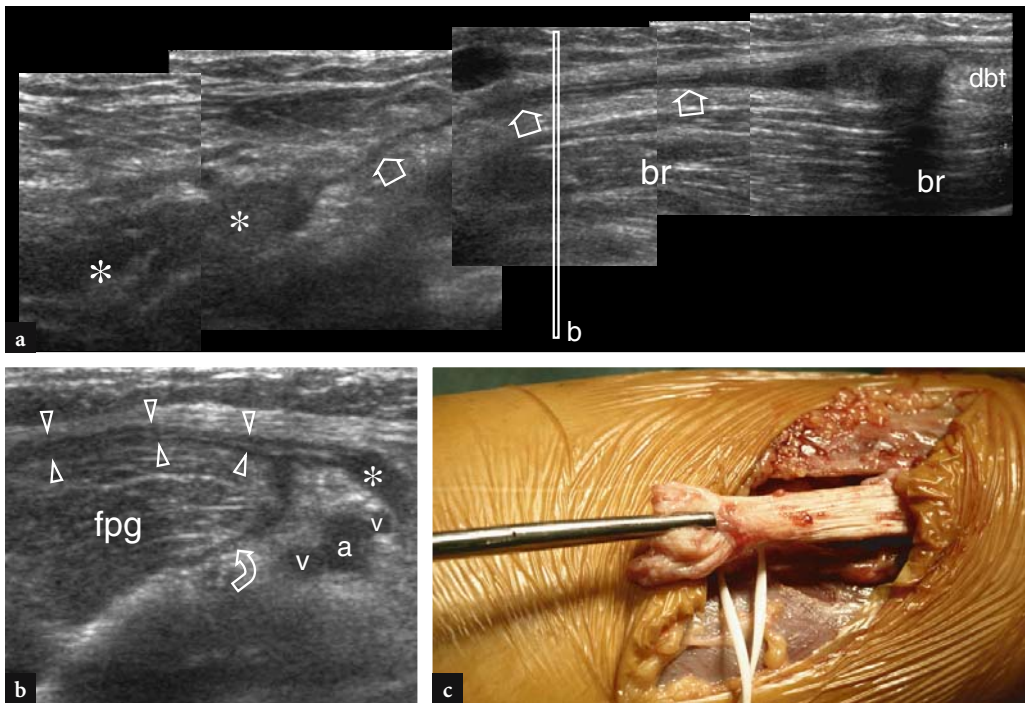
Fig. 8.29a–c. Acute complete rupture of the distal biceps tendon associated with a torn bicipital aponeurosis. **a** Long-axis 12−5 MHz US image over the brachialis muscle (*br*) demonstrates a markedly retracted tendon edge (*dbt*), the hematoma at the rupture site (*asterisks*) and the absence of the tendon (*arrows*). **b** Short axis 12−5 MHz US image obtained at the level (*vertical white bar*) indicated in a reveals fluid (*arrowheads* and *curved arrow*) in the soft tissues surrounding the flexor-pronator group (*fpg*) of muscles, suggestive of a coincident injury of the lacertus fibrosus. In this case, the injury of the bicipital aponeurosis was surgically confirmed. *a*, brachial artery; *v*, cubital veins. **c** Gross operative view of the same case
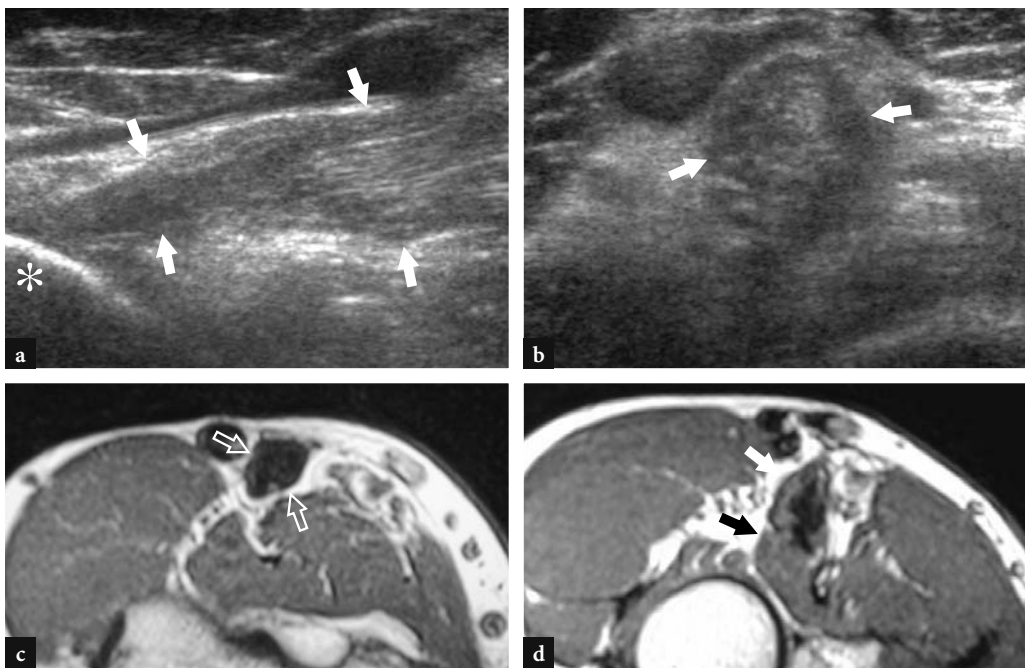
Fig. 8.30a–d. Partial rupture of the distal biceps tendon. **a** Long-axis and **b** short-axis 12−5 MHz US images obtained at level distal to the elbow joint with **c, d** correlative transverse T1w SE MR images demonstrate a thickened and heterogeneous tendon (*arrows*) inserting on the radial tuberosity (*asterisk*)
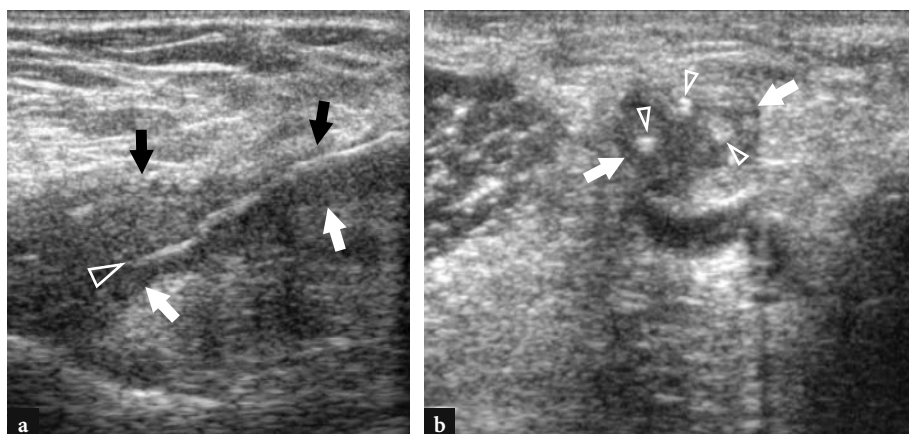
Fig. 8.31a,b. Postoperative distal biceps tendon. After surgical repair, **a** long-axis and **b** short-axis 12−5 MHz US images reveal a thickened and wavy distal biceps tendon (*arrows*). Adhesions and irregularities in the peritendinous tissues are also seen. Observe the sutures, which appear as bright echoes (*arrowheads*) within the tendon substance

distal biceps tendon and the radial tuberosity to reduce friction during pronation of the forearm (Skaf et al. 1999). Bicipitoradial bursitis is a rare condition that may result from several causes (infection, inflammatory arthropathy, amyloidosis, etc.) but it is most commonly secondary to repetitive mechanical trauma as well as to tendinosis and tearing of the distal biceps. On clinical grounds, swelling of the bicipitoradial bursa can be appreciated as a nonspecific mass in the antecubital fossa often associated with antecubital pain, especially upon elbow motion and forearm rotation. Because the clinical picture of bursitis is similar to tendinitis and the deep location of the bursa makes it difficult to palpate, a definite diagnosis of cubital bursitis relies mainly on imaging findings.

When the bicipitoradial bursa is only mildly distended, US may have difficulty in distinguishing it from the adjacent distal biceps tendon that appears hypoechoic due to anisotropy (Miller and Adler 2000). Usually, transverse scans with the forearm supinated perform better in delineating the bursal shape.

At US, bicipitoradial bursitis appears as a hypoechoic mass located in proximity to the distal biceps tendon (Liessi et al. 1996). It may have septa, thick walls and echogenic content. Rice bodies have been described in this bursa with US (Spence et al. 1998). When distended by a large amount of fluid, the bicipitoradial bursa can surround the distal portion of the distal biceps tendon completely, thus mimicking a tenosynovitis (Fig. 8.32). Bicipitoradial bursitis must be differentiated from synovial and ganglion cysts and other soft-tissue masses. Ganglia commonly arise from the anterior capsule and may expand at a variable distance from the joint, dissecting the soft tissues of the forearm (Steiner et al. 1996). Visualization of a pedicle that connects the cyst with the elbow joint cavity may help the diagnosis. Calcified bursitis may be encountered in patients with renal osteodystrophy (Fig. 8.33). For asymptomatic bursitis no treatment is necessary, whereas most symptomatic patients are successfully treated with rest, physiotherapy and anti-inflammatory drugs.
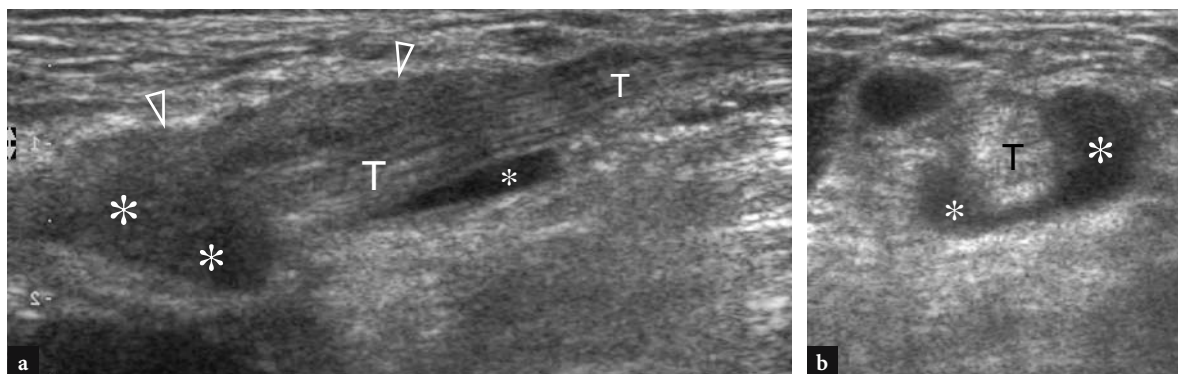

Fig. 8.32a,b. Bicipitoradial bursitis. **a** Longitudinal and **b** transverse 12−5 MHz US images over the antecubital fossa at level distal to the joint line show fluid distension of the bicipitoradial bursa (*asterisks*) which almost completely surrounds the adjacent normal distal biceps tendon *(T)*, thus mimicking a tenosynovitis process
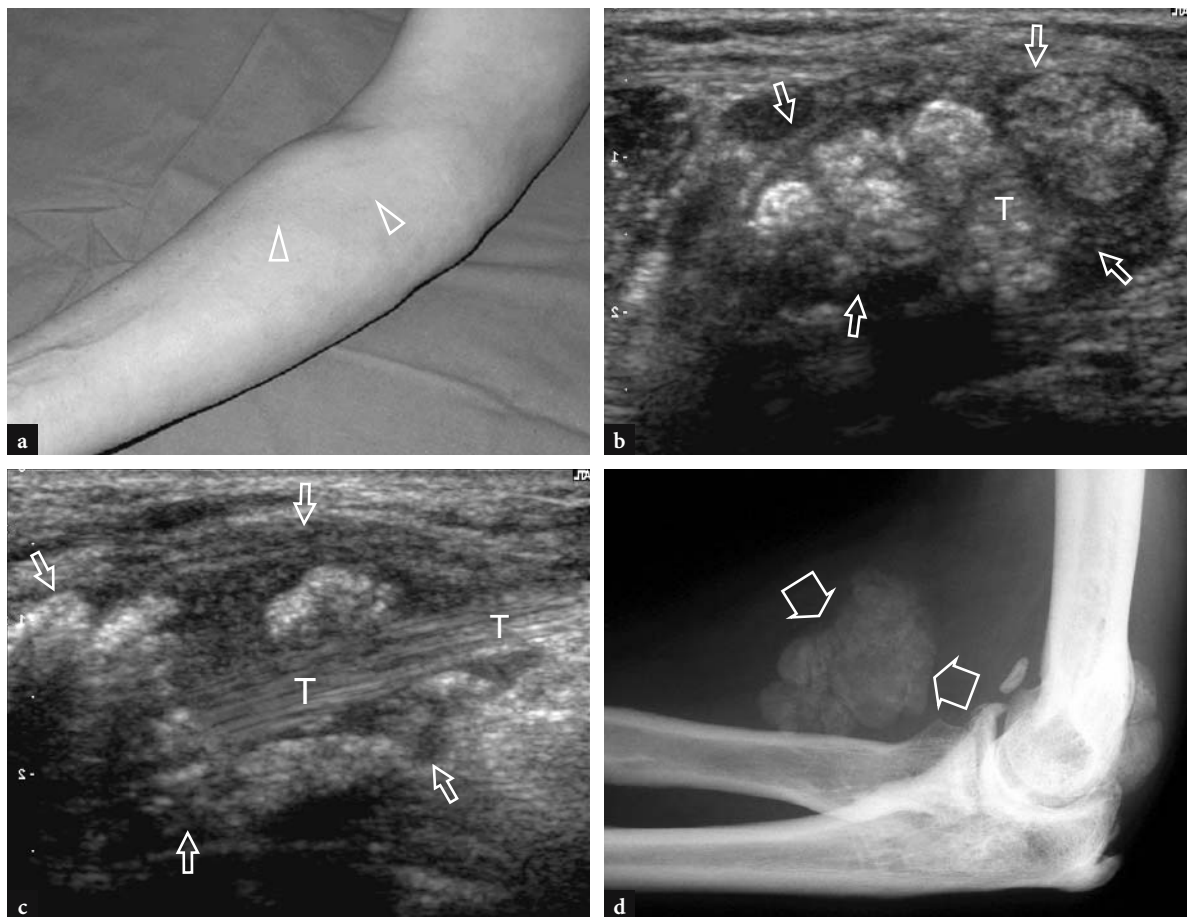
Fig. 8.33a–d. Calcified bicipitoradial bursitis in a woman with chronic renal failure who presented with a palpable mass in the antecubital fossa and difficulties in pronation. **a** Photograph shows focal soft-tissue swelling (*arrowheads*) over the anterior proximal forearm. **b** Transverse and **c** longitudinal 12−5 MHz US images reveal extensive hyperechoic deposits (*arrows*) with faint posterior acoustic shadowing related to calcifications with the bicipitoradial bursa. The bursa exhibits thickened walls and the distal portion of the biceps tendon (*T*) is completely surrounded by calcifications. **d** Correlative lateral radiograph shows the bulk of calcifications (*arrows*) in the antecubital fossa

8.5.2
Medial Elbow Pathology

8.5.2.1
Medial Epicondylitis (Epitrochleitis)

Medial epicondylitis, commonly referred to as "golfer's elbow", "medial tennis elbow" or "pitcher's elbow", occurs far less commonly than lateral epicondylitis and usually presents with pain and tenderness over the anterior aspect of the medial epicondyle that is enhanced by grasping and by resisted pronation of the forearm. Some sporting activities requiring repetitive valgus stress to the elbow joint, such as golf, javelin throwing and squash, may predispose to this condition. Medial epicondylitis is produced by degeneration and tearing of the common flexor tendon relative to overuse of the flexor-pronator group of muscles. Enthesopathy is frequently observed instead of tendinopathy. In this condition, joint effusion is absent and the elbow retains a full range of movements. The US appearance of medial epicondylitis is similar to the appearance of the other degenerative tendinopathies that involve the attachment of tendons to bone and includes hypoechoic changes in the tendon substance secondary to tendinosis or to partial-thickness tears (Fig. 8.34) (FERRARA and MARCELIS 1997). Complete tear of the common flexor tendon is rare. In this clinical setting, US can help to distinguish tendinopathy from a lesion of the underlying medial collateral ligament. Ulnar neuropathy may be associated with tendinosis of the common flexor tendon.
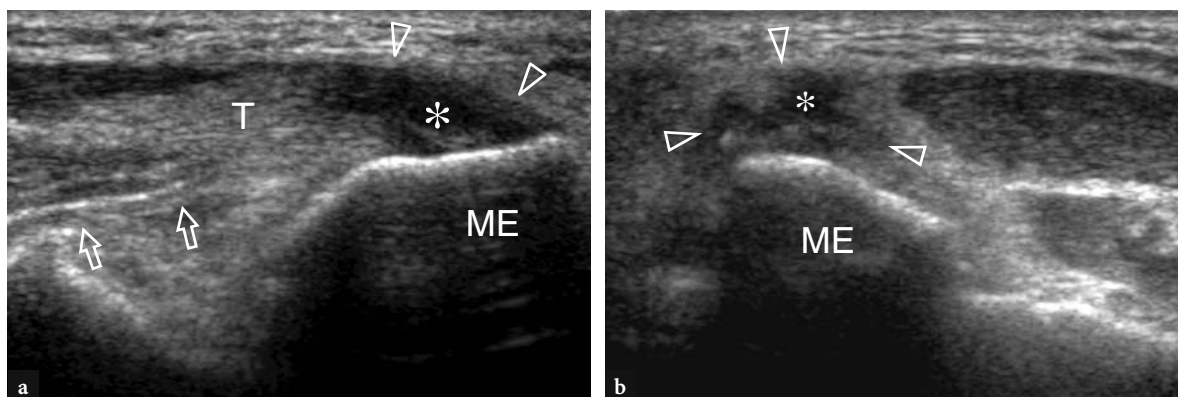
Fig. 8.34a,b. Medial epicondylitis. **a** Longitudinal and **b** transverse 12−5 MHz US images at the medial elbow in a golf player with chronic elbow pain reveal a swollen common flexor tendon (*arrowheads*) with a full-thickness hypoechoic area (*asterisk*) compatible with severe tendinosis. A normal-appearing medial collateral ligament (*arrows*) underlies the abnormal tendon origin. *ME*, medial epicondyle; *T*, proximal portion of the common flexor tendon

8.5.2.2
Medial Collateral Ligament Injury

The medial collateral ligament is stronger than the lateral collateral ligament. Its degeneration and tearing with or without an injury of the adjacent common flexor tendon may be secondary to acute or chronically repeated overstretching in valgus stress during the acceleration phases of throwing or may result from a fall or from posterior dislocation of the elbow (see Sect. 8.5.5.4). Baseball pitching is the sporting activity most commonly associated with medial collateral ligament injuries and medial joint instability. When the anterior band is injured, high-resolution US reveals a thickened hypoechoic ligament with surrounding effusion slightly posterior and deep to the medial epicondyle (Vanderschueren et al. 1998; Jacobson and van Holsbeeck 1998; Ward et al. 2003). Calcifications can also be associated with ligamentous tears (Nazarian et al. 2003). In cases of complete rupture, US examination may show either a gap or focal hypoechoic areas in the proximal and distal portion of the ligament (Fig. 8.35) (de Smet et al. 2002). To improve the diagnostic confidence, high-frequency US examination can provide dynamic assessment of the degree of medial joint laxity in both neutral and valgus stressed positions (de Smet et al. 2002). In a series of asymptomatic baseball pitchers, the medial elbow joint space of the throwing arm was significantly wider during valgus stressing than the joint space in the elbow of the nonthrowing arm (Nazarian et al. 2003). In symptomatic patients, widening of the trochlea-ulna joint and soft tissue falling into the distracted joint space suggest a medial collateral ligament injury

(de Smet et al. 2002). Dynamic US scanning may be particularly useful in the event of partial-thickness tears, in which the ligament is continuous but lax (Fig. 8.9). Examination of the noninjured elbow should be obtained to compare the amount of joint widening that occurs during valgus stressing.

8.5.2.3
Epitrochlear Lymphadenopathies

Just proximal to the elbow and adjacent to the medial epicondyle and the medial neurovascular bundle, small lymph nodes may enlarge as a result of reactive or septic inflammation (Barr and Kirks 1993). One of the leading causes of medial epitrochlear regional
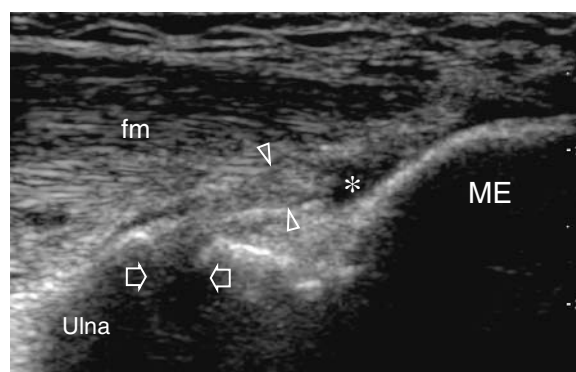

Fig. 8.35. Medial collateral ligament injury. Longitudinal 12−5 MHz US image obtained with valgus stress over the anterior band of the medial collateral ligament (*arrowheads*) shows a focal hypoechoic area in the proximal ligament and mild widening of the elbow joint (*arrows*) compatible with a ligamentous injury. *ME*, medial epicondyle; *fm*, flexor muscles

lymphadenopathy is "cat-scratch" disease, an infection caused by a gram-negative bacterium, *Bartonella henselae*, usually transmitted by scratches of the hand by an animal (most patients have a history of exposure to a cat!). However, enlarged lymph nodes in the epitrochlear area may also be involved by other disorders, including benign and malignant forms. US reveals the appearance of reactive lymph nodes consisting of oval hypoechoic masses with an echogenic hilum, often hypervascular at color Doppler imaging (Fig. 8.36). This appearance is typical and works well to rule out other soft-tissue masses, such as neurogenic tumors or sarcomas. The US examination should be extended up to the axillary region in order to rule out the possible coexistence of axillary lymphadenopathies. In cat-scratch disease, lymphadenopathies may be multiple and contiguous. Clinically, they are accompanied by painful soft-tissue swelling and systemic symptoms, such as fever and malaise. The involved nodes have a hypervascular pattern at color and power Doppler imaging and tend to develop central necrosis and liquefaction (Carcía et al. 2000; Gielen et al. 2003). Hyperechoic infiltration of the perinodal fat due to cellulitis is a characteristic finding (Fig. 8.37a). Enlarged lymph nodes most often regress over weeks to months. Whatever the cause of epitrochlear lymphadenopathies, US may exclude a local soft-tissue mass, thus obviating the need for biopsy or resection of this pseudotumor (Gielen et al. 2003). With time from the acute process, and especially in the elderly, the reactive nodes may undergo diffuse, massive adipose infiltration leading to a broad and hyperechoic medulla and progressive atrophy of the outer cortex (Fig. 8.37b). In these cases, the examiner should be careful not to mistake these atrophic nodes for lipomas or other hyperechoic soft-tissue masses. Detection of a thin continuous hypoechoic rim related to the atrophic cortex of the node may help the diagnosis (Fig. 8.37b).

8.5.3
Lateral Elbow Pathology

8.5.3.1
Lateral Epicondylitis

The most common disorder involving the lateral elbow is lateral epicondylitis, also known as "tennis elbow", caused by repetitive traction on the osteotendinous attachment of the common extensor tendon (Regan et al. 1992). This condition can be the result of
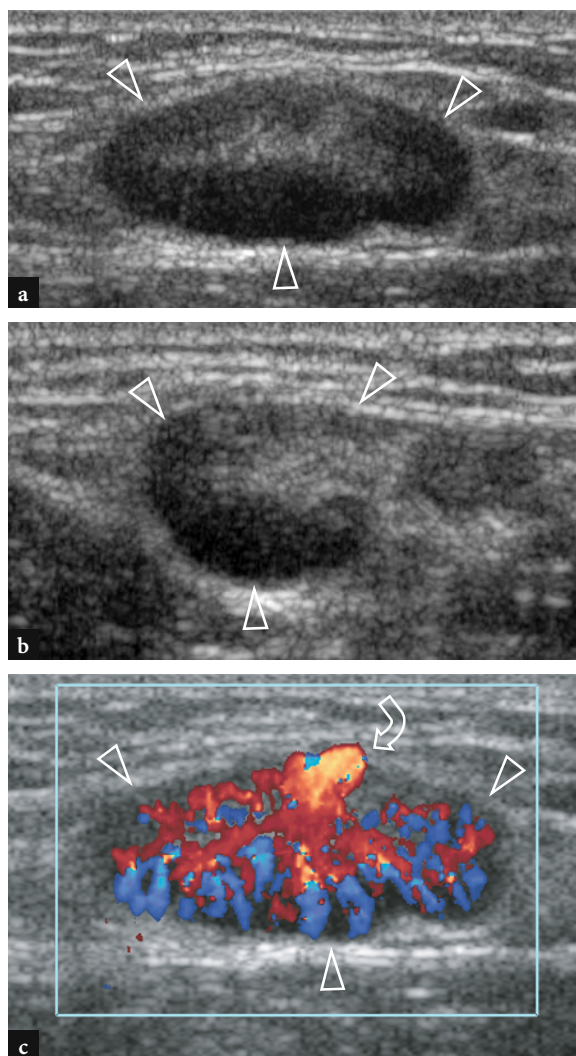
Fig. 8.36a–c. Epitrochlear lymphadenopathy. **a** Long-axis and **b** short-axis 12−5 MHz US images over the medial elbow in a patient with a painful palpable mass associated with the medial epicondyle. US identifies an oval hypoechoic mass with echogenic hilum consistent with a superficial lymph node (*arrowheads*). **c** Color Doppler imaging reveals a hypervascular pattern of the node with a vessel pedicle (*arrow*) that enters the hilum and branches through the hypoechoic cortex. This lymph node regressed 2 weeks after medical treatment

chronic microtrauma secondary to repetitive overuse related to professional or recreational activities leading to progressive degeneration and/or partial tears of the common extensor tendon (tendinopathy) or to damage to the bone insertion (enthesopathy). The extensor carpi radialis brevis is the more commonly affected component of the common extensor tendon. Although lateral epicondylitis typically occurs in tennis players who injure this tendon–especially during the backhand stroke, in which the extensors
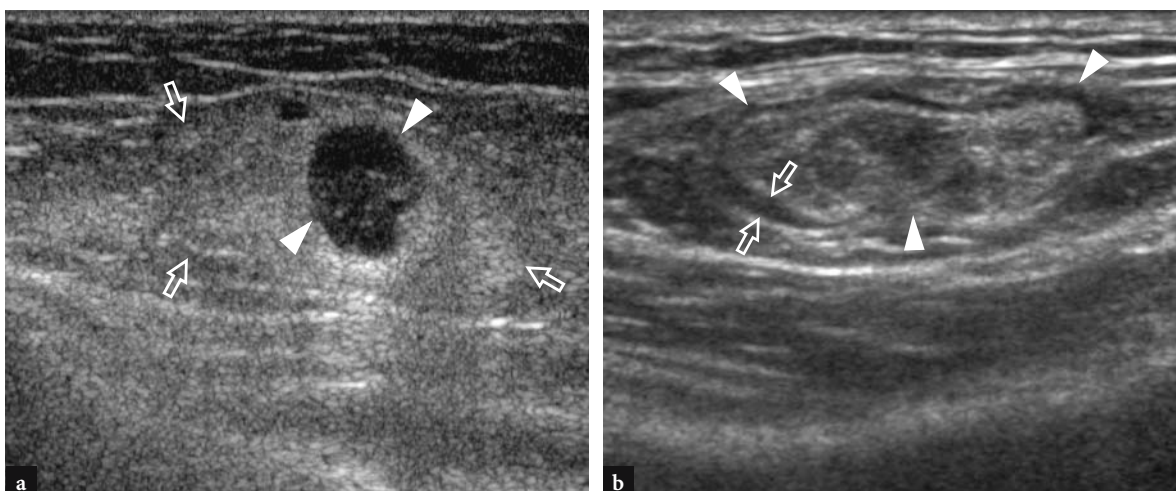
Fig. 8.37a,b. Epitrochlear lymphadenopathies in two different individuals with **a** active cat-scratch disease and **b** without any signs of infectious or inflammatory abnormalities. In **a**, the inflamed node is completely hypoechoic (*arrowheads*) with loss of definition of the echogenic hilum and appears surrounded by abnormally hyperechoic fat (*arrows*) due to perinodal cellulitis. In **b**, massive adipose infiltration has occurred in an epitrochlear lymph node (*arrowheads*) leading to a broad hyperechoic medulla. The cortical portion is markedly reduced in thickness and appears as a thin peripheral hypoechoic rim (*arrows*)

are subjected to a greater tensioning–this condition is seen far more commonly in nonathletes. In tendinopathy, patients report a localized pain over the common extensor tendon during or just after repetitive muscle activation, whereas in enthesopathy, pain is confined to the tendon's insertional area. Physical examination reveals localized tenderness over the lateral aspect of the elbow radiating down to the proximal forearm or well localized over the lateral aspect of the epicondyle respectively. Intra-articular effusion is not an associated finding. In chronic longstanding disease, pain at rest and limitation in joint extension can be noted.

The diagnosis is usually based on clinical findings and does not require imaging studies. US may be useful to confirm the clinical diagnosis in doubtful or refractory cases, to reveal the extent and severity of the disease and to monitor the response to therapy. The main US features of lateral epicondylitis are pre-insertional hypoechoic swelling of the tendon with focal or diffuse areas of decreased reflectivity in the tendon substance and loss of the fibrillary pattern related to tendinosis, fluid adjacent to the common tendon and ill-defined tendon margins (Figs. 8.38, 8.39) (MAFFULLI et al. 1990; CONNELL et al. 2001; MILLER et al. 2002d; LEVIN et al. 2005). In a recent series, the mean size of the focal hypoechoic areas was 8.7 mm (range 3–15 mm) (CONNELL et al. 2001). Although early tendon abnormalities may be confined to the superficial fibers (Fig. 8.38a,b), involvement of the deep fibers of the extensor carpi radialis brevis component is more common and may even extend down to the joint capsule (Fig. 8.38c,d). Similarly, the anterolateral and mid-portion of the common extensor tendon is more commonly involved, whereas the posterior portion usually remains unaffected (Fig. 8.38b) (CONNELL et al. 2001). In high-grade tendinosis, the angiofibroblastic infiltration based on migration of fibroblasts and vascular granulation tissue within the tendon substance causes a striking hypervascular pattern of the intratendinous hypoechoic areas at color and power Doppler imaging (Fig. 8.39b). Spurring at the common extensor tendon insertion and cortical irregularities at the anterolateral surface of the lateral epicondyle may also be recognized, although bony changes do not correlate with disease activity. Intratendinous calcifications may also be seen as part of crystal deposition diseases (Fig. 8.40). In partial tears, the common extensor tendon may appear thinned compared with the opposite side. In practice, discrimination of focal areas of tendinosis and partial tears can be difficult and US is reliable for recognizing a partial tear only when discrete anechoic cleavage planes with no fibers intact are visible in the tendon substance (CONNELL et al. 2001). These tears typically appear as longitudinal splits oriented from the bony insertion distally (Fig. 8.41). Thickening of peritendinous soft tissues and a thin layer of superficial fluid over the extensor tendon are also more often observed with partial tears. In complete tears, US identifies a fluid-filled gap separating the tendon from its bony attachment site (Fig. 8.42) (JACOBSON and VAN HOLSBEECK 1998; CONNELL et al. 2001). Overall, US
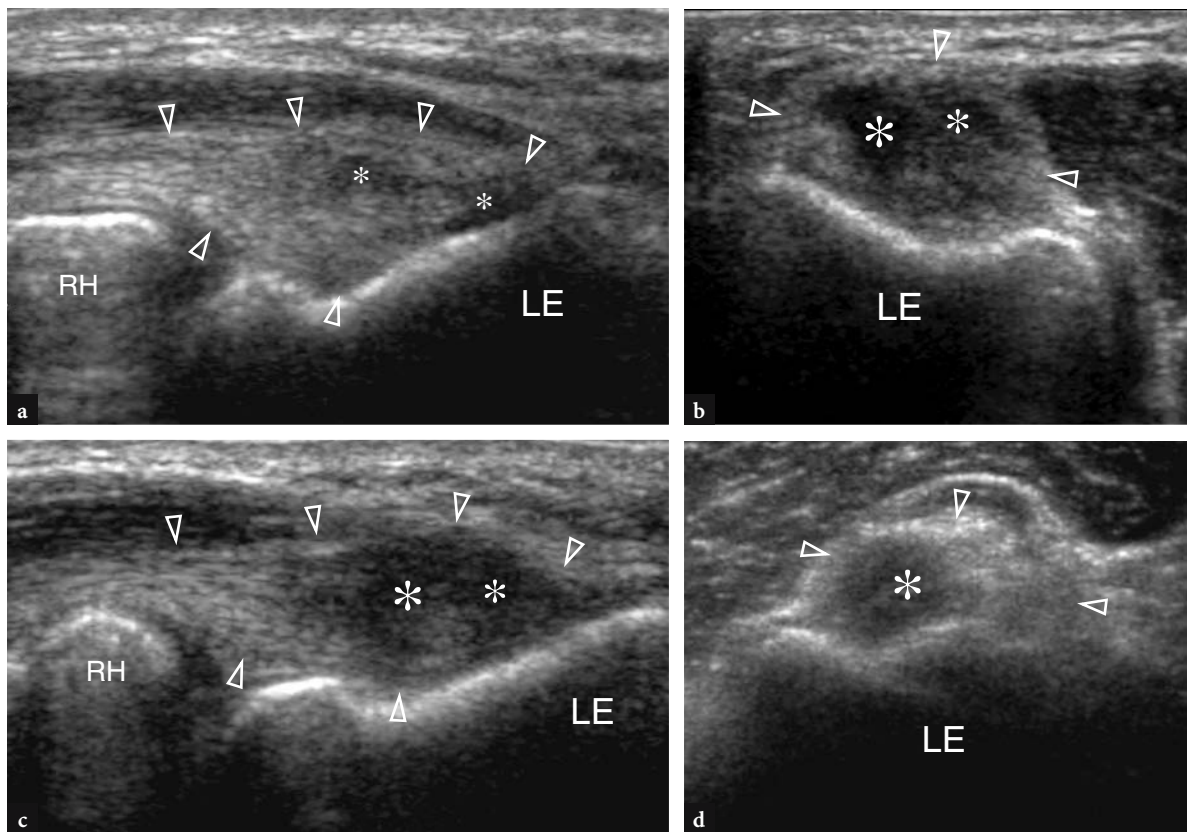
Fig. 8.38a–d. Lateral epicondylitis: spectrum of US appearances in a weightlifter with bilateral lateral elbow pain. **a** Long-axis and **b** short-axis 12−5 MHz US images over the right common extensor tendon origin reveal a hypoechoic focus (*asterisks*) of tendinosis in the superficial fibers of an otherwise normal-appearing tendon (*arrowheads*). **c** Long-axis and **d** short-axis 12−5 MHz US images over the left common extensor tendon origin demonstrate a large hypoechoic area (*asterisks*) affecting both superficial and deep fibers of the tendon (*arrowheads*), indicating severe tendinopathy. On cross-section, the abnormal hypoechoic areas with loss of fibrillary echotexture (*asterisks*) are seen involving the full thickness of the anterior half of the tendon (*arrowheads*). In both elbows, observe the integrity of the deepest fibers in relation to the lateral collateral ligament. *LE*, lateral epicondyle; *RH*, radial head

has proved to be as specific but not as sensitive as MR imaging for evaluating epicondylitis (MILLER et al. 2002). On the other hand, US of the common extensor tendon has high sensitivity but low specificity in the detection of symptomatic cases (Levin et al. 2005).

Conservative treatment with rest, anti-inflammatory drugs, physiotherapy and local steroid injections gives satisfactory results in most cases of lateral epicondylitis. Surgical intervention with excision of the degenerated tissue, resection of the common extensor tendon and debridement of the extensor tendon origin with release of the annular ligament may be advocated in refractory cases. Confirmation of the disease and exclusion of other causes of lateral elbow pain which may mimic or accompany lateral epicondylitis, such as posterior interosseous nerve entrapment or lateral collateral ligament inju-

ries, should, however, be ascertained with imaging modalities, and possibly with US, before submitting the patient to surgery.

8.5.3.2
Lateral Collateral Ligament Injury

In lateral epicondylitis, the lateral elbow ligamentous complex, and especially the lateral ulnar collateral ligament, should be routinely assessed because this ligament is commonly injured in association with tears of the common extensor tendon as a result of the same forces or overuse mechanisms on adjacent structures (BREDELLA et al. 1999). An unsuspected tear of this ligament may be the cause of conservative therapy failure in patient with lateral epicon-
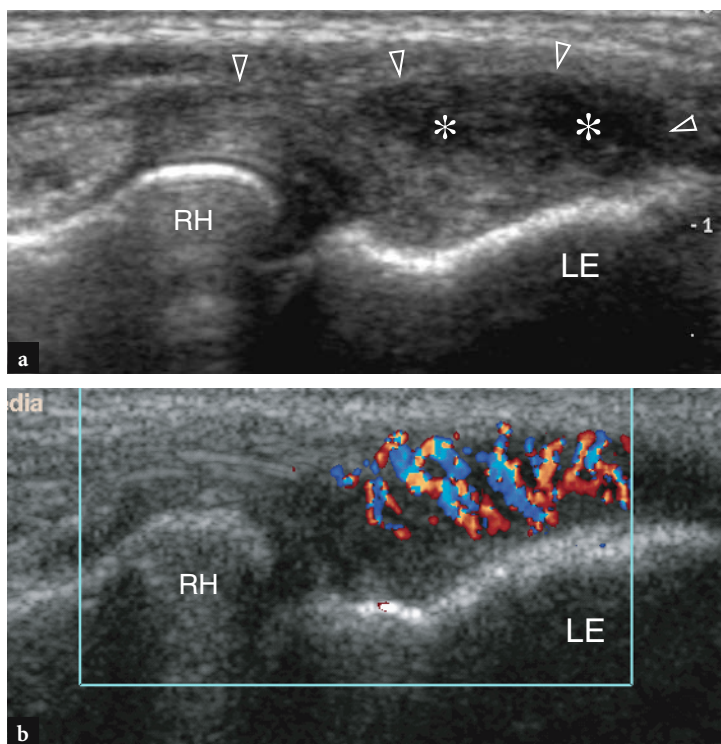
Fig. 8.39a,b. Lateral epicondylitis in a professional tennis player with a history of chronic right lateral elbow pain. **a** Long-axis gray-scale 12−5 MHz US image reveals a hypoechoic focus (*asterisks*) in the most superficial fibers of the common extensor tendon origin (*arrowheads*), whereas the deep fibers are preserved. **b** Color Doppler imaging demonstrates a striking hypervascular pattern composed of series of tiny vessels throughout the intratendinous hypoechoic areas, characteristic of tendinosis. *LE*, lateral epicondyle; *RH*, radial head
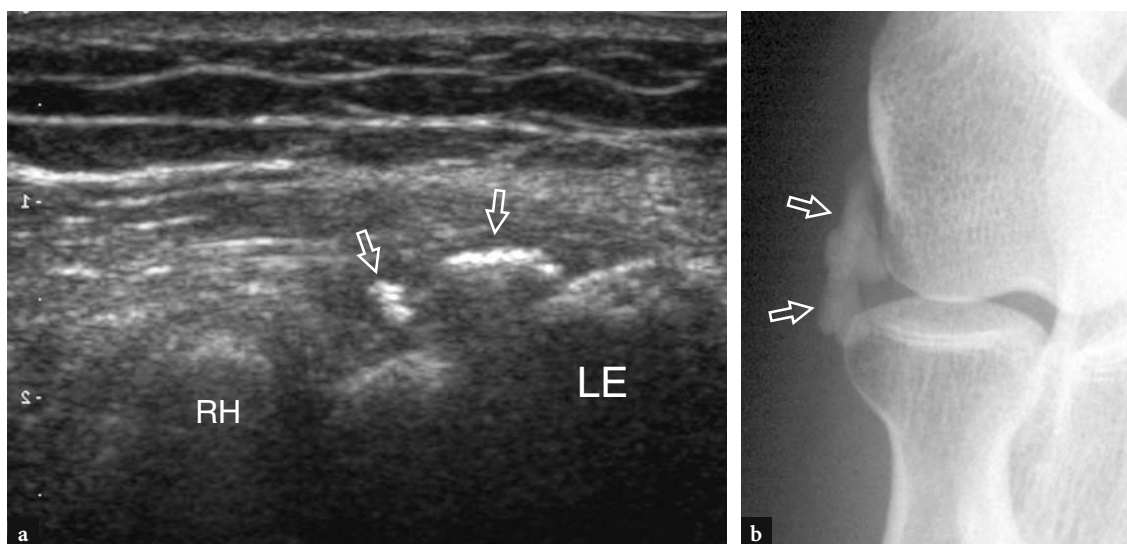
Fig. 8.40a,b. Calcifying lateral epicondylitis. **a** Long-axis 12−5 MHz US image with **b** radiographic correlation in a patient with calcium pyrophosphate crystals deposition disease and recent onset of lateral elbow pain demonstrates large calcified foci (*arrows*) within the common extensor tendon origin. *LE*, lateral epicondyle; *RH*, radial head
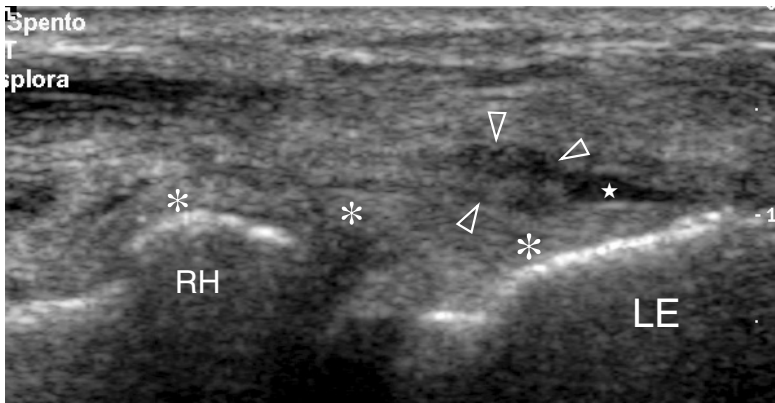
Fig. 8.41. Partial-thickness tear of the common extensor tendon. Long-axis 12–5 MHz US image in a manual laborer who presented with acute onset of lateral elbow pain reveals a linear hypoechoic split (*star*) extending from the lateral epicondyle (*LE*) through the substance of the common extensor tendon origin. The torn deep fibers (*arrowheads*) are retracted just distal to the hypoechoic area. Note the integrity of the underlying lateral ulnar collateral ligament (*asterisks*). *RH*, radial head
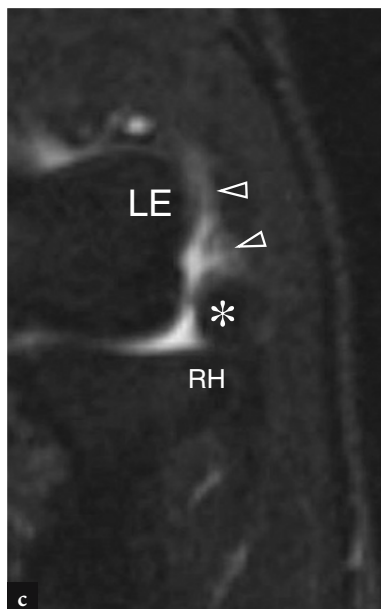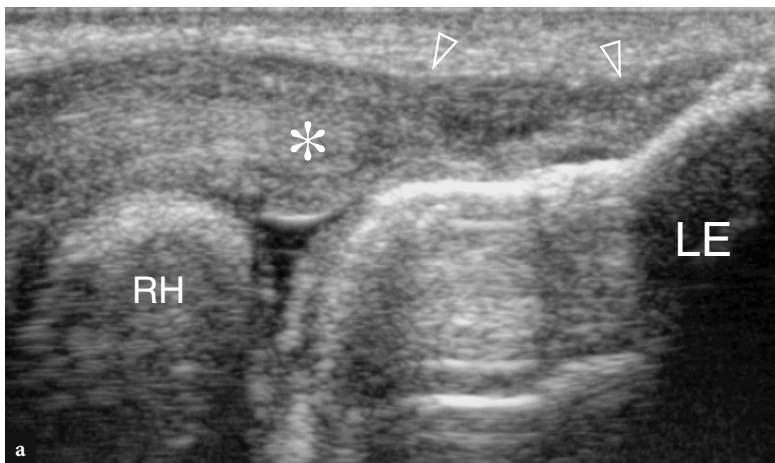

Fig. 8.42a–c. Complete rupture of the common extensor tendon. **a** Long-axis 12–5 MHz US image in a golfer player who complained of longstanding elbow pain with coronal **b** T1w SE and **c** fat-suppressed T2w SE MR imaging correlation shows a retracted common extensor tendon. Note the gap (*arrowheads*) related to the tear that separates the avulsed tendon edge (*asterisk*) from the lateral epicondyle (*LE*). *RH*, radial head

dylitis. In addition, when the torn lateral ulnar collateral ligament is not recognized preoperatively, the operative release of the common extensor tendon may be responsible for worsening of symptoms and onset of posterolateral rotatory instability of the elbow (see Sect. 8.5.5.4).

When the more superficial extensor carpi radialis brevis is torn, the deep lateral ulnar collateral ligament becomes more clearly distinguishable with US as a cord-like fibrillary structure located over the joint space (Fig. 8.41). An isolated ligament tear appears as discontinuity of the deepest fibers of the extensor tendon origin, whereas tears involving both the ligament and the common extensor tendon cause a full-thickness interruption of fibers over the lateral aspect of the radiocapitellar joint and soft tissue hematoma around the proximal margin of the capitellum (CONNELL et al. 2001). Dynamic scanning during careful varus stressing can disclose lateral ulnar collateral ligament injury by depicting widening of the lateral elbow joint space compared with the opposite normal elbow (Fig. 8.43).

In "pulled elbow", a common injury among children due to slipping of the annular ligament over the radial head following forceful pronation, US is able to depict an increased distance between the radial head and the humeral capitellum probably due to the impingement of the annular ligament (KOSUWON et al. 1993) - see also chapter 19.

8.5.3.3
Supinator Syndrome (Posterior Interosseous Neuropathy)

Supinator syndrome, also referred to as "posterior interosseous syndrome" or "radial tunnel syndrome", is a rare compression neuropathy of the upper limb affecting the posterior interosseous nerve just near or behind the supinator muscle (SPINNER 1968). This nerve is vulnerable to injury at the proximal edge of the superficial belly of the supinator muscle that forms a free, strong, fibrous arch, the "arcade of Frohse". At this site, the posterior interosseous nerve may be tethered and entrapped by fibrous bands,
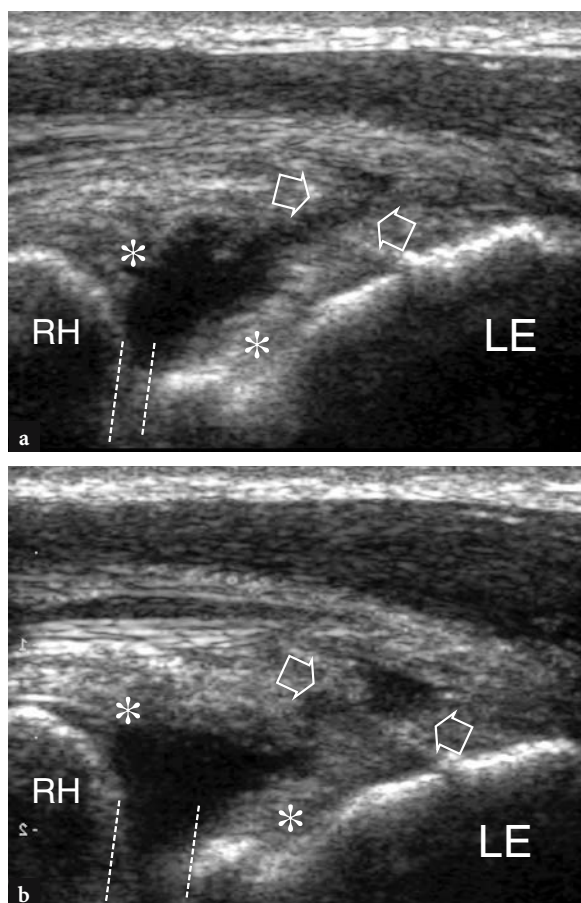

Fig. 8.43a–c. Complete tear of the common extensor tendon and the lateral ulnar collateral ligament. **a, b** Longitudinal 12−5 MHz US images obtained over the common extensor tendon origin **a** in neutral position and **b** with varus stressing. In **a**, US identifies a large horizontal hypoechoic cleft through the full thickness of the common extensor tendon origin (*arrows*) and the lateral ulnar collateral ligament (*asterisks*). In **b**, varus stress on the elbow shows widening of the radio-capitellar joint space (*dashed lines*). *RH*, radial head; *LE*, lateral epicondyle. **c** Correlative STIR MR image confirms the complete rupture of both structures (*arrowheads*)

fan-shaped recurrent radial vessels or by tightness of the passage within the superficial and deep layers of the supinator. In addition, it may be compressed by a variety of soft-tissue masses, such as paraosteal lipomas and deep ganglia. Radial head and neck fractures, including Monteggia fracture-dislocations, may also displace and encase the posterior interosseous nerve by callus as it passes through the supinator tunnel. Clinically, the posterior interosseous neuropathy produces a clinical picture distinct from a lesion of the radial nerve in the arm. In fact, the patient has a "finger drop" rather than the characteristic "wrist drop" of a radial neuropathy, because muscle weakness spares the extensor carpi radialis (Fig. 8.44). Extension of the fingers at the metacarpophalangeal joints is impaired and there is deficit of abduction and extension of the thumb. In addition, posterior interosseous neuropathy may cause burning pain and tenderness over the lateral elbow, possibly mimicking a "resistant lateral epicondylitis".

High-resolution US is able to identify the impingement of the posterior interosseous nerve in the supinator area. The compressed nerve typically appears swollen and hypoechoic proximal to or inside the supinator muscle (BODNER et al. 2002). In post-traumatic settings, the nerve may appear displaced by a malaligned radial head and may exhibit alternate thickened and thinned segments between the superficial and deep bellies of the supinator muscle as a possible result of stretching injury (Fig. 8.45). In addition, the nerve may be seen encased by hypoechoic scar tissue following a radial fracture (Fig. 8.46).

Decompressive surgery of the posterior interosseous nerve is indicated if there is continuous worsening or no recovery of function with a few months.

8.5.4
Posterior Elbow Pathology

8.5.4.1
Distal Triceps Tendon Tear

Distal triceps tendon tear is an uncommon condition that mostly occurs at or close to the olecranon process of the ulna, often associated with a fleck of bone attached to the retracted tendon as a result of avulsion fracture (Fig. 8.47). The mechanism involves either forced flexion of the elbow against a contracting triceps, as occurs during a fall on an outstretched arm, or relates to a direct blow onto the olecranon process. Local steroid injection into the olecranon bursa, anabolic steroid abuse and pre-existing tendinosis may also have a role in the tendon rupture. As a rule, complete tears occur more
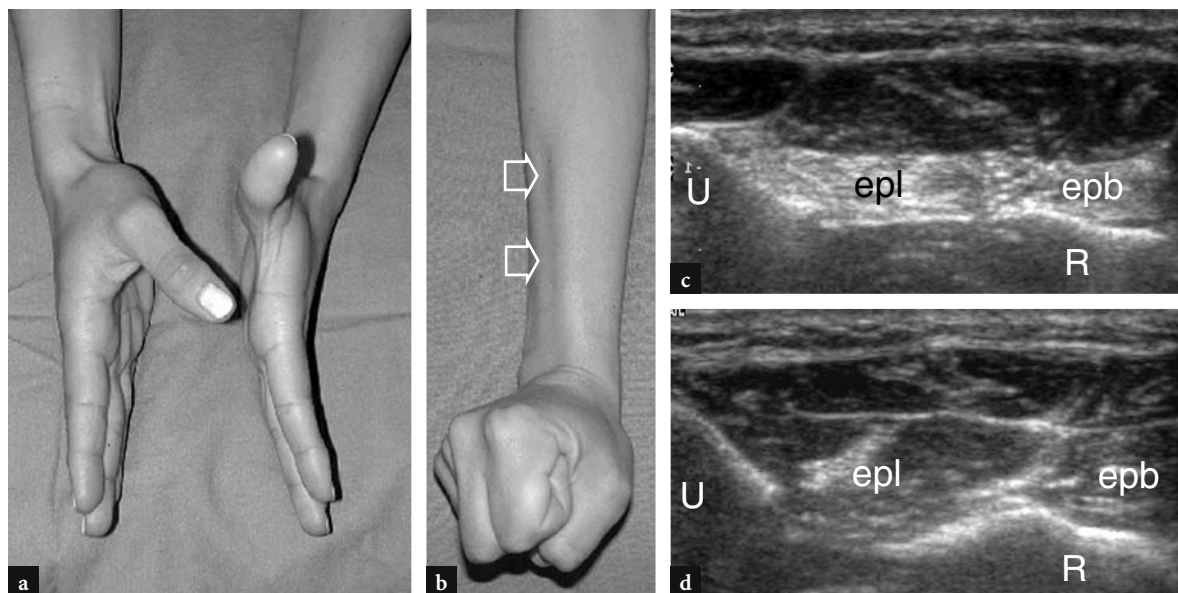

Fig. 8.44a–d. Posterior interosseous nerve syndrome in a young woman who presented with **a** intense weakness in extending the right fingers, especially involving thumb movements, and **b** a longitudinal skin depression (*arrow*) over the dorsum of the forearm following a contusion to the lateral elbow. **c** Transverse 12–5 MHz US image at the middle dorsal forearm reveals loss in bulk and a hyperechoic appearance of the extensor pollicis longus *(epl)* and extensor pollicis brevis *(epb)* muscles relative to fatty atrophy. Surgery confirmed the traumatic injury of the posterior interosseous nerve. **d** Normal contralateral side. *U*, ulna; *R*, radius
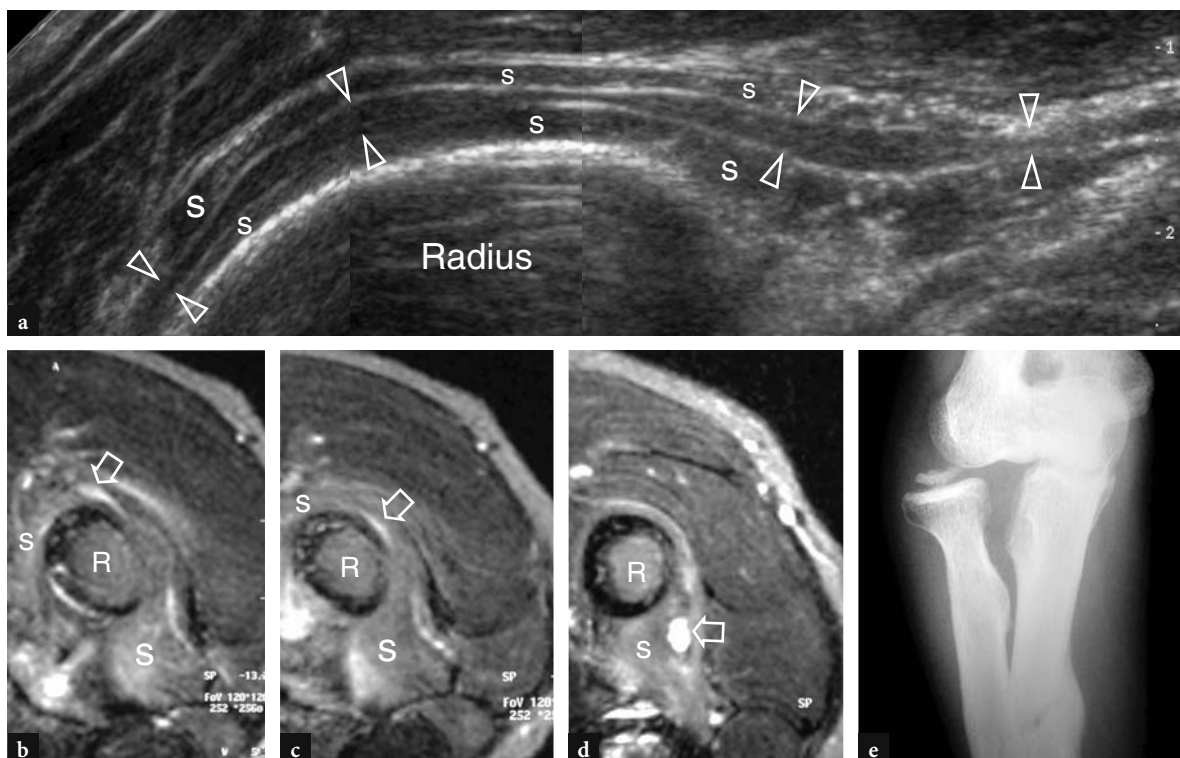
Fig. 8.45a–e. Posterior interosseous nerve syndrome in a patient with malaligned Monteggia fracture-dislocation (type IV). **a** Extended field-of-view 12−5 MHz US image reconstructed according to the longitudinal axis of the supinator tunnel demonstrates the posterior interosseous nerve (*arrowheads*) which alternates thickened and thinned portions as it traverses the supinator muscle (*s*). **b–d** Serial T2*GRE MR images reveal slight hyperintensity in the supinator muscle (*s*) due to denervation edema. The nerve (*arrows*) appears markedly hyperintense. *R*, radius. **e** Radiograph shows the malalignment of the radius, which appears subluxated anterolaterally
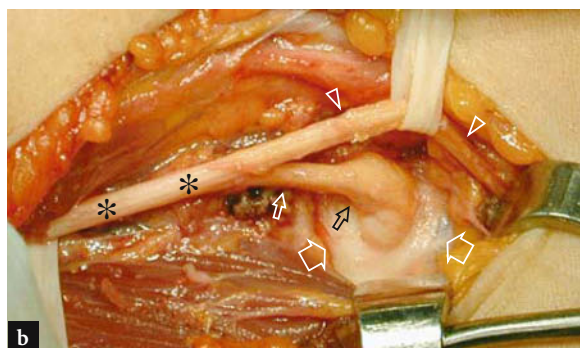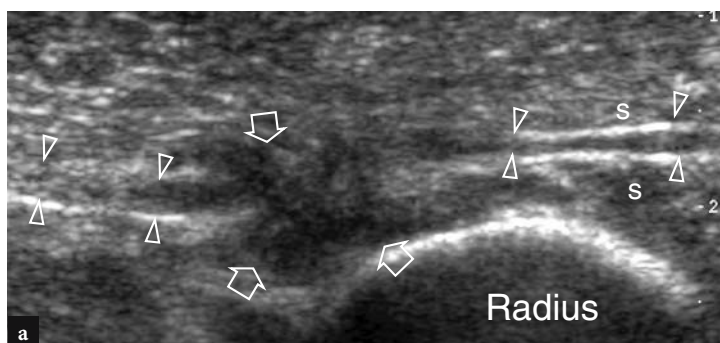

Fig. 8.46a,b. Posterior interosseous nerve syndrome. **a** Transverse 12−5 MHz US image obtained over the supinator area in patient with a previous radial head fracture and radial nerve deficit demonstrates the posterior interosseous nerve (*arrowheads*) entrapped within a hypoechoic scar (*arrows*) in the area of the supinator muscle (*s*). **b** Gross operative view shows the main trunk of the radial nerve (*asterisks*) as it splits into the superficial cutaneous sensory branch (*arrowheads*) and the deep posterior interosseous nerve (*narrow arrows*). This latter nerve is irregularly swollen as it passes over the bone (*large arrows*) as a result of the scar encasement visible in **a**

Fig. 8.47a–c. Avulsion fracture of the olecranon in a boy following a bicycle accident. **a** Reconstructed midsagittal 12−5 MHz US image over the posterior elbow with **b** lateral radiographic correlation demonstrates the avulsion fracture of the olecranon process *(1)* from the ulnar shaft *(2)* due to a traction mechanism by the distal triceps tendon *(arrows)*. Note the coexisting avulsion of the cartilaginous growth plate *(asterisks)*. **c** Lateral radiograph of the opposite healthy side shows incomplete ossification *(curved arrow)* between the olecranon and the ulnar shaft

frequently than partial tears, whereas disruption of either the muscle bellies or the myotendinous junction is rare. Complete rupture of the distal triceps tendon presents clinically with complete inability to extend the elbow, given the absence of other muscles that can assist in this movement. In the acute phase, however, the clinical diagnosis may be hampered by local soft-tissue swelling, inflammatory edema and pain that limit the physical examination. In such cases, US may be useful both to confirm the tendon injury and to differentiate between complete tears that require immediate surgery to avoid retraction of the tendon and partial tears that may be treated conservatively. In acute complete ruptures, US demonstrates the distal triceps tendon as wavy, retracted and surrounded by fluid (Fig. 8.48) (KAEMPFFE and LERNER 1996). US examination is also reliable to delineate the degree of tendon retraction and can help in the diagnosis of atypical ruptures, such as in cases of tears occurring at the myotendinous junction (Fig. 8.49). Due to the close anatomic relation of the distal triceps tendon with the medial epicondyle and the cubital tunnel, an acute ulnar nerve compression syndrome may occur secondary to a distal triceps tendon tear (DUCHOW et al. 2000). Degenerative tendinosis can be appreciated as a thickened hypoechoic tendon.

8.5.4.2
Olecranon Bursitis

Olecranon bursitis, the most common superficial bursitis in the body, appears clinically as a lump overlying the olecranon process due to fluid distension or hypertrophy of the synovial membrane. The most common cause of olecranon bursitis is repetitive local contusion (student's elbow, miner's elbow) that leads to a painless local swelling covered by normal skin. Calcific enthesopathy of the distal triceps tendon is a predisposing factor. However, bursal distension can be appreciated in a variety of systemic disorders, such as rheumatoid arthritis, gout, hydroxyapatite and calcium pyrophosphate deposition diseases, as well as in septic conditions (e.g. *Staphylococcus*, tuberculosis); also patients under chronic hemodialysis treatment may occasionally have olecranon bursitis. When bursitis is secondary to infection or gout, bursal swelling is typically painful and associated with skin warmth and erythema due to local inflammatory changes. Because systemic findings are often absent in septic bursitis, the likelihood of an infected bursa must always be kept in mind. Similarly, when the patient has a history of tuberculous disease, a specific etiology of bursitis should first be suspected.
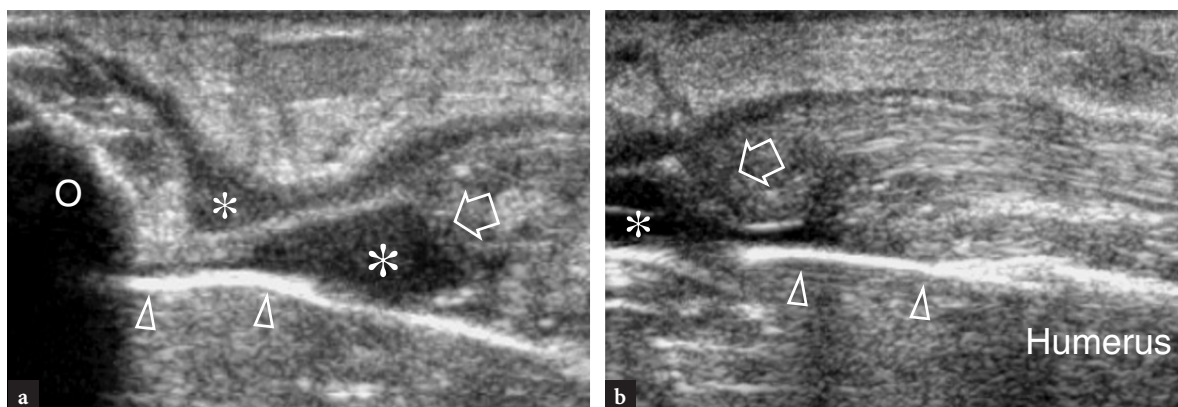
Fig. 8.48a,b. Complete distal triceps tendon rupture in a patient who had undergone osteosynthesis for a supracondylar fracture of the humerus. Midsagittal 12−5 MHz US images over the posterior elbow obtained in **a** extension and **b** mild flexion show a large defect (*asterisks*) in the distal triceps tendon (*arrow*) which appears retracted as a result of disinsertion from the olecranon *(O)*. Tear resulted from the lower edge of the internal fixation plate (*arrowheads*) which projected into the posterior fossa causing conflict with the overlying tendon
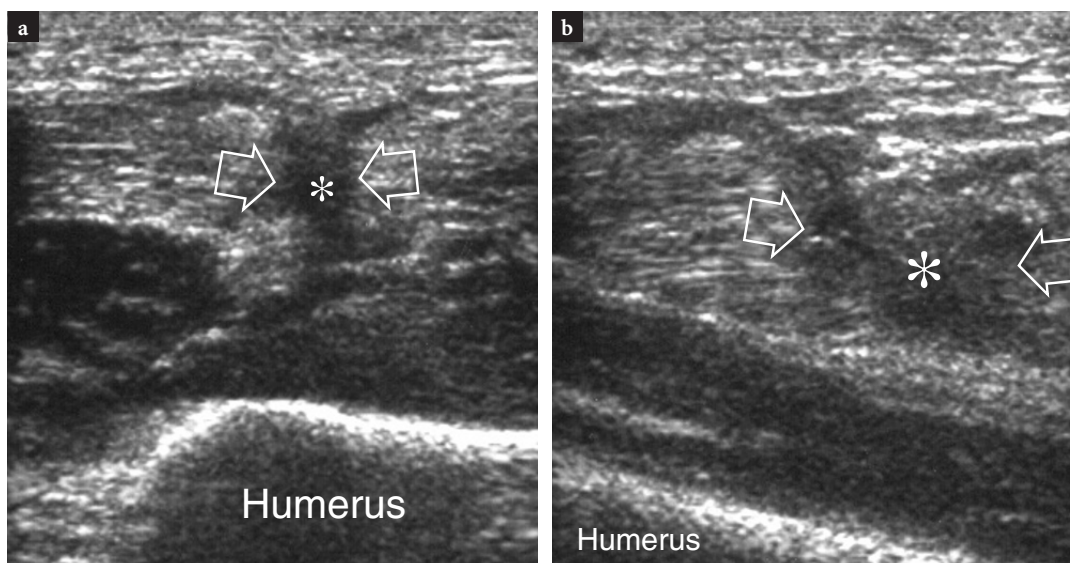

Fig. 8.49a,b. Partial tear at the distal myotendinous junction of the triceps. Long-axis 12−5 MHz US images obtained with the elbow extended (**a**) and mildly flexed (**b**) demonstrate a gap (*arrows*) in the posterior fibers of the triceps filled with hypoechoic hematoma (*asterisk*). The hypoechoic gap widens as the elbow flexes

US demonstrates olecranon bursitis as a localized fluid collection and/or synovial wall hypertrophy within the subcutaneous tissue immediately posterior to the olecranon (Fig. 8.50). Soft-tissue hyperemia is often recognized with color and power Doppler imaging as an accompanying finding (Lin et al. 2000). The hypervascular pattern typically distributes in a rim-like peribursal pattern. In crystal deposition diseases, the US appearance of bursal fluid is more likely hyperechoic and associated with thickened and echogenic bursal walls (Fig. 8.51). In hemorrhagic and septic bursitis, the fluid may result in a complex appearance: edema of surrounding soft tissues and cellulitis are frequently associated (Fig. 8.52). However, these characteristics are too subtle to allow a definitive diagnosis based on US findings alone, and needle aspiration of fluid, possibly obtained under US guidance, is usually required for analysis and culture. In extreme cases, chronic synovial proliferation and fibrosis may make the bursa indistinguishable from a solid tumor. Calcified bursitis may occur in patients with chronic renal failure (Fig. 8.53). In rheumatoid arthritis, the bursal fluid may occasionally be seen dissecting the superficial soft tissues of the forearm
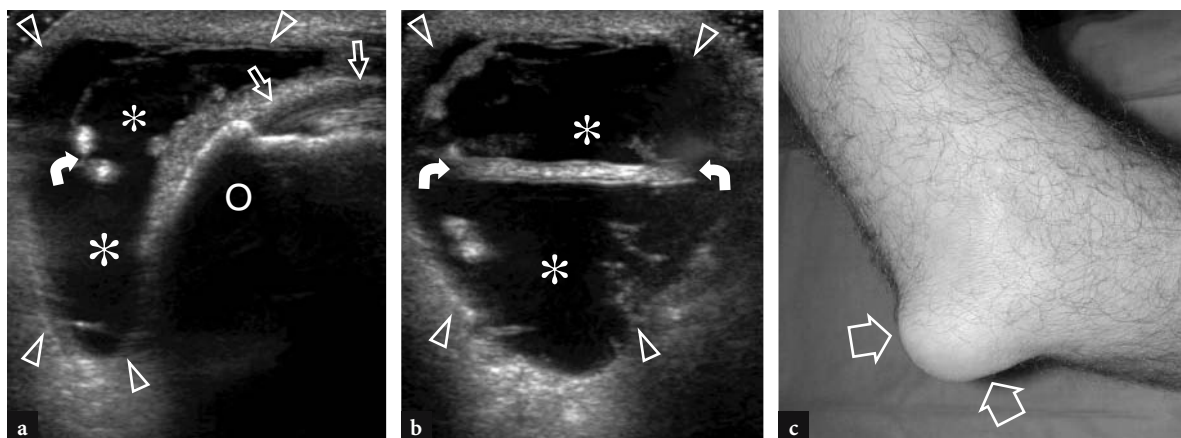
Fig. 8.50a–c. Chronic traumatic olecranon bursitis in a manual laborer who had recently injured several times his posterior right elbow. **a** Midsagittal and **b** transverse 12–5 MHz US images over the olecranon process *(O)* show a markedly distended olecranon bursa *(arrowheads)* containing thick septa *(curved arrows)* and anechoic effusion *(asterisks)*. *Straight arrows*, distal triceps tendon. **c** Photograph showing the bursal lump *(arrows)* on the posterior elbow
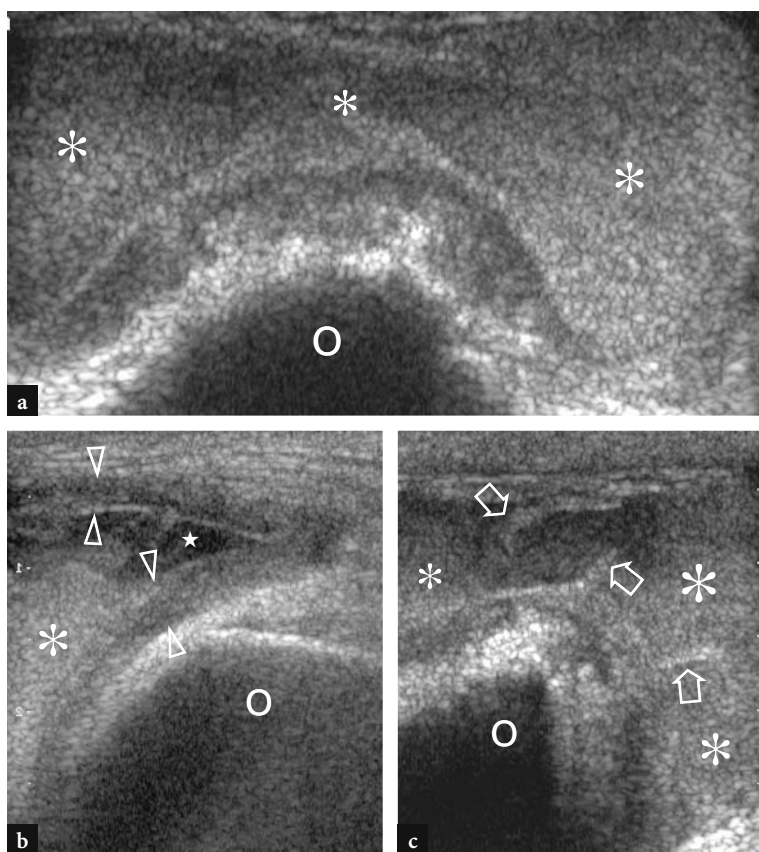

Fig. 8.51a–c. Hydroxyapatite olecranon bursitis. **a** Transverse and **b,c** longitudinal 12–5 MHz US images of a painful soft-tissue mass over the olecranon *(O)* show the olecranon bursa filled with homogeneous highly echogenic fluid *(asterisks)* that could be seen fluctuating during probe compression. The bursa exhibits thickened walls *(arrowheads)* and septa *(arrows)*. In this case, needle aspiration of the bursal fluid revealed calcium milk solution

following bursal rupture. In such patients, subcutaneous nodules can be seen in the olecranon region and along the proximal ulna. These nodules should be considered in the differential diagnosis as they can mimic olecranon bursitis or a solid neoplasm Distal

to the olecranon bursa, an additional small subolecranon bursa can exist at the posterior aspect of the proximal ulnar shaft. In rare instances, this bursa can be involved by the same processes affecting the larger olecranon one (Fig. 8.54).
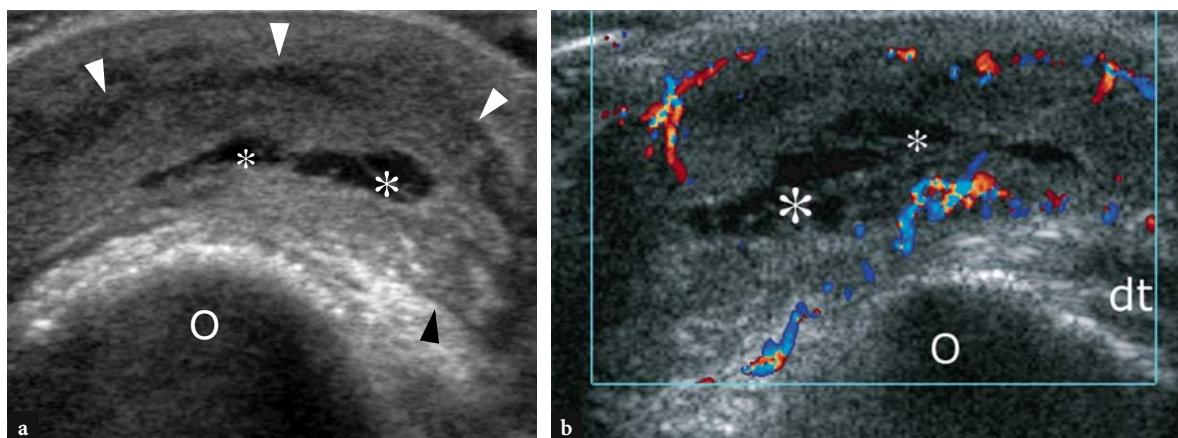
Fig. 8.52a,b. Tuberculous olecranon bursitis. **a** Longitudinal gray-scale and **b** color Doppler 12−5 MHz US images in a patient with painful soft-tissue swelling over the posterior elbow. The olecranon bursa (*arrowheads*) shows irregular wall thickening and ill-defined margins due to coexisting peribursal cellulitis. Only a small amount of intrabursal fluid is seen (*asterisks*). dt, distal triceps tendon; *O*, olecranon
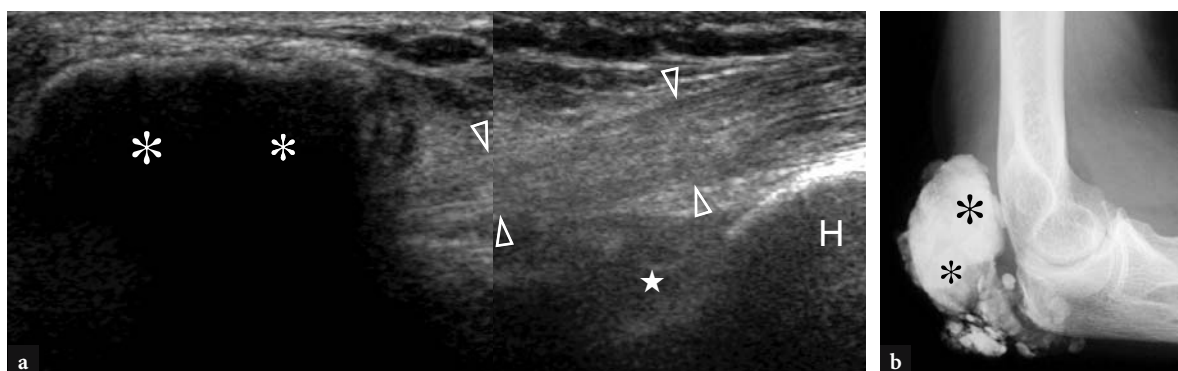

Fig. 8.53a,b. Calcific olecranon bursitis in a patient with renal osteodystrophy. **a** Posterior midsagittal 12−5 MHz US image with **b** lateral radiographic correlation demonstrates a large calcification (*asterisks*) that lies superficial to the insertion of the distal triceps tendon (*arrowheads*) reflecting an extensively calcified bursa. Note the relation of the mass with the posterior olecranon fossa (*star*) and the humeral shaft (H)
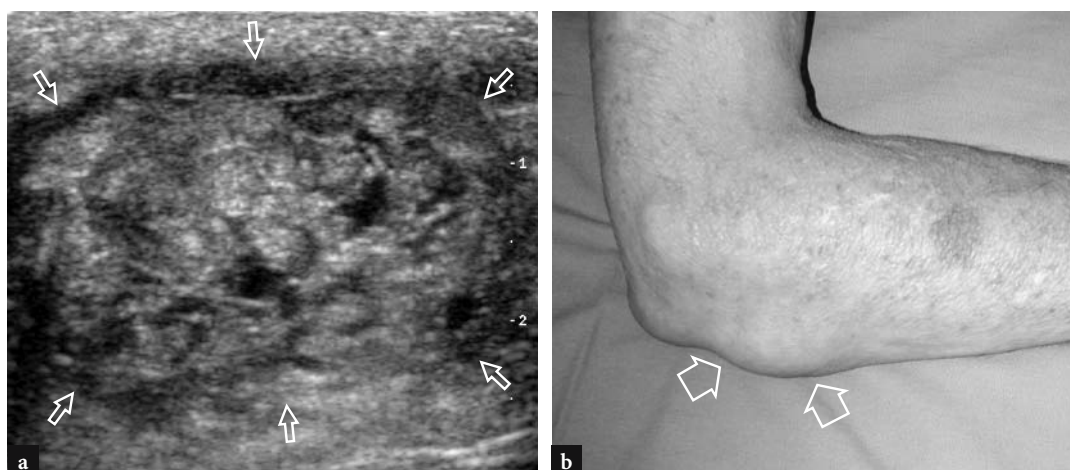

Fig. 8.54a,b. Subolecranon bursitis nodule in a patient with severe rheumatoid arthritis. **a** Transverse 12−5 MHz US image reveals a painless heterogeneous soft-tissue mass (*arrows*) with mixed echotexture located in the subcutaneous tissue over the proximal posterior ulna, compatible with subolecranon bursitis. **b** Photograph of the same case shown in **a**

8.5.4.3
Cubital Tunnel Syndrome

Ulnar nerve compression inside the cubital tunnel, the second most common entrapment syndrome of the upper limb after carpal tunnel syndrome, may occur either at the condylar groove or at the edge of the arcuate ligament (proper cubital tunnel). There are several causes of ulnar nerve damage, including direct extrinsic compression of the nerve against a shallow condylar groove, bone abnormalities (cubitus valgus, deformities from previous elbow fractures, osteoarthritis with medial osteophytes and loose bodies, heterotopic ossification) and a variety of space-occupying soft-tissue lesions, including thickening of the capsule and the medial collateral ligament, ganglia and accessory muscles (anconeus epitrochlearis muscle) (Stewart 1993). Clinically, the entrapment of the ulnar nerve at the elbow presents insidiously with medial elbow pain and a spectrum of complaints ranging from sensory symptoms in the ring and little fingers to weakness of the ulnar-innervated hand muscles. Wasting of hand muscles is best appreciated at the first interosseous space and hypothenar eminence and causes a typical semiflexion deformity of the ring and little fingers that is commonly referred to as "claw hand" (Fig. 8.55). In addition, the little finger may stay slightly abducted (Wartenberg sign).

The diagnosis is essentially based on electrophysiologic studies. US typically demonstrates an abrupt narrowing and displacement of the nerve within the tunnel, possibly in association with a thickened retinaculum or a space-occupying lesion (Fig. 8.56) (Puig et al. 1999; Martinoli et al. 2000; Okamoto et al. 2000). Proximal to it, the compressed nerve appears swollen with loss of the fascicular pattern and, in some cases, hypervascularity at color Doppler imaging. As assessed by quantitative analysis with US, the nerve cross-sectional area at the epicondyle is significantly larger in patients with cubital tunnel syndrome than in healthy subjects or in the opposite normal elbow (Okamoto et al. 2000; Chiou et al. 1998). An ulnar nerve area ≥ 7.5 mm^2 at the level of the epicondyle has been indicated as the threshold value for cubital tunnel syndrome (Chiou et al. 1998). These data are somewhat contradictory with a more recent paper which indicates 7.9 mm^2 as the mean cross-sectional area for the normal ulnar nerve at the elbow (Jacob et al. 2004). Besides assessing the ulnar nerve, a wide spectrum of extrinsic causes for nerve entrapment may be recognized with US as well, including congenital anomalies such as an accessory anconeus epitrochlearis muscle (Fig. 8.57), and acquired disease which
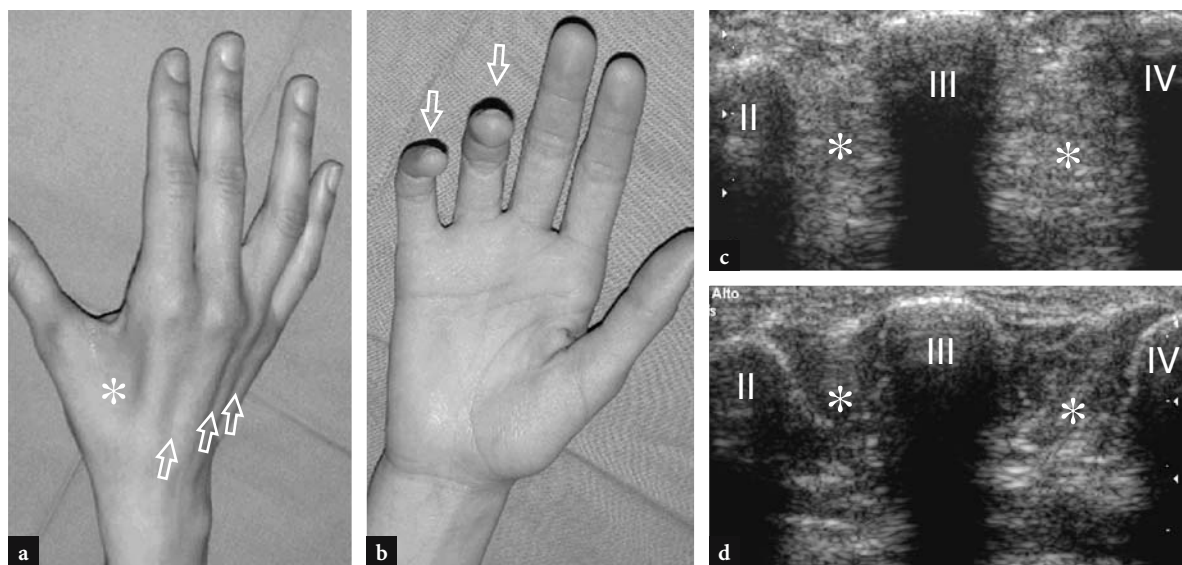

Fig. 8.55a–d. Claw-like deformity in the right hand of a young patient with severe ulnar neuropathy at the cubital tunnel level. **a** Photograph of the dorsal aspect of the hand reveals loss in bulk of the dorsal interosseous muscles (*arrows*) that lie in the intermetacarpal spaces. The atrophy of the ulnar-innervated hand muscles is more obvious at the first intermetacarpal space (*asterisk*). **b** Photograph of the palmar aspect of the hand shows the fourth and fifth fingers extended at the metacarpophalangeal joint and flexed at the interphalangeal joints. **c** Transverse 12–5 MHz US image at the dorsal aspect of the hand demonstrates a hyperechoic appearance of the dorsal interosseous muscles (*asterisks*) related to neurogenic fatty atrophy. **d** Contralateral healthy side. II–III–IV, metacarpals
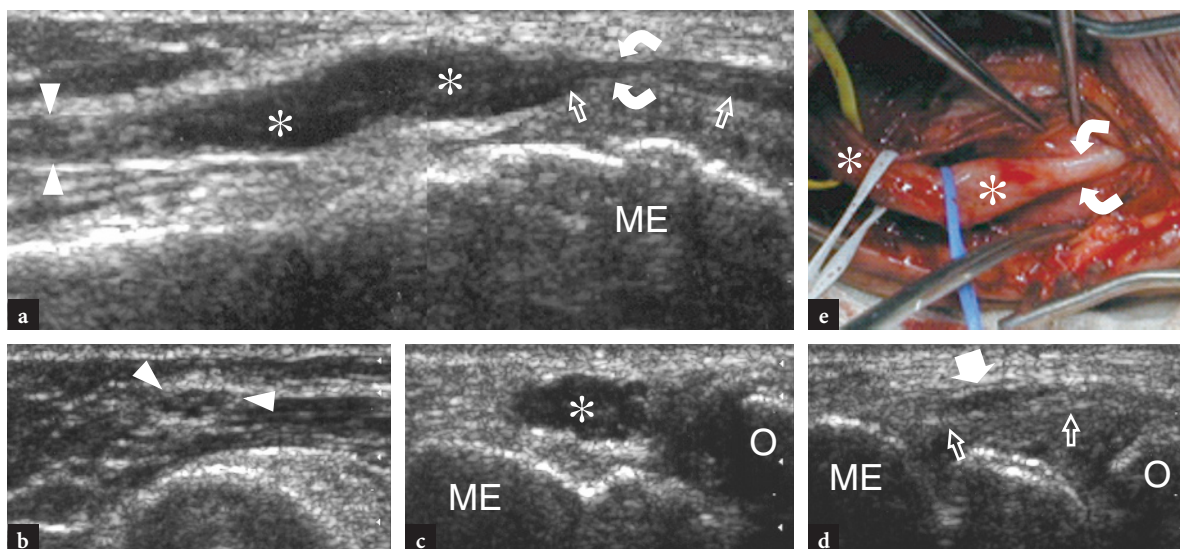
Fig. 8.56a–e. Cubital tunnel syndrome. **a** Long-axis 12−5 MHz US image of the cubital tunnel in a patient with cubitus valgus demonstrates the ulnar nerve (*arrowheads*), which appears increasingly swollen and hypoechoic with absent fascicular pattern (*asterisks*) as it progresses towards the compression point (*curved arrow*). Observe the elevated floor of the tunnel relative to thickening of the medial capsule and medial ligamentous complex (*arrows*). **b–d** Transverse 12−5 MHz US images show **b** a normal-appearing ulnar nerve (*arrowheads*) at the distal arm, **c** a swollen and hypoechoic nerve (*asterisks*), just proximal to the tunnel, and **d** an abrupt narrowing in the cross-sectional area of the ulnar nerve (*white arrow*) beneath the Osborne retinaculum and superficial to the thickened floor (void arrows) of the tunnel. *ME*, medial epicondyle; *O*, olecranon. **e** Gross operative view of the same case.
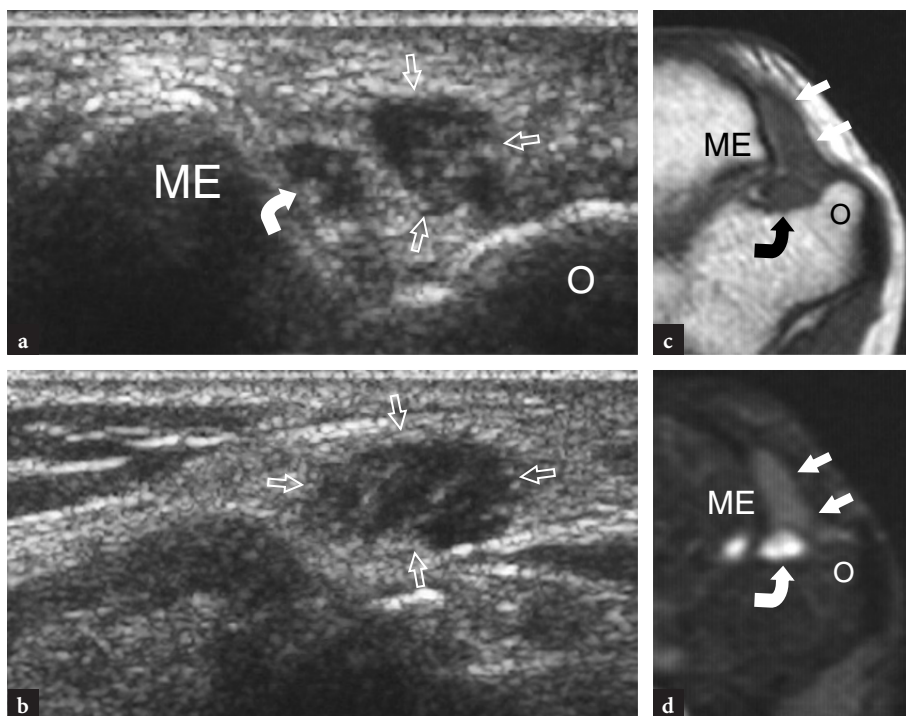

Fig. 8.57a–d. Cubital tunnel syndrome in a patient with anconeus epitrochlearis muscle. **a** Short-axis and **b** long-axis 12−5 MHz US images of the cubital tunnel reveal the anconeus epitrochlearis muscle (*straight arrows*) that lies between the medial epicondyle (*ME*) and the olecranon (*O*) in close relation with a swollen ulnar nerve (*curved arrow*). Correlative transverse **c** T1w SE and **d** fat-suppressed T2w SE MR images demonstrate the aberrant muscle (*straight arrows*) within the cubital tunnel. In **d**, the ulnar nerve (*curved arrow*) appears markedly hyperintense as a result of compression neuropathy. *ME*, medial epicondyle; *O*, olecranon
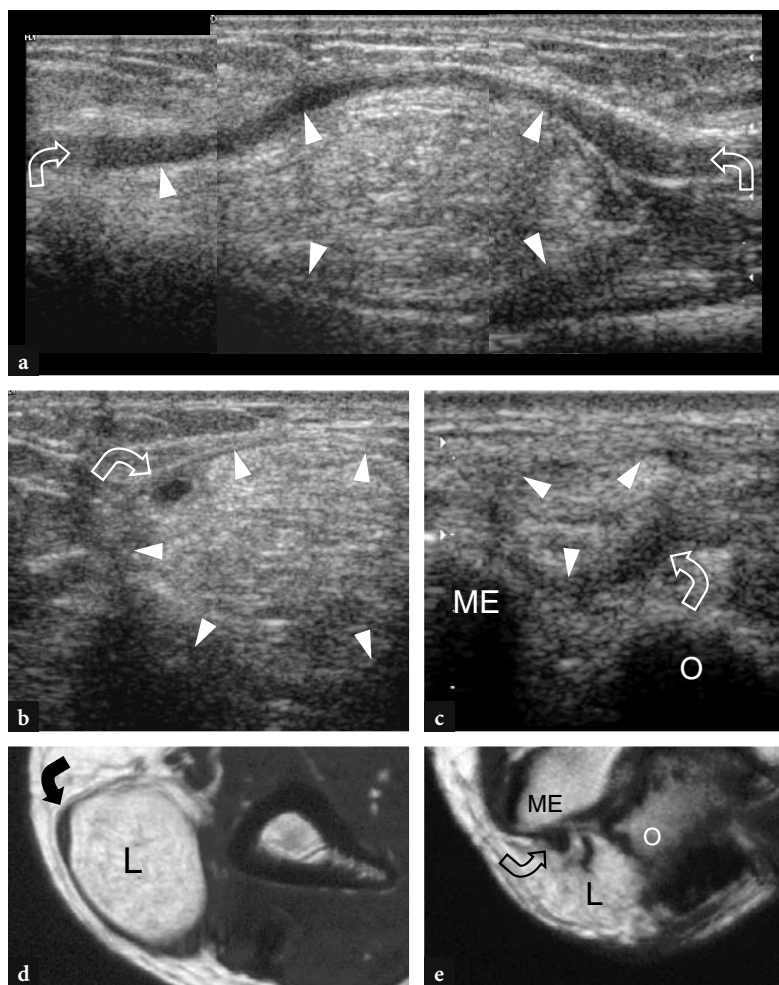
Fig. 8.58a–e. Cubital tunnel syndrome in a patient presenting with a superficial soft-tissue mass on the posteromedial elbow. **a** Reconstructed longitudinal and **b** transverse 12–5 MHz US images obtained just proximal to the cubital tunnel demonstrate the ulnar nerve (*curved arrow*) that shows a bowing course over an oval solid hyperechoic lesion (*arrowheads*) with well-defined margins, consistent with a lipoma. Note the close relationship of the mass with the nerve. **c** Transverse 12–5 MHz US image obtained at the cubital tunnel level shows the lipoma (*arrowheads*) that infolds within the tunnel leading to compression of the ulnar nerve (*curved arrow*). *ME*, medial epicondyle; *O*, olecranon. **d,e** Correlative transverse T1w SE MR images obtained **d** at the distal arm and **e** at the cubital tunnel levels confirm the lipomatous nature of the space-occupying lesion *(L)*. Curved arrow, ulnar nerve; *ME*, medial epicondyle; *O*, olecranon

in turn leads to an increased content–i.e., lipoma (Fig. 8.58)–or a decreased size–i.e. fracture residuals (Fig. 8.59)–of the tunnel.

Surgical decompression of the ulnar nerve at the elbow may include slitting the Osborne fascia and the aponeurosis of the flexor carpi ulnaris leaving the nerve inside the cubital tunnel. Alternatively, the nerve may be transposed out of the condylar groove and the cubital tunnel, anterior to the medial epicondyle and superficial to the flexor muscles (Fig. 8.60). This surgical option is preferred in cases of ulnar neuropathies caused by bone and joint disease. After surgical transposition, persistent symptoms are usually related to an excessive angling of the ulnar nerve as it passes deep to the arcuate ligament or to incomplete stabilization of the nerve in its new position. US is able to identify scar tissue along the course of the nerve in patients with recurrent symptoms or relapse of compressive causes (Fig. 8.61).

8.5.4.4
Ulnar Nerve Instability

In the congenital partial or complete absence of the cubital tunnel retinaculum, the ulnar nerve may subluxate over the tip of the epicondyle or dislocate anterior to it with a transient snapping sensation during flexion of the elbow, to return inside the tunnel when the joint is extended. Ulnar nerve instability at the cubital tunnel can be considered a normal variant, being reported in between 16% and 47% of asymptomatic healthy people, subluxation being the most common form (CHILDRESS 1975; OKAMOTO et al. 2000). The condition is bilateral in almost three quarters of cases and asymptomatic at both clinical examination and nerve conduction studies. Patients may occasionally complain of only mild discomfort with tingling and paresthesias when the flexed elbow hits a firm surface such as the edge of a desk. In rare instances, however, chronic
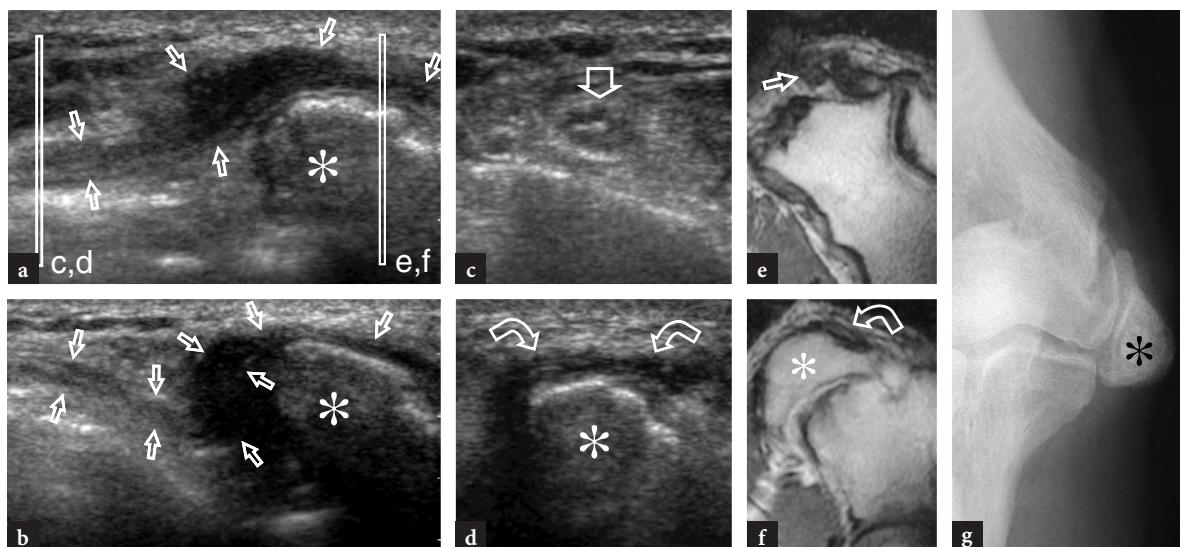
Fig. 8.59a–g. Cubital tunnel syndrome in a patient with recent onset of symptoms related to right ulnar neuropathy who had undergone a fracture of the medial epicondyle when he was an adolescent. **a,b** Longitudinal 12−5 MHz US images of the cubital tunnel obtained **a** during flexion and **b** full extension of the elbow. **a** With elbow flexion, an anomalous bone (*asterisk*) can be appreciated as a hyperchoic image bulging within the tunnel and displacing a swollen and hypoechoic ulnar nerve (*arrows*). **b** With elbow extension, the nerve (*arrows*) forms an abnormal loop cranial to the anomalous bone (*asterisk*) and appears flattened and compressed against its superficial aspect. **c,d** Transverse 12−5 MHz US images with **e,f** T1w SE MR imaging correlation obtained **c, e** at the distal arm and **d, f** at the level of the medial epicondyle with extended elbow reveal a normal-appearing nerve (*straight arrow*) cranial to the compression point and a flattened hypoechoic nerve (*curved arrows*) over the anomalous bone (*asterisk*). **g** Plain radiograph shows an old fracture of the medial epicondyle (*asterisk*) with the fragment displaced toward the joint line
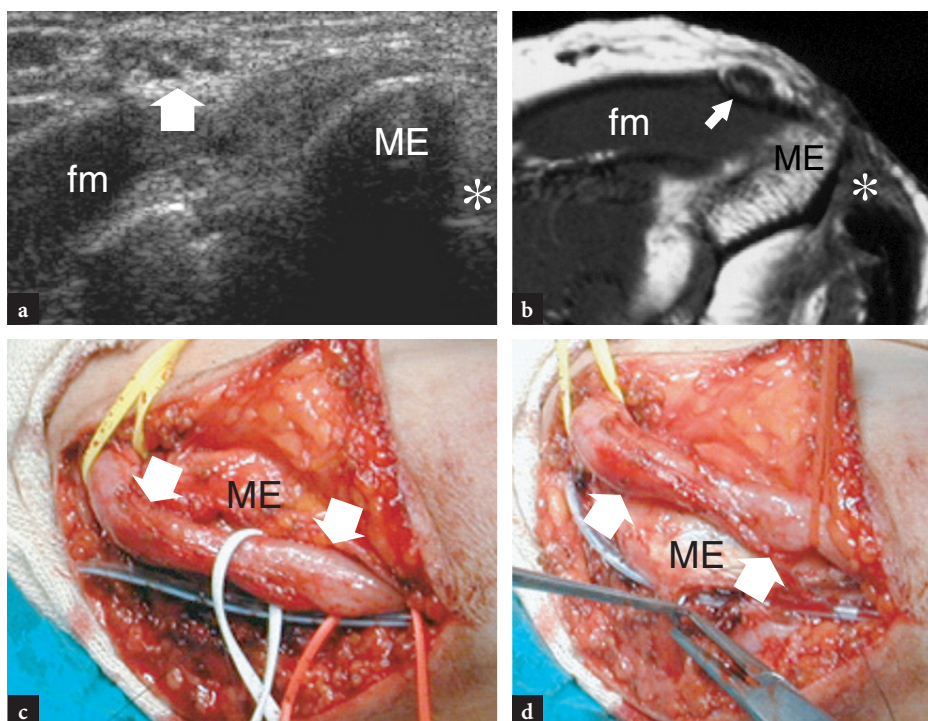

Fig. 8.60a–d. Postoperative ulnar nerve. **a** Transverse 12−5 MHz US image over the medial elbow with **b** T1w SE MR imaging correlation shows anterior transposition of the ulnar nerve (*arrow*) relative to the medial epicondyle *(ME)*. The nerve is subcutaneous and lies over the flexor muscles *(fm)*. Note the empty condylar groove (*asterisk*). **c,d** Gross operative views obtained **c** before and **d** after anterior transposition of the ulnar nerve (*arrows*) relative to the medial epicondyle *(ME)*
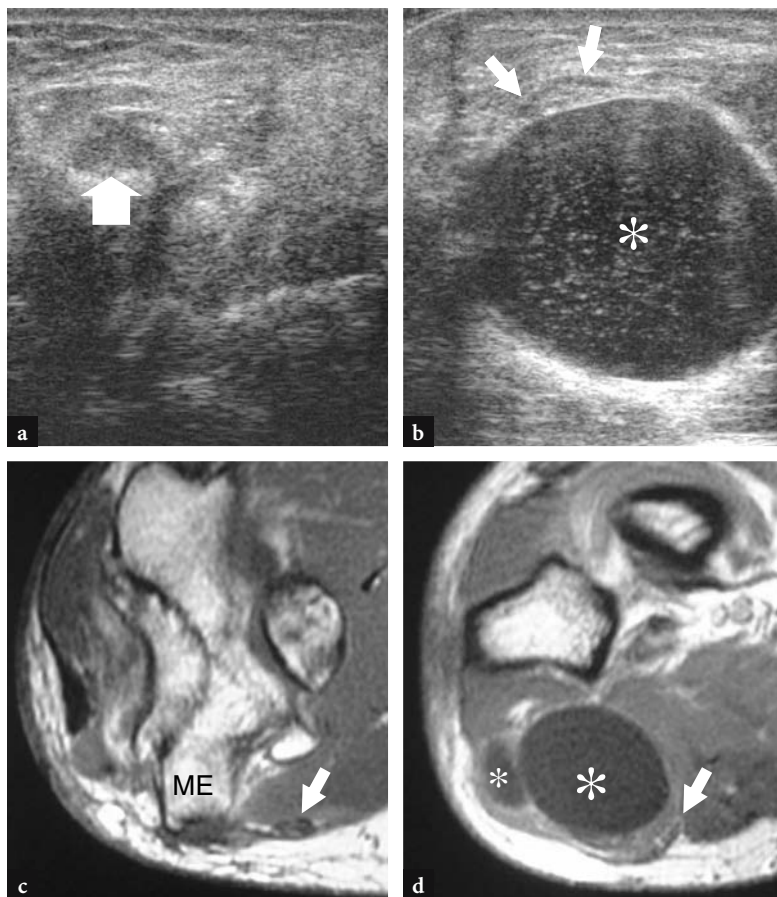
Fig. 8.61a–d. Postoperative patient with recurrence of symptoms after decompressive surgery of the ulnar nerve at the cubital tunnel for a ganglion cyst. **a,b** Transverse 12–5 MHz US images obtained **a** at the cubital tunnel level and **b** at the proximal forearm with **c,d** T1w SE MR imaging correlation show a relapsed cyst (*asterisks*) which constricts the transposed ulnar nerve (*arrow*). The patient underwent surgery again and the postoperative course was finally uneventful. *ME*, medial epicondyle

microtrauma of the nerve over the medial epicondyle due to repetitive dislocation can cause friction neuritis with symptoms and signs of ulnar nerve impairment. In such cases, nerve instability should be treated with surgical transposition of the nerve in order to avoid more serious damage.

Dynamic US scanning is an ideal means to depict the instability of the ulnar nerve during progressive elbow flexion, to recognize nerve abnormalities related to friction neuritis as well as to establish whether ulnar neuropathy is produced by compressive causes or instability because of the overlap in clinical findings (Jacobson and van Holsbeeck 1998; Jacobson et al. 2001). In subluxation, the nerve is seen moving over the apex of the medial epicondyle during full active elbow flexion but no further. In dislocation, the nerve may be seen snapping completely out of the cubital tunnel and migrating over the common flexor tendon origin (Fig. 8.62). During dynamic scanning, the snapping sensation may be felt by the examiner through the transducer. Careful scanning technique is needed to avoid excessive pressure with the probe over the epicondyle, which can prevent the nerve

from dislocating. In cases of symptomatic friction neuritis, the ulnar nerve appears markedly swollen and hypoechoic with loss of fascicular echotexture, probably reflecting localized intraneural edema and fibrotic changes (Fig. 8.63). However, these abnormalities may occasionally be encountered in healthy subjects too, without any implication of disease.

8.5.4.5
Snapping Triceps Syndrome

With elbow flexion, anterior dislocation of the medial head of triceps muscle relative to the medial epicondyle can occur in combination with dislocation of the ulnar nerve. In this condition, referred to as "snapping triceps syndrome", the dislocation of the muscle leads to concurrent dislocation of the adjacent ulnar nerve as these structures are contiguous (Fig. 8.64). Two palpable "snaps" are typically appreciated over the medial elbow, the first one reflecting dislocation of the ulnar nerve and the second, dislocation of the medial head of triceps muscle. The clinical presen-
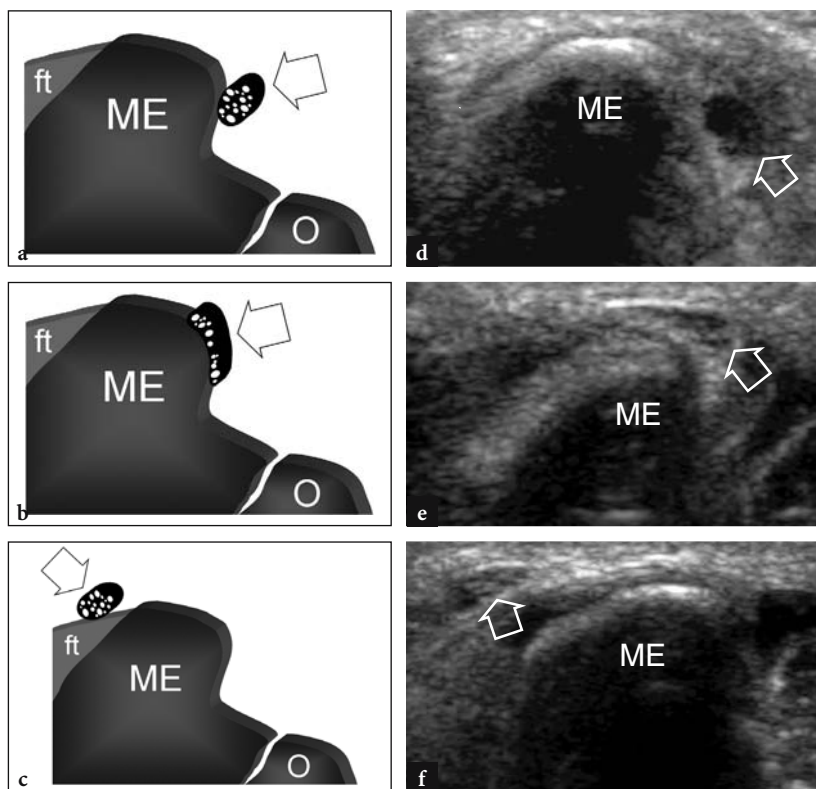
Fig. 8.62a–f. Dynamic study of the cubital tunnel in ulnar nerve dislocation. **a–c** Schematic drawings and **d–f** respective series of transverse 12−5 MHz US images obtained **a,d** with extended elbow and during progressive degrees of elbow flexion (**b,e** and **c,f**). When the elbow is extended, the ulnar nerve *(arrow)* is contained within the tunnel. Elbow flexion gradually pushes the nerve over the medial epicondyle *(ME)* until it snaps completely out of the cubital tunnel to lie superficial to the common flexor tendon origin *(ft)*. *O*, olecranon
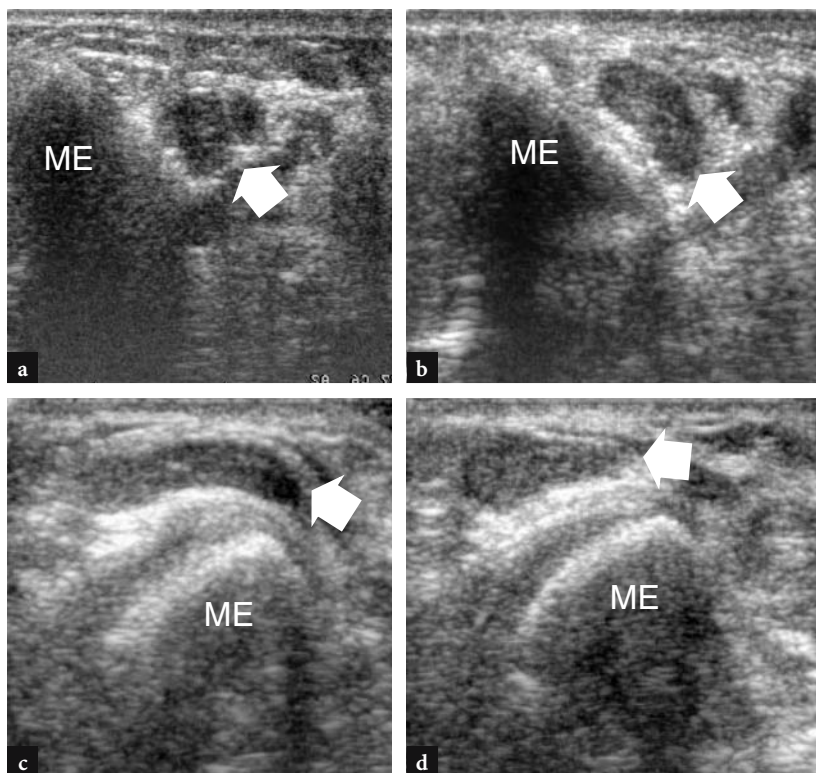

Fig. 8.63a–d. Dynamic study of the cubital tunnel in a patient with recurrent ulnar nerve dislocation and clinical symptoms of ulnar neuropathy. **a–d** Series of transverse 13−8 MHz US images acquired **a** with extended elbow and **b–d** throughout elbow flexion show a markedly swollen and hypoechoic nerve *(arrow)* that flattens and dislocates over the medial epicondyle *(ME)* during elbow flexion. In the symptomatic patient, this finding is suggestive of ulnar neuropathy based on a friction mechanism
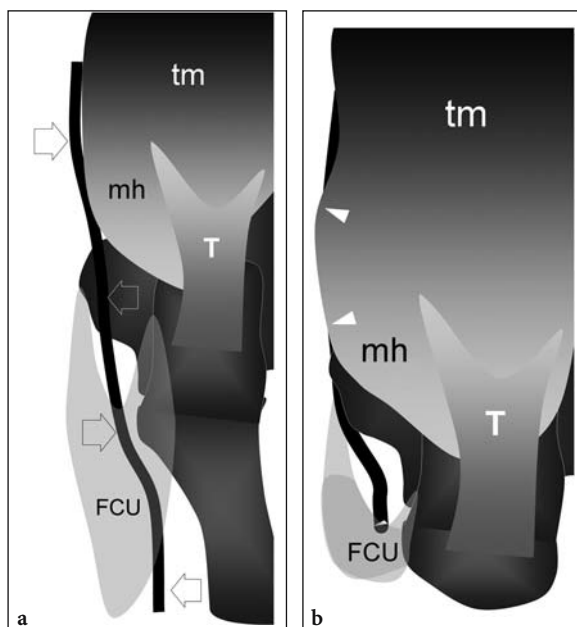
Fig. 8.64a,b. Snapping triceps syndrome. Schematic drawings of the posterior aspect of the elbow in **a** extension and **b** 90° flexion demonstrate the ulnar nerve (*arrows*) as it passes through the cubital tunnel and a prominent medial head (*mh*) of the triceps muscle (*tm*). Note the absence of the Osborne retinaculum when compared with **Fig. 8.7c.** With elbow flexion, the medial edge of the triceps (*arrowheads*) and the ulnar nerve move anterior to the tip of the epicondyle. *T*, distal triceps tendon; *fcu*, flexor carpi ulnaris

tation of this syndrome is variable and may include medial elbow pain, snapping sensation, ulnar neuropathy or a combination of these szymptoms (Spinner and Goldner 1998). Somewhat similar to the isolated dislocation of the ulnar nerve, the snapping triceps may however remain asymptomatic and probably unrecognized in most cases. Although the cause of snapping triceps is still unknown, some possible congenital and acquired conditions have been advocated to explain this syndrome, such as a hypertrophied triceps muscle, an accessory triceps tendon and abnormal medial head of the triceps muscle, as well as post-traumatic osseous abnormalities. Differentiation between snapping triceps syndrome and isolated ulnar nerve dislocation as causes for medial elbow snapping is important in symptomatic subjects as the surgical treatments differ. For this purpose, dynamic US scanning is accurate in allowing direct visualization of transient dislocation of both structures during active flexion and extension of the elbow (Fig. 8.65) (Jacobson et al. 2001).

8.5.5
Bone and Joint Disorders

8.5.5.1
Synovitis

A variety of inflammatory diseases can affect the elbow. The main pathologic findings are joint effusion, synovial hypertrophy and destructive bone abnormalities. Physical examination reveals a swollen joint with local inflammatory changes and a reduced range of movements. Incomplete elbow extension can be due either to increased intra-articular fluid or to destructive changes of the articular surfaces. Clinically, joint effusion can be palpated as a localized swelling and tenderness over the anterolateral aspect of the joint, at the level of the radio-capitellar joint, or posteriorly at both sides of the triceps tendon. The accumulation of joint fluid can be reliably recognized with US by examining the distended recesses of the elbow joint, including the larger coronoid fossa and the smaller radial fossa anteriorly and the olecranon fossa posteriorly (Fig. 8.66) (DeMaeseneer et al. 1998). Small amounts of fluid initially collect in the olecranon recess and are best revealed with US while keeping the elbow flexed. In fact, the interposition of the olecranon in elbow extension may make visualization of a small amount of joint fluid more difficult in this recess (DeMaeseneer et al. 1998). With increasing quantities, synovial processes cause progressive elevation of the anterior and posterior fat pads giving them a crescent-shaped appearance of them (Figs. 8.67, 8.68) (Koski 1990; DeMaeseneer et al. 1998). With the elbow extended, the anterior fat pad is pushed by the brachialis against the bone and less fluid tends to collect in the coronoid and radial fossae compared with when the elbow is flexed (DeMaeseneer et al. 1998). The recesses located inferiorly to the anterior fat pad, including the annular one, fill with fluid only in cases with large amounts of joint effusion (Fig. 8.69). In the case of small effusions, and
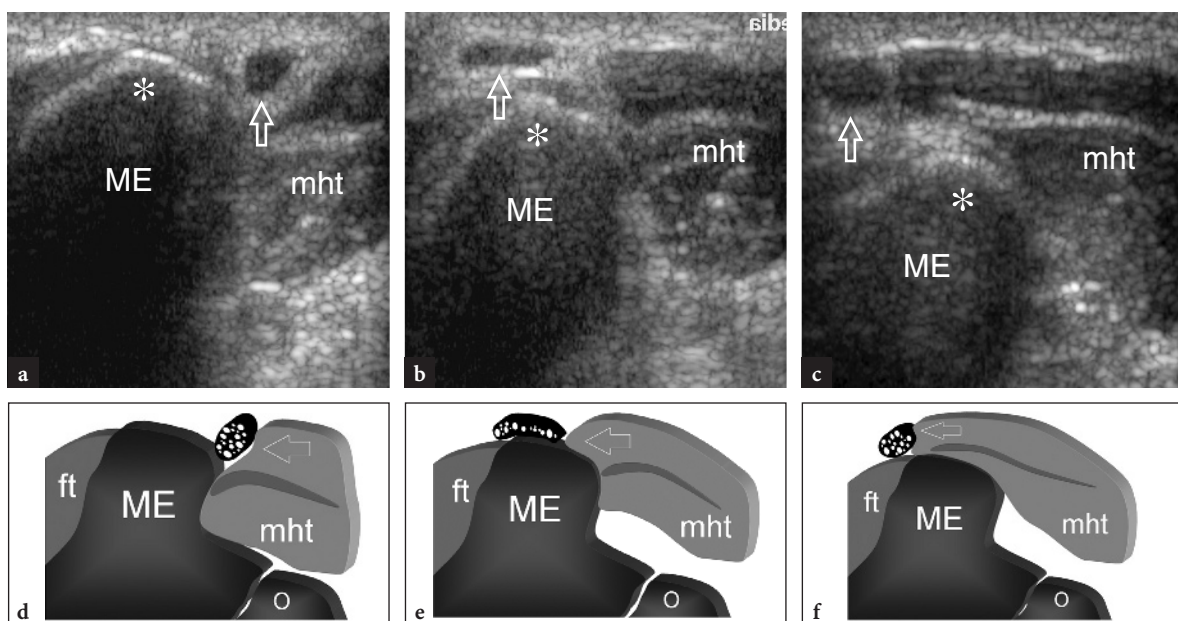
Fig. 8.65a–f. Dynamic study of the cubital tunnel in snapping triceps syndrome. **a–c** Series of transverse 12–5 MHz US images with **d–f** correlative schematic drawings obtained (**a,d**) with the elbow extended and (**b,e** and **c,f**) throughout elbow flexion. With extended elbow, the ulnar nerve *(arrow)* and the medial head of the triceps muscle (mht) are contained within the cubital tunnel. During progressive degrees of elbow flexion, the triceps pushes the ulnar nerve over the tip *(asterisk)* of the medial epicondyle *(ME)* until it snaps out of the tunnel. Then the triceps snaps out too. *ft*, common flexor tendon origin; *O*, olecranon
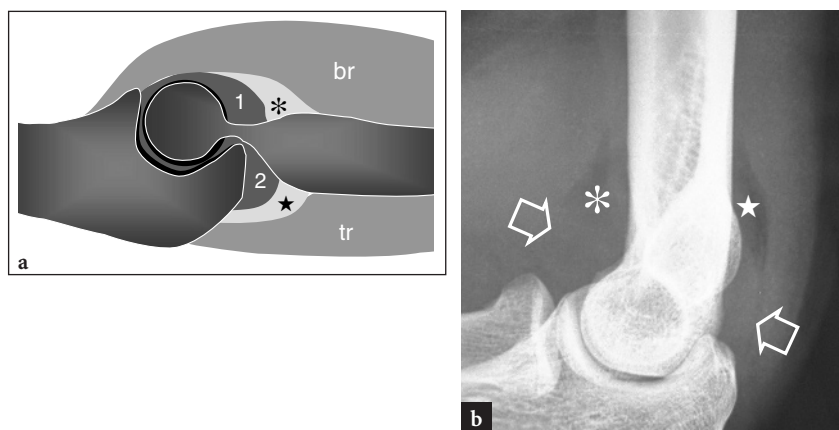

Fig. 8.66a,b. Elbow joint effusion. **a** Schematic drawing of a midsagittal view through an extended elbow demonstrates fluid in the anterior *(1)* and posterior *(2)* portions of the joint. Deep to the brachialis *(br)* and triceps *(tr)* muscles, the anterior *(asterisk)* and posterior *(star)* fat pads are elevated by intra-articular fluid. **b** Lateral radiograph in a patient with abundant joint effusion reveals elevation of the anterior *(asterisk)* and posterior *(star)* fat pads from the surface of the humerus, leading to a "positive fat pad sign", and increased density *(arrows)* at the level of the anterior and posterior recesses, reflecting synovitis

especially in children, careful scanning technique is required not to confuse the articular cartilage of the humerus with fluid. The cartilage interference sign may be helpful for this differentiation. In addition, fluid can be squeezed away by pressure with the transducer (DeMaeseneer et al. 1998). In chronic hypertrophic arthritides, such as rheuma-toid arthritis, herniation of synovial pannus in the periarticular soft tissues of the elbow and joint fluid accumulation can distend the anterior periradial recess to mimic a "cystic mass" in the antecubital region (Miles and Lamont 1989). US demonstrates the pannus as hypoechoic synovial tissue associated with intra-articular anechoic effusion and erosions
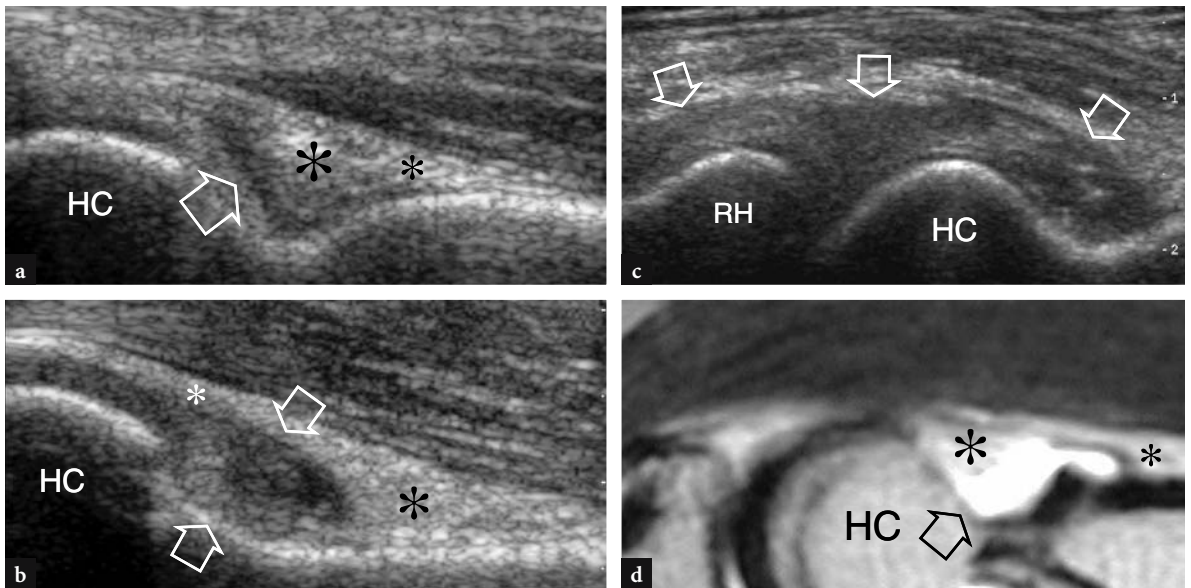
Fig. 8.67a–d. Synovitis of the elbow joint: anterior joint recess. Longitudinal 12–5 MHz US images over the anterior coronoid recess **a** in normal state and **b,c** in two cases of joint synovitis presenting with **b** mild and **c** marked distention of the anterior synovial spaces by fluid and hypertrophied synovium. In normal conditions, a thin layer of fluid (*arrow*) may be encountered in the anterior coronoid recess, deep to the anterior fat pad (*asterisks*). This is a normal finding. When joint fluid expands into the anterior joint spaces, the anterior fat pad (*asterisks*) becomes elevated to assume a typical crescentic or "sail-like" appearance. In markedly distended joints, the anterior bulging of the joint cavity is more conspicuous and may extend down to the joint level. *HC*, humeral capitellum; *RH*, radial head. **d** Corresponding T2w SE MR image of the case illustrated in **b**
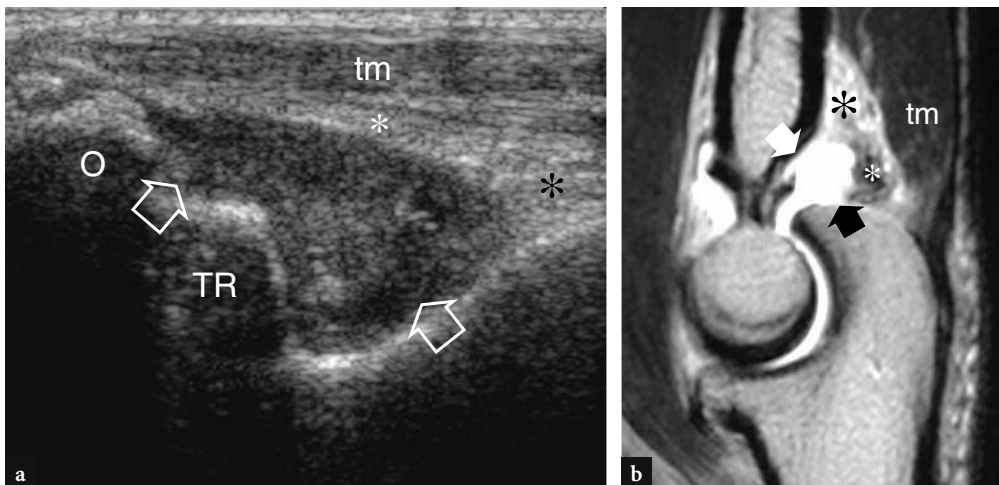

Fig. 8.68a,b. Synovitis of the elbow joint: posterior joint recess. **a** Longitudinal 12–5 MHz US image over the posterior olecranon recess with **b** T2w SE MR imaging correlation in a patient with rheumatoid arthritis presenting with painful elbow and loss of extension. US shows a bulk of hypoechoic synovial pannus filling the recess (*arrows*). Deep to the triceps muscle *(tm)*, the posterior fat pad (*asterisks*) is elevated by the pannus. Note the prominence of the tip of the olecranon *(O)* and the humeral trochlea *(TR)* bulging within the recess

of the hyaline cartilage and subchondral bone on the joint surfaces (Fig. 8.70). In the olecranon fossa, care should be taken not to confuse the synovial pannus with the normal fat pad that may appear slightly hypoechoic (Fig. 8.71). In doubtful cases, graded compression with the probe can help to distinguish between them. When there are clinical concerns for septic arthritis, US-guided aspiration of the joint fluid can be performed (Jacobson and van Holsbeeck 1998; Lim-Dunham et al. 1995).
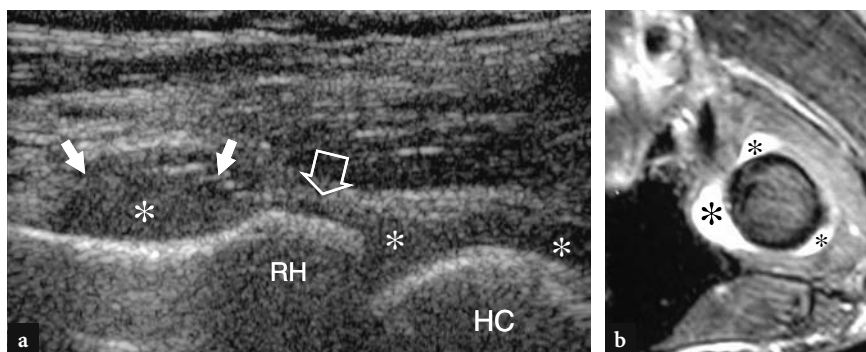
Fig. 8.69a,b. Synovitis of the elbow joint: annular (periradial) recess. **a** Longitudinal 12−5 MHz US image over the anterior aspect of the radio-capitellar joint with **b** transverse T2w SE MR imaging correlation in a patient with rheumatoid arthritis reveals filling of the annular recess (*white arrows*) by hypoechoic synovial fluid (*asterisks*). The annular recess lies around the radial metaphysis and communicates with the joint cavity through a thin passageway (*open arrow*) deep to the annular ligament. Note the rounded profile of the humeral capitellum *(HC)* and the squared profile of the radial head *(RH)*
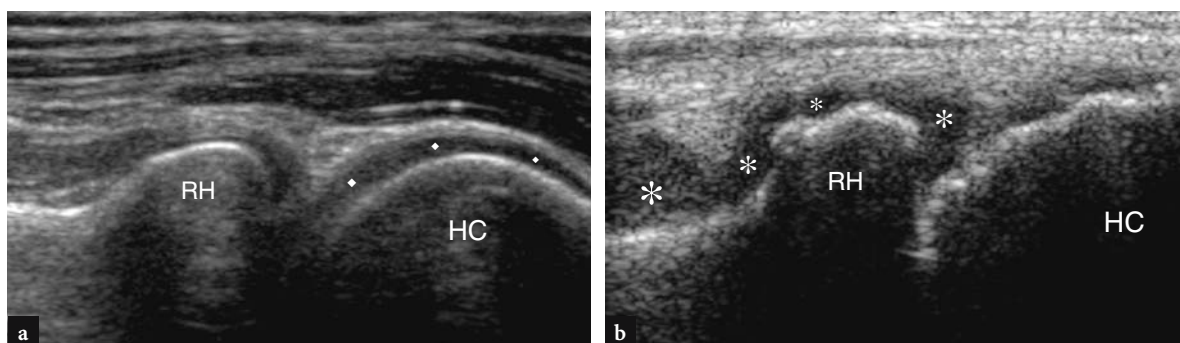

Fig. 8.70a,b. Rheumatoid arthritis. **a,b** Longitudinal 12−5 MHz US images over the anterior aspect of the radio-capitellar joint **a** in a normal subject and **b** in a patient with severe longstanding rheumatoid arthritis. In **a**, note the articular cartilage (*rhombi*) and the regular profile of the subchondral bone of the humeral capitellum *(HC)* and radial head *(RH)*. In **b**, there is complete loss of the cartilage layer and the surface of bones appears diffusely irregular, reflecting erosions. Synovial pannus (*asterisks*) can be seen within the joint space and distending the annular recess
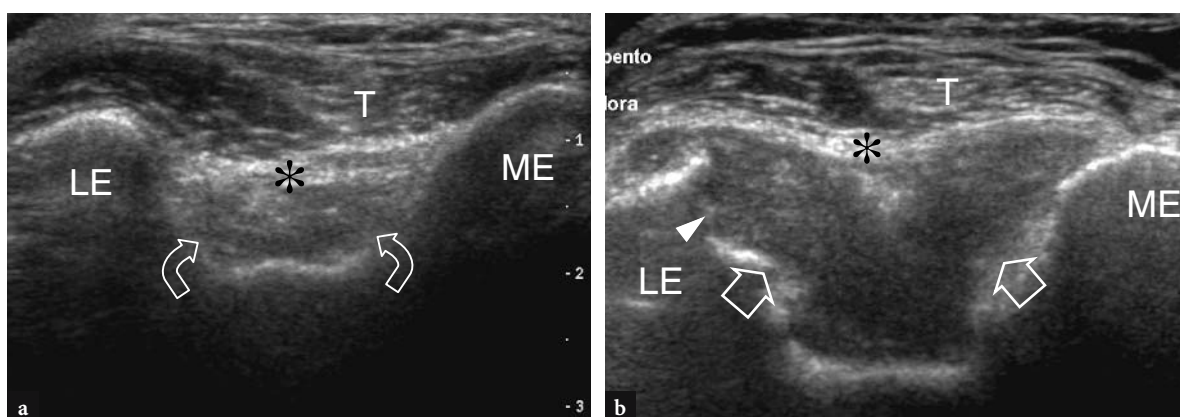
Fig. 8.71a,b. Synovitis of the elbow joint: pitfall. **a,b** Transverse 12−5 MHz US images over the posterior olecranon recess **a** in a normal subject and **b** in a patient with rheumatoid arthritis and an olecranon recess (*arrows*) appears markedly distended by fluid. In **a**, the normal hypoechoic fat contained. In **b** the olecranon fossa, between the lateral *(LE)* and medial *(ME)* epicondyles, should not be confused with the synovitis process shown in **b**. In doubtful cases, careful dynamic examination with elbow flexion and extension movements may be helpful for the diagnosis. Note the erosion (*arrowhead*) on the posteromedial aspect of the lateral epicondyle. *T*, distal triceps tendon

8.5.5.2
Osteoarthritis and Osteochondral Damage

Osteoarthritis of the elbow is basically post-traumatic in nature. It is typically seen in male patients with a history of manual labor (vibration tools), sport-related overuse or fracture malalignment. The dominant extremity is more frequently involved. Given the physiologic attitude of the elbow joint to valgus posture, the external radio-capitellar compartment is most commonly affected. Clinical findings are related to the degenerative process itself (stiffness and loss of motion, usually extension, related to spurring, swelling due to synovitis, local pain), compression of the ulnar nerve inside the cubital tunnel (local pain and tenderness, tingling of the ring and little fingers and, in chronic compression, wasting of the ulnar-innervated intrinsic hand muscles) as well as intra-articular loose bodies (intermittent joint locking and effusion).

Intra-articular loose bodies commonly migrate into the dependent portions of the joint and in the humeral depressions above the joint line, particularly the olecranon fossa, resulting in mechanical symptoms such as intermittent locking and loss of extension. In patients without a synovial effusion, the intra-articular location of a fragment can be established by demonstrating it between the articular cartilage and the anterior and posterior intracapsular fat pads. The small radial annular recess is rarely involved by loose bodies. Dynamic examination performed during flexion and extension of the elbow may be helpful in mobilizing the joint fluid and small loose bodies as well as for differentiating

them from local heterotopic ossification and spurring (Fig. 8.72) (BIANCHI and MARTINOLI 2000). In primary synovial chondromatosis, multiple chondral or osteochondral loose bodies typically display nearly equal size and can vary in number from a few to hundreds (Fig. 8.73). Advanced disease may result in disintegration of the articular surfaces. As already described in other anatomic sites, in the initial phase of disease the treatment includes removal of the loose bodies and synovectomy to prevent recurrence. Similar to a loose body, the os supratrochleare dorsale is an intra-articular ossicle located in the olecranon fossa that may be associated with pain and progressive loss of elbow extension with locking symptoms (OBERMANN and LOOSE 1983). This accessory ossicle is generally believed to be the result of a congenital anomaly rather than the consequence of previous trauma and may cause deepening and remodeling of the olecranon fossa as it increases in size. Differentiation between an os supratrochleare dorsale and a loose body is clinically not relevant because both fragments are treated by surgical removal.

In adolescents, US is also able to recognize deformities of the humeral capitellum in osteochondritis dissecans (TAKAHARA et al. 1998, 2000a,b). This condition typically occurs in 13- to 16-year-olds, mainly as a result of chronic lateral impaction or repetitive valgus stress. The anterolateral articular surface of the capitellum is typically involved with localized subchondral bone flattening and subsequent fragmentation and loosening of bone fragments (TAKAHARA et al. 2000a). US examination is best performed with an anterior approach while
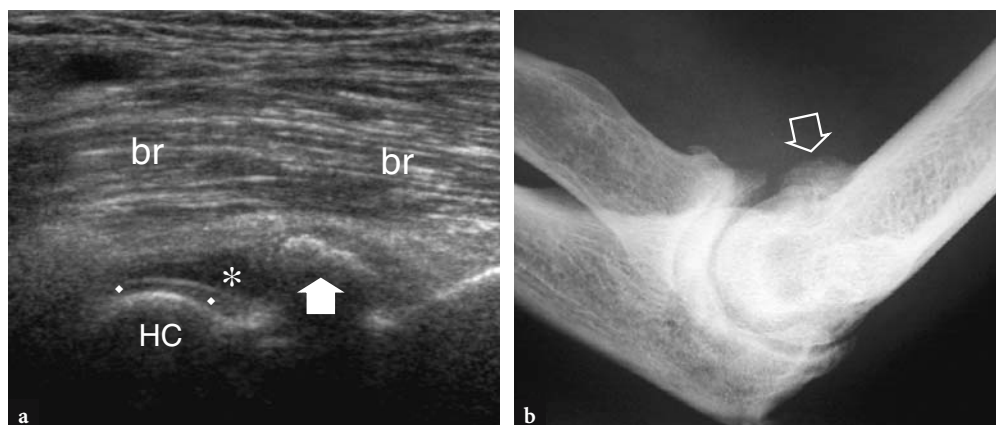
Fig. 8.72a,b. Anterior spur mimicking a loose body. **a** Longitudinal 12–5 MHz US image with **b** lateral radiographic correlation demonstrates a prominent spur (*arrow*) over the coronoid fossa of the humerus. The spur is intracapsular in location and appears bordered by fluid (*asterisk*). During elbow movements, it remained still. Note the thin hypoechoic layer of articular cartilage (*rhombi*) that covers the humeral capitellum *(HC)*. *Br*, brachialis muscle

Fig. 8.73a–d. Primary synovial chondromatosis. **a** Longitudinal and **b** transverse 12–5 MHz US images over the anterior coronoid recess demonstrate multiple intra-articular loose bodies as hyperechoic fragments (*arrowheads*) of similar size with posterior acoustic shadowing lying inside the recess. Note the elevation of the anterior fat pad (*asterisks*) over the fragments and the thin hypoechoic layer of articular cartilage (*rhombi*) that overlies the humeral capitellum *(HC)*. *br*, brachialis muscle. **c** Lateral radiograph and **d** transverse T1w GRE MR imaging of the same case showing the loose bodies (*arrowheads*)

keeping the elbow extended (to view the proximal and middle parts of the anterior capitellum) and with a posterior approach while keeping the elbow flexed (to view the middle and distal parts of the anterior capitellum) (TAKAHARA et al. 2000b). Detached bony fragments are depicted as echogenic foci in the osteochondral defect. US has also proved to be accurate in determining whether the lesion is stable or unstable (loosened fragments), with good (89%) agreement with surgical findings and MR imaging (TAKAHARA et al. 2000b). In these patients, delay in the appropriate management can be avoided by an early US examination. Similar abnormalities may be encountered in Panner disease, a condition related to avascular necrosis of the ossification center of the capitellum that occurs in 5–11 years old children secondary to traumatic injures. Somewhat comparable to Legg-Calvé-Perthes disease in the hip, this latter condition has a benign outcome with no residual deformity of the capitellum and absence of loose body formation (VANDERSCHUEREN et al. 1998).

8.5.5.3
Occult Fractures

Due to the anatomic complexity of the elbow joint, some undisplaced fractures, such as those involving the radial head and neck and the coronoid process, may remain occult radiographically, even when additional projections are performed. When cast immobilization is not employed as a prophylactic measure to avoid overtreatment, persistent pain and disability may lead the referring physician to acquire a US examination to rule out any possible soft-tissue abnormality about the elbow. With careful scanning technique, high-resolution US is able to identify acute elbow fractures based on detection of a step-off deformity or focal discontinuity of the hyperechoic cortical line (Fig. 8.74). In these cases, however, additional radiographic or MR imaging studies should always be obtained to confirm the US diagnosis. Dynamic scanning during careful passive-assisted pronation and supination of the forearm with the probe placed
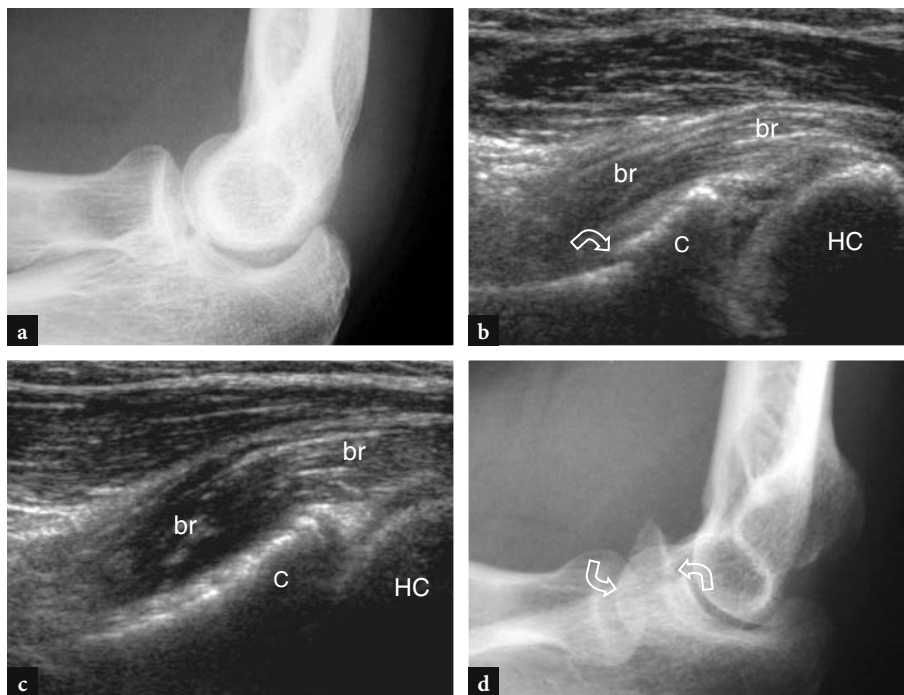
Fig. 8.74a–d. Occult fracture of the right coronoid process in a woman following a ski accident. **a** The patient had a negative radiographic examination performed soon after the injury. **b** Two weeks later, she was submitted to US examination due to persistent elbow pain and loss of extension. US identified an interruption (*curved arrow*) of the hyperechoic cortical profile of the coronoid process (*C*), just cranial to the insertion of the brachialis *(br)*. There was associated mild intra-articular effusion. *HC*, humeral capitellum. **c** Left healthy side for comparison. **d** Additional oblique view of the right elbow confirms the fracture

in the transverse plane over the radial head may be useful to exclude any fracture at this site. In doubtful cases, associated US signs, such as joint effusion, can be easily detected in intra-articular fractures and may suggest a more detailed analysis of the bone contour (Major and Crawford 2002). On the other hand, the absence of effusion in elbow injuries with negative plain radiographs may make further bone investigation with MR imaging unnecessary (Kessler et al. 2002). More than in adults, US seems to have a potential role for the evaluation of elbow fractures in children. In fact, there are difficulties in assessing bony abnormalities about the elbow in skeletally immature patients using plain radiographs because of the absence of the secondary centers of ossification (Fig. 8.75). When a radiographic sign of joint effusion is present but a fracture is not visualized, US may help in distinguishing the separation of the distal humeral epiphysis (Dias et al. 1988; Ziv et al. 1996) from elbow dislocation in neonates, as well as in detecting or excluding radial head (Lazar et al. 1998) and supracondylar fractures (Davidson et al. 1994; Brown and Eustace 1997).

8.5.5.4
Posterior Dislocation Injury and Instability

Elbow dislocation is most common in children less than 10 years old and accounts for 5–8% of all fractures and dislocations in adults, being second only to the shoulder. Usually, the ulna and radius dislocate posteriorly following a hyperextension mechanism, such as during a fall on the outstretched hand. The posterior translation can cause impaction fractures (i.e., coronoid process, humeral capitellum) and a variety of soft-tissue lesions, involving joint and ligaments, vessels and nerves. In such cases, US can occasionally be required to demonstrate soft-tissue complications, such as heterotopic ossification, contusion of the brachialis muscle and injuries to the brachial artery and the median and ulnar nerves (Figs. 8.76, 8.77). After a dislocation, instability of the elbow joint may result following progressive disruption of the lateral ulnar collateral ligament (posterolateral rotatory instability), tearing of the anterior and posterior joint capsule and then rupture of the medial collateral ligamentous complex (multidirectional instability).

Fig. 8.75a–c. Radial fracture in a 5-year-old child presenting with left lateral elbow pain and disability after a fall. **a** Longitudinal 12−5 MHz US image at the anterolateral elbow demonstrates increased distance between the humeral capitellum *(HC)* and the radial epiphysis related to an intervening hyperechoic joint effusion *(asterisks)*. Note the hyperechoic dot *(arrowheads)* within the radial epiphysis representing the ossification center. At the radial metaphysis, US reveals a focal irregularity of the hyperechoic cortical line *(arrow)* suggesting a fracture. *R*, radius. **b** Contralateral healthy side for comparison. **c** Lateral radiograph of the left elbow confirms the diagnosis of radial fracture *(arrow)*
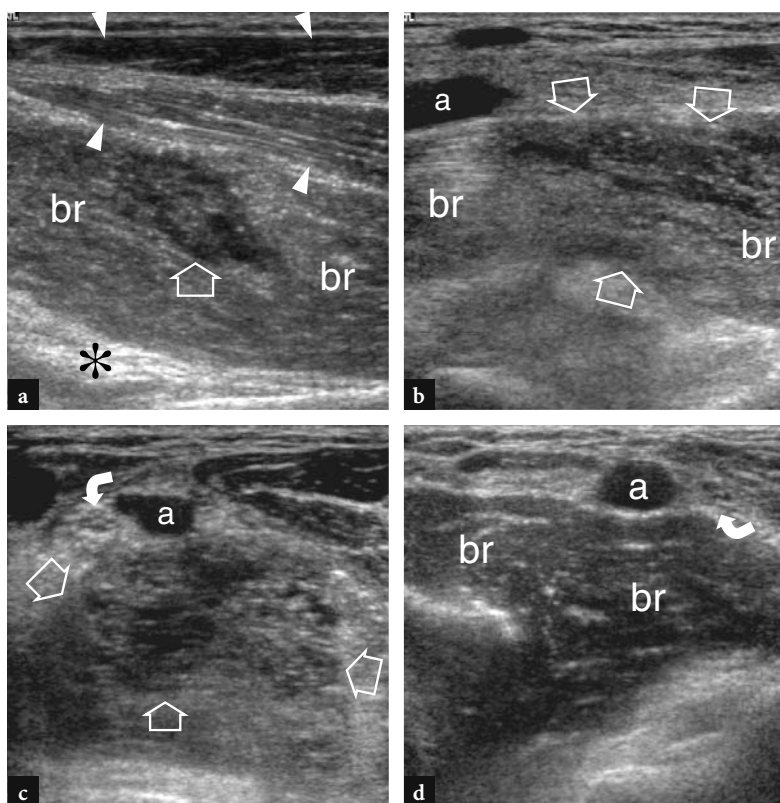

Fig. 8.76a–d. Partial tear of the brachialis muscle as a consequence of posterior dislocation injury. **a,b** Longitudinal and **c** transverse 12−5 MHz US images of the anterior elbow obtained in the supracondylar area demonstrate a wide hypoechoic defect *(large arrows)* in the substance of the brachialis muscle *(br)* related to hematoma. The torn muscle tissue is surrounded by anechoic spaces. Note the relationship of the injured brachialis with the normal distal biceps muscle *(arrowheads)*, brachial artery *(a)* and median nerve *(curved arrow)*. **d** Contralateral healthy side. Corresponding transverse 12−5 MHz US image shown in **c** reveals an intact brachialis
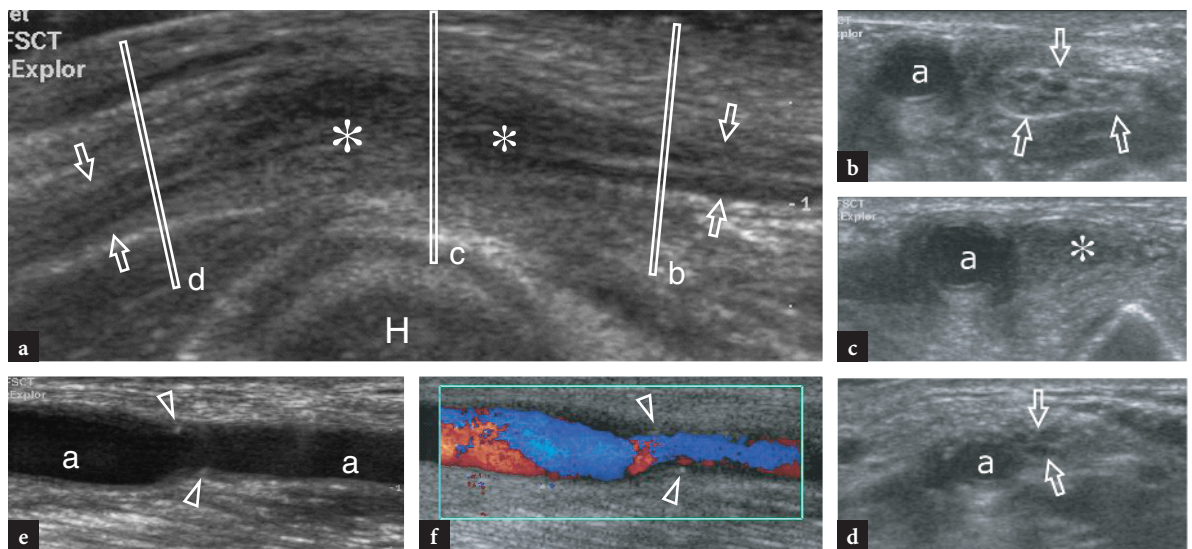
Fig. 8.77a–f. Traumatic injury of the median nerve and brachial artery following posterior dislocation of the elbow. The patient received primary surgical repair. **a** Long-axis 12−5 MHz US image over the trochlea *(H)* demonstrates fusiform swelling with an indistinct outer surface and hypoechoic changes *(asterisks)* of the median nerve *(arrows)* relative to a post-traumatic fusiform neuroma. **b–d** Short-axis 12−5 MHz US images obtained at the level *(vertical white bar)* indicated in a reveal nerve enlargement and loss of the internal fascicular pattern *(asterisk)* at the site of injury (**b**) compared with more proximal (**a**) and distal (**c**) levels. Note the close relation of the nerve with the adjacent brachial artery (**a**). **e,f** Long-axis gray-scale **e** and color Doppler **f** 12−5 MHz US images of the injured brachial artery show the site of vascular reconstruction *(arrowheads)*

8.5.6
Elbow Masses

Both solid and cystic masses can be encountered in the soft tissues of the elbow as incidental findings. Most are benign and have an indolent behavior, such as lipomas, ganglia and neural tumors, and can be easily diagnosed with US based on previously described criteria (Figs. 8.78, 8.79). Only occasionally, elbow masses may cause pain and specific symptoms related to their specific anatomic relationship with elbow structures, including joint impairment and nerve compression (see Fig. 8.57). In such cases, surgical excision is always indicated to ensure recovery of function. Also, US can be useful to distinguish normal findings that can simulate disease. At the
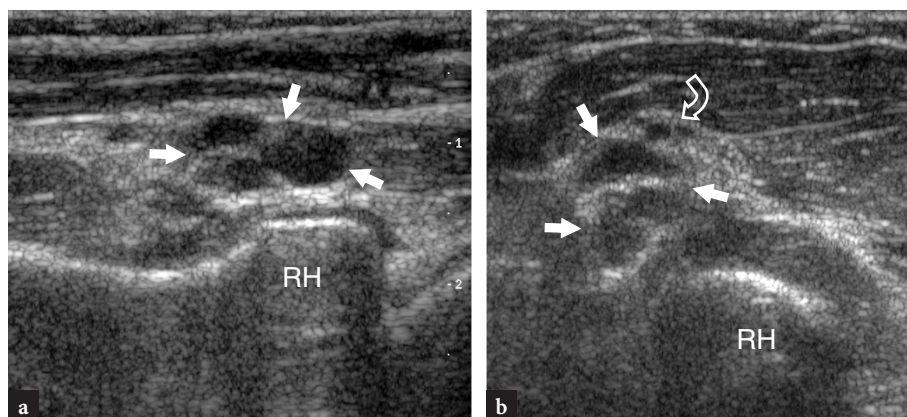

Fig. 8.78a,b. Ganglion cyst of the elbow in a patient who complained of mild paresthesias radiating over the dorsal thumb. **a** Longitudinal and **b** transverse 12−5 MHz US images over the radial head *(RH)* reveal a small lobulated anechoic fluid-filled mass *(straight arrows)* consistent with a ganglion, adjacent to the radial nerve *(curved arrow)*. The ganglion had a thin pedicle in connection with the radio-capitellar joint, confirming its articular extension
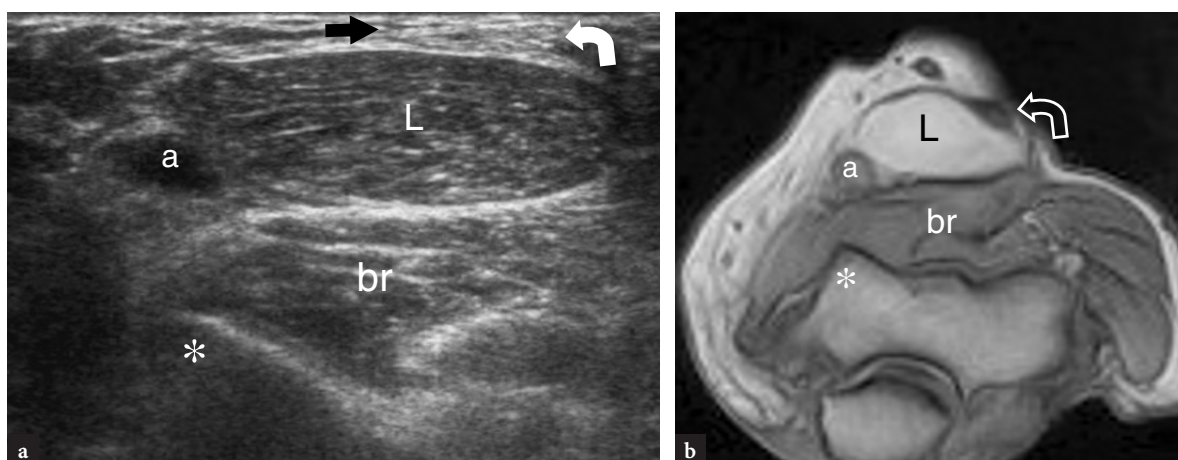
Fig. 8.79a,b. Lipoma in a patient with painless soft-tissue swelling over the anterior elbow. **a** Transverse 10−5 MHz US image over the distal humerus with **b** T1w GRE MR imaging correlation demonstrates an oval hypoechoic soft-tissue mass *(L)* located superficial to the brachialis muscle *(br)* that displaces the brachial artery *(a)* and the distal biceps tendon *(arrows)*. In this particular case, the echotexture of lipoma is quite similar to the underlying brachialis and should not be interpreted as a normal muscle. *Asterisk*, medial edge of the humeral trochlea

elbow, this most often occurs in young women who seek advice because of a painless lump located anterior to the medial epicondyle that is best appreciated with full joint extension. This pseudomass is due to the anterior prominence of the medial portion of the epicondyle that becomes evident in females with hyperlax joints when extending the elbow >180°. In these cases, US can readily exclude any local space-occupying mass.

References

Abiri MM, Kirperkar M, Ablow RC (1989) Osteomyelitis: detection with US. Radiology 172:509−511

Agins HJ, Chess JL, Hoekstra DV et al (1988) Rupture of the distal insertion of the biceps brachii tendon. Clin Orthop 234:34−38

Awaya H, Schweitzer ME, Feng SA et al (2001) Elbow synovial fold syndrome: MR imaging findings. AJR Am J Roentgenol 177:1377−1381

Barr LL, Babcock DS (1991) Sonography of the normal elbow. AJR Am J Roentgenol 157:793−798

Barr LL, Kirks DR (1993) Ultrasonography of acute epitrochlear lymphadenitis. Pediatr Radiol 23:72−73

Bianchi S, Martinoli C (2000) Detection of loose bodies in joints. Radiol Clin North Am 37:679−690

Bodner G, Harpf C, Meirer R et al (2002) Ultrasonographic appearance of supinator syndrome. J Ultrasound Med 21:1289−1293

Bredella MA, Tirman PF, Fritz RC et al (1999) MR imaging findings of lateral ulnar collateral ligament abnormalities in patients with lateral epicondylitis. AJR Am J Roentgenol 173:1379−1382

Brown J, Eustace S (1997) Neonatal transphyseal supracondy-

lar fracture detected by ultrasound. Pediatr Emerg Care 13:410−412

Capasso G, Testa V, Cappabianca S et al (1998) Recurrent dislocation of the ulnar nerve in athletes: a report of two cases. Clin J Sport Med 8:56−58

Carcìa CJ, Varela C, Abarca K et al (2000) Regional lymphadenopathy in cat-scratch disease: ultrasonographic findings. Pediatr Radiol 30:640−643

Childress HM (1975) Recurrent ulnar-nerve dislocation at the elbow. Clin Orthop 108:168−173

Chiou HJ, Chou YH, Cheng SP (1998) Cubital tunnel syndrome: diagnosis by high-resolution ultrasonography. J Ultrasound Med 17:643−648

Clarke RP (1988) Symptomatic lateral synovial fringe (plica) of the elbow joint. Arthroscopy 4:112−116

Connell D, Burke F, Coombes P et al (2001) Sonographic examination of lateral epicondylitis. AJR Am J Roentgenol 176:1763−1777

Davidson RS, Markovitz RI, Dormans J et al (1994) Ultrasonographic evaluation of the elbow in infants and young children after suspected trauma. J Bone Joint Surg Am 76:1804−1812

De Smet AA, Winter TC, Best TM et al (2002) Dynamic sonography with valgus stress to assess elbow ulnar collateral ligament injury in baseball pitchers. Skeletal Radiol 31:671−676

DeMaeseneer M, Jacobson JA, Jaovisidha S et al (1998) Elbow effusions: distribution of joint fluid with flexion and extension and imaging implications. Invest Radiol 33:117−125

Dias JJ, Lamont AC, Jones JM (1988) Ultrasonic diagnosis of neonatal separation of the distal humeral epiphysis. Bone Joint Surg Br 70:825−828

Duchow J, Kelm J, Kohn D (2000) Acute ulnar nerve compression syndrome in a powerlifter with triceps tendon rupture: a case report. Int J Sports Med 21:308−310

Falchook FS, Zlatkin MB, Erbacher GE et al (1994) Rupture of the distal biceps tendon: evaluation with MR imaging. Radiology 190:659−663

Ferrara MA, Marcelis S (1997) Ultrasound of the elbow. J Belge Radiol 80:122−123

Fitzgerald SW, Curry DR, Erickson SJ et al (1994) Distal biceps tendon injury: MR imaging diagnosis. Radiology 191:203−206

Gelberman RH, Yamaguchi K, Hollstien SB et al (1998) Changes in interstitial pressure and cross-sectional area of the cubital tunnel and of the ulnar nerve with flexion of the elbow. J Bone Joint Surg Am 80:492−501

Gielen J, Wang XL, Vanhoenacker F et al (2003) Lymphadenopathy at the medial epitrochlear region in cat-scratch disease. Eur Radiol (13:363-1369)

Jacob D, Creteur V, Courthaliac C et al (2004) Sonoanatomy of the ulnar nerve in the cubital tunnel: a multicentre study by the GEL. Eur Radiol 14:1770-1773

Jacobson JA, van Holsbeeck MT (1998) Musculoskeletal ultrasonography. Orthop Clin North Am 29:135−167

Jacobson JA, Jebson PJL, Jeffers AW et al (2001) Ulnar nerve dislocation and snapping triceps syndrome: diagnosis with dynamic sonography: report of three cases. Radiology 220:601−605

Kaempffe FA, Lerner RM (1996) Ultrasound diagnosis of triceps tendon rupture. A report of 2 cases. Clin Orthop 332:138−142

Kessler T, Winkler H, Weiss C et al (2002) Ultrasound diagnosis of the elbow joint in fracture of the head of the radius. Orthopade 31:268−270

Koski JM (1990) Ultrasonography of the elbow joint. Rheumatol Int 10:91−94

Kosuwon W, Mahaisavariya B, Saengnipanthkul S et al (1993) Ultrasonography of pulled elbow. J Bone Joint Surg Br 75:421−422

Lazar RD, Waters PM, Jaramillo D (1998) The use of ultrasonography in the diagnosis of occult fracture of the radial neck. J Bone Joint Surg Am 80:1361−1364

Levin D, Nazarian LN, Miller TT et al (2005) Lateral epicondylitis of the elbow: US findings. Radiology 237:230-234

Liessi G, Cesari S, Spaliviero B et al (1996) The US, CT and MR findings of cubital bursitis: a report of five cases. Skeletal Radiol 25:471−475

Lim-Dunham JE, Ben-Ami TE, Yousefzadeh DK (1995) Septic arthritis of the elbow in children: the role of sonography. Pediatr Radiol 25:556−559

Lin J, Jacobson JA, Fessell DP et al (2000) An illustrated tutorial of musculoskeletal sonography. II. Upper extremity. AJR Am J Roentgenol 175:1071−1079

Lozano V, Alonso P (1995) Sonographic detection of the distal biceps tendon rupture. J Ultrasound Med 14:389−391

Maffulli N, Regine R, Carrillo F et al (1990) Tennis elbow: an ultrasonographic study in tennis players. Br J Sport Med 24:151−154

Major NM, Crawford ST (2002) Elbow effusions in trauma in adults and children: is there an occult fracture? AJR Am J Roentgenol 178:413−418

Markowitz RI, Davidson RS, Harty MP et al (1992) Sonography of the elbow in infants and children. AJR Am J Roentgenol 159:829−833

Martinoli C, Bianchi S, Gandolfo N et al (2000) Ultrasound of nerve entrapments in osteofibrous tunnels. Radiographics 20:199−217

Martinoli C, Bianchi S, Giovagnorio F et al (2001) Ultrasound of the elbow. Skeletal Radiol 30:605−614

Miles KA, Lamont AC (1989) Ultrasonic demonstration of the elbow fat pad. Clin Radiol 40:602−604

Miller JH, Beggs I (2001) Detection of intra-articular bodies in the elbow with saline arthrosonography. Clin Radiol 56:231−234

Miller T, Adler RS (2000) Sonography of tears of the distal biceps tendon. AJR Am J Roentgenol 175:1081−1086

Miller TT, Shapiro MA, Schults E, Kalish PE (2002) Comparison of sonography and MRI for diagnosing epicondylitis. J Clin Ultrasound 30:193−202

Nazarian LN, McShane JM, Ciccotti MC et al (2003) Dynamic US of the anterior band of the ulnar collateral ligament of the elbow in asymptomatic major league baseball pitchers. Radiology 227:149−154

Obermann WR, Loose HW (1983) The os supratrochleare dorsale: a normal variant that may cause symptoms. AJR Am J Roentgenol 141:123−127

Okamoto M, Abe M, Shirai H et al (2000) Diagnostic ultrasonography of the ulnar nerve in cubital tunnel syndrome. J Hand Surg [Br] 25:499−502

Popovic N, Ferrara MA, Daenen B et al (2001) Imaging overuse injury of the elbow in professional team handball players: a bilateral comparison using plain films, stress radiography, ultrasound, and magnetic resonance imaging. Int J Sports Med 22:60−67

Puig S, Turkof E, Sedivy R et al (1999) Sonographic diagnosis of recurrent ulnar nerve compression by ganglion cysts. J Ultrasound Med 18:433−436

Regan W, Wold LE, Conrad R et al (1992) Microscopic histopathology of chronic refractory lateral epicondylitis. Am J Sports Med 20:746−749

Rosenberg ZS, Bencardino J, Beltran J (1997) MR imaging of normal variants and interpretation pitfalls of the elbow. MRI Clin North Am 5:481−499

Sasaki J, Takahara M, Ogino T et al (2002) Ultrasonographic assessment of the ulnar collateral ligament and medial elbow laxity in college baseball players. J Bone Joint Surg Am 84:525−531

Seiler JG, Parker LM, Chamberland PDC et al (1995) The distal biceps tendon: two potential mechanisms involved in its rupture. Arterial supply and mechanical impingement. J Shoulder Elbow Surg 4:149−156

Skaf AY, Boutin RD, Dantas RWM et al (1999) Bicipitoradial bursitis: MR imaging findings in eight patients and anatomic data from contrast material opacification of bursae followed by routine radiography and MR imaging in cadavers. Radiology 212:111−116

Spence LD, Adams J, Gibbons D et al (1998) Rice body formation in bicipitoradial bursitis: ultrasound, CT, and MRI findings. Skeletal Radiol 27:30−32

Spinner M (1968) The arcade of Frohse and its relationship to posterior interosseous nerve paralysis. J Bone Joint Surg Br 50:809−812

Spinner RJ, Goldner RO (1998) Snapping of the medial head of the triceps and recurrent dislocation of the ulnar nerve. J Bone Joint Surg Am 80:239−247

Steiner E, Steinbach LS, Schnarkowski P et al (1996) Ganglia and cysts around joints. Radiol Clin North Am 34:395−425

Stewart JD (1993) Compression and entrapment neuropathies. In: Dyck PJ, Thomas PK (eds) Peripheral neuropathy, 3rd edn. Saunders, Philadelphia, pp 1354−1379

Takahara M, Shundo M, Kondo M et al (1998) Early detection of osteochondritis dissecans of the capitellum in young

baseball players. Reports of three cases. J Bone Joint Surg Am 80:892–897

Takahara M, Ogino T, Takagi M et al (2000a) Natural progression of osteochondritis dissecans of the humeral capitellum: initial observations. Radiology 216:207–212

Takahara M, Ogino T, Tsuchida H et al (2000b) Sonographic assessment of osteochondritis dissecans of the humeral capitellum. AJR Am J Roentgenol 174:411–415

Vanderschueren G, Prasad A, van Holsbeeck M (1998) Ultrasound of the elbow. Semin Musculoskel Radiol 2:223–235

Ward S, Teefey S, Paletta G et al (2003) Sonography of the medial collateral ligament of the elbow: a study of cadavers and healthy adult male volunteers. AJR Am J Roentgenol 180:389–394

Ziv M, Litwin A, Katz K et al (1996) Definitive diagnosis of fracture-separation of the distal humeral epiphysis in neonates by ultrasonography. Pediatr Radiol 26:493–496